

**Characterization of the TPQ Cofactor in Amine  
Oxidases and the Heme Cofactor  
in Cystathionine Beta-Synthase  
by Resonance Raman Spectroscopy.  
Implications for Catalytic Properties**

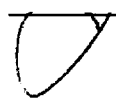
Edward L. Green


B.S., Pacific University, 1996

A dissertation submitted to the faculty of the  
OGI School of Science & Engineering  
Oregon Health & Science University  
in partial fulfillment of the  
requirements for the degree  
Doctor of Philosophy  
in  
Biochemistry and Molecular Biology


October 2001

The dissertation "Characterization of the TPQ Cofactor in Amine Oxidases and the Heme Cofactor in Cystathionine Beta-Synthase by Resonance Raman Spectroscopy. Implications for Catalytic Properties" by Edward L. Green has been examined and approved by the following Examination Committee:

 \_\_\_\_\_  
Joanne Sanders-Loehr, Advisor  
Professor

\_\_\_\_\_  
 \_\_\_\_\_  
Ninian J. Blackburn  
Professor

\_\_\_\_\_  
Thomas M. Loehr  
Professor

 \_\_\_\_\_  
James F. Hare  
Associate Professor  
Oregon Health Sciences University

## **DEDICATION**

**This dissertation is dedicated to my wife and my son.**

## ACKNOWLEDGMENTS

First, I wish to express my deepest thanks to my research advisors, Professors Joann Sanders-Loehr and Thomas M. Loehr, who have given to me a new understanding of what it means to be a scientist and have provided me with many learning opportunities. I would not be where I am today if it wasn't for their immense patience over the past five years. I would also like to thank Professor Ninian Blackburn for his guidance, seminar discussions, and for taking the time to examine this dissertation. I also wish to thank Professor James Hare for the time spent carefully reviewing my dissertation. I am also grateful to our collaborators: Drs. Judith Klinman, Benjamin Schwartz, Julie Plastino, and Joann Dove for providing me with the HPAO and mutant proteins and for many enlightening discussions, and to Drs. Ruma Banerjee and Shin Taoka for providing the CBS proteins. I would like to thank Drs. Pierre Moënne-Loccoz, Nobuhumi Nakamura, Jonathan Cohen, Jingyuan Ai, Hong-wei Huang, Colin Andrew, and the entire metalloprotein group for their immense help and friendship during my Ph.D. studies. Special appreciation to my grandparents, my parents, my extended family, my coworkers at IDC, and many former teachers for providing me with love, support, and encouragement during my long period of studies. Finally, I wish to give the biggest thanks to my beautiful wife Theresa and my son Harrison for always being there in times of need and for the great love, patience, and support they have both given to me.

## TABLE OF CONTENTS

DEDICATION . . . . .	iii
ACKNOWLEDGMENTS . . . . .	iv
TABLE OF CONTENTS . . . . .	v
LIST OF TABLES . . . . .	ix
LIST OF FIGURES . . . . .	x
LIST OF SCHEMES . . . . .	xii
ABSTRACT . . . . .	xiii

### CHAPTER 1 CHARACTERIZATION OF THE TPQ COFACTOR IN AMINE OXIDASES AND THE HEME COFACTOR IN CYSTATHIONINE $\beta$ -SYNTHASE BY RESONANCE RAMAN SPECTROSCOPY. IMPLICATIONS FOR CATALYTIC PROPERTIES . . . . . 1

1.1	Introduction . . . . .	1
1.2	Overview of Copper-Containing Amine Oxidases . . . . .	4
1.2.1	Active Site Structure . . . . .	5
1.2.2	Biogenesis Mechanism of TPQ . . . . .	5
1.2.3	Catalytic Mechanism . . . . .	9
1.3	Overview of Cystathionine $\beta$ -Synthase . . . . .	9
1.3.1	Active Site Structure . . . . .	11
1.3.2	Catalytic Mechanism . . . . .	11
1.4	Focus of Present Research . . . . .	13

### CHAPTER 2 RATES OF OXYGEN AND HYDROGEN EXCHANGE AS INDICATORS OF TPQ COFACTOR ORIENTATION IN AMINE OXIDASES . 16

2.1	Introduction . . . . .	16
-----	------------------------	----

2.2	Experimental Procedures . . . . .	20
2.2.1	Protein Preparation . . . . .	20
2.2.2	Resonance Raman Spectroscopy . . . . .	20
2.2.3	Isotope Exchange in WT-HPAO and Mutants . . . . .	21
2.2.4	Isotope Incorporation during Biogenesis of HPAO . . . . .	21
2.2.5	Isotope Exchange in ECAO, AGAO, PSAO, and Model Compound . . . . .	22
2.2.6	Exchange Rate Calculation . . . . .	22
2.3	Results and Discussion . . . . .	23
2.3.1	Oxygen Exchange in WT-HPAO and ECAO . . . . .	23
2.3.2	Hydrogen Exchange in WT-HPAO, ECAO, and Model Compound . . . . .	30
2.3.3	Oxygen Exchange in PSAO . . . . .	30
2.3.4	O and H Exchange in AGAO . . . . .	35
2.3.5	O and H Exchange in the D319 Mutants of HPAO . . . . .	38
2.3.6	O and H Exchange in E406Q and N404A Mutants of HPAO . . . . .	43
2.4	Conclusions . . . . .	44
2.4.1	Prediction of TPQ Orientation from Exchange Rates . . . . .	44
2.4.2	Structural Basis for Differences in Exchange Rates . . . . .	48
2.4.3	Functional Significance of Cofactor Mobility . . . . .	50

## CHAPTER 3 DETECTION AND CHARACTERIZATION OF REACTION

	INTERMEDIATES IN AMINE OXIDASE . . . . .	51
3.1	Introduction . . . . .	51
3.1.1	Catalytic Base Mutants . . . . .	53
3.1.2	Flanking Residue Mutations . . . . .	53
3.2	Experimental Procedures . . . . .	55
3.2.1	Sample Preparation . . . . .	55
3.2.2	Resonance Raman Spectroscopy . . . . .	56
3.3	Results and Discussion . . . . .	57
3.3.1	Ammonia Adduct of D319N and Methylamine Adduct of D319E . . . . .	57
3.3.2	Methylamine Adduct of N404A . . . . .	62
3.4	Conclusions . . . . .	64

<b>CHAPTER 4</b>	<b>RESONANCE RAMAN CHARACTERIZATION OF THE HEME COFACTOR IN CYSTATHIONINE <math>\beta</math>-SYNTHASE. IDENTIFICATION OF THE Fe-S(Cys) VIBRATION IN THE SIX-COORDINATE LOW-SPIN HEME .</b>	<b>67</b>
4.1	Introduction . . . . .	67
4.2	Materials and Methods . . . . .	68
4.2.1	Chemicals . . . . .	68
4.2.2	Enzyme Labeling and Purification . . . . .	69
4.2.3	Resonance Raman Samples . . . . .	69
4.2.4	Resonance Raman Spectroscopy . . . . .	70
4.3	Results and Discussion . . . . .	72
4.3.1	Resonance Raman of Oxidized Cystathionine $\beta$ -Synthase . . . . .	72
4.3.2	Homocysteine Binding to Cystathionine $\beta$ -Synthase . . . . .	75
4.3.3	Resonance Raman of Reduced Cystathionine $\beta$ -Synthase . . . . .	75
4.3.4	Spectrum of Oxidized Cystathionine $\beta$ -Synthase Treated with HgCl <sub>2</sub> . . . . .	76
4.3.5	Spectrum of Reduced Cystathionine $\beta$ -Synthase Treated with HgCl <sub>2</sub> . . . . .	76
4.3.6	CO Adduct of Cystathionine $\beta$ -Synthase . . . . .	78
4.3.7	Summary . . . . .	78
<b>CHAPTER 5</b>	<b>CONCLUSIONS AND FUTURE DIRECTIONS . . . . .</b>	<b>81</b>
5.1	Characterization of Biogenesis in Amine Oxidases . . . . .	81
5.2	Determination of TPQ Orientation . . . . .	83
5.2.1	Productive Orientation . . . . .	83
5.2.2	Flipped Orientation . . . . .	84
5.2.3	Mobile Orientation . . . . .	85
5.3	Characterization of Reaction Intermediates . . . . .	86
5.3.1	Identification of Deprotonated Iminoquinone . . . . .	87
5.3.2	Identification of Product Schiff Base . . . . .	88
5.4	Future Copper Amine Oxidase Work . . . . .	89
5.5	Characterization of the Heme Cofactor in CBS . . . . .	91

5.5.1	Determination of Heme Axial Ligands . . . . .	91
5.5.2	Ligation and Spin-State Changes with HgCl <sub>2</sub> . . . . .	94
5.5.3	Examination of Homocysteine Binding . . . . .	94
5.6	Future Directions for Cystathionine $\beta$ -Synthase Research . . . . .	95
LITERATURE CITED . . . . .		97
BIOGRAPHICAL SKETCH . . . . .		107



## LIST OF TABLES

2.1	Comparison of Isotopic Shifts Due to $^{18}\text{O}$ Incorporation at the C2 and C5 Position of the TPQ Ring in AGAO and HPAO . . . . .	28
2.2	Raman Frequencies and Half-times for Isotope Exchange in Amine Oxidases . . . . .	29
2.3	Rates of Solvent Isotope Exchange as Indicators of Cofactor Orientation . .	45

## LIST OF FIGURES

1.1	Structure diagrams of the four major quinone cofactors . . . . .	2
1.2	Structural representations of different porphyrin-containing cofactors . . . . .	3
1.3	Active site of HPAO showing the distances (in Å) between groups . . . . .	6
1.4	Postulated organization of the tetrameric and truncated dimer forms of cystathionine $\beta$ -synthase . . . . .	12
2.1	Proposed reaction cycle for amine oxidation in HPAO . . . . .	18
2.2	Resonance Raman spectra of copper-containing amine oxidases and models . . . . .	24
2.3	Effect of oxygen isotopes of Raman spectrum of WT-HPAO . . . . .	25
2.4	Proposed mechanisms for H and O exchange on TPQ . . . . .	26
2.5	Raman spectra of tBQO <sup>-</sup> model compound at different times after dilution into D <sub>2</sub> O buffer . . . . .	31
2.6	Effect of pH on the Raman spectrum of PSAO . . . . .	33
2.7	Raman spectra of PSAO as a function of time of exposure to H <sub>2</sub> <sup>18</sup> O . . . . .	34
2.8	Raman spectra of AGAO as a function of time of exposure to D <sub>2</sub> O . . . . .	36
2.9	Effect of ionic strength on the rate of D exchange in AGAO at pH 7.1 . . . . .	37
2.10	Resonance Raman spectra of WT-HPAO and mutants of HPAO . . . . .	39
2.11	Raman spectra of D319E mutant of HPAO as a function of time of reaction with H <sub>2</sub> <sup>18</sup> O . . . . .	40
2.12	Fraction of C5= <sup>18</sup> O formed as a function of time of incubation of the D319E mutant in H <sub>2</sub> <sup>18</sup> O . . . . .	41
2.13	Effect of D <sub>2</sub> O on Raman spectrum of D319E mutant of HPAO . . . . .	42
2.14	Immobilized water molecules in the active site of HPAO as detected in the crystal structure at 2.4 Å resolution . . . . .	49

3.1	Flipped (nonproductive) intermediates observed during reaction of amine oxidases with methylamine or ammonia . . . . .	54
3.2	Reaction of D319E with methylamine . . . . .	58
3.3	Resonance Raman spectra of the ammonia adduct of D319N . . . . .	59
3.4	Resonance Raman spectra of the methylamine adduct of D319E . . . . .	60
3.5	Resonance Raman spectra of methylamine adducts . . . . .	63
4.1	Electronic absorption spectra of cystathionine $\beta$ -synthase in oxidized, reduced, and reduced + CO forms . . . . .	71
4.2	High-frequency Raman spectra of nonlabeled ferric cystathionine $\beta$ -synthase and non-labeled ferrous cystathionine $\beta$ -synthase . . . . .	73
4.3	Low-frequency Raman spectra of unlabeled ferric cystathionine $\beta$ - synthase and global $^{34}\text{S}$ -labeled ferric cystathionine $\beta$ -synthase. . . . .	74
4.4	Resonance Raman spectra of unlabeled ferric and ferrous CBS after treatment with $\text{HgCl}_2$ . . . . .	77
4.5	Resonance Raman spectrum of the CO adduct of ferrous cystathionine $\beta$ -synthase . . . . .	79
5.1	Plot of observed (Fe-CO) versus (C-O) frequencies for six-coordinate CO adducts of ferrous hemoproteins . . . . .	93

## **LIST OF SCHEMES**

1.1	Proposed biogenesis mechanism of TPQ . . . . .	8
1.2	Proposed mechanism for the oxidative deamination of a primary amine . .	10
1.3	Proposed mechanism for cystathionine formation . . . . .	14

## ABSTRACT

**Characterization of the TPQ Cofactor in Amine Oxidases and the Heme Cofactor  
in Cystathionine Beta-Synthase by Resonance Raman Spectroscopy.  
Implications for Catalytic Properties.**

Edward L. Green, B.S.

Ph.D., OGI School of Science & Engineering

October 2001

Thesis Advisor: Dr. Joann Sanders-Loehr

The copper-containing amine oxidases contain the organic cofactor, 2,4,5-trihydroxyphenylalanine (TPQ), whose C5=O participates in the oxidative deamination of primary amines. Differing rates of solvent exchange for the C5=O and C3-H of the TPQ cofactor have been observed by resonance Raman (RR) spectroscopy in different amine oxidases. Rapid C5=O exchange and slow or non-observable C3-H exchange lead to the prediction of a productive TPQ orientation for the amine oxidases from *Hansenula polymorpha* (HPAO), *Arthrobacter globiformis* (AGAO), pea seedling (PSAO) at pH 7.1, and the E406Q-HPAO mutant. In contrast, slow C5=O exchange and fast C3-H exchange leads to the prediction of a flipped TPQ orientation for PSAO at low pH, and the D319E-HPAO and D319N-HPAO mutants. Finally, for the amine oxidase from *Escherichia coli* (ECAO) and the N404A-HPAO mutant, a mobile cofactor is predicted.

RR spectroscopy has also been used to identify the dead-end complexes formed during catalytic turnover with HPAO mutants. Thus, the flanking-residue mutant, N404A, reacts with methylamine to form a deprotonated product Schiff base. The catalytic-base mutants, D319E and D319N, form a deprotonated iminoquinone species

with methylamine and ammonium chloride, respectively. The deprotonated state of these intermediates is indicative of a flipped cofactor orientation (with C5 directed away from the substrate-binding pocket), thereby explaining their dead-end character.

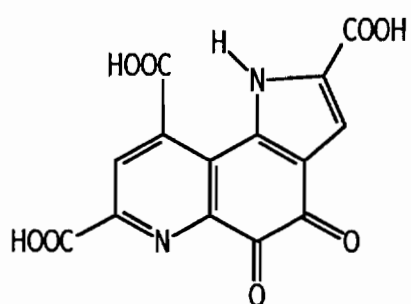
RR spectroscopy of the heme cofactor in cystathionine  $\beta$ -synthase has enabled us to identify the heme axial ligands as His and Cys in both the ferrous and ferric states. The Cys ligand was elucidated through global  $^{34}\text{S}$  substitution and the identification of the Fe-S(Cys) stretch at  $312\text{ cm}^{-1}$  ( $-3\text{ cm}^{-1}$  in  $^{34}\text{S}$ ). The His ligand was verified through examination of the ferrous-CO complex where the  $\nu(\text{Fe-CO})$  and  $\nu(\text{CO})$  frequencies at  $497$  and  $1961\text{ cm}^{-1}$ , respectively, correlate with a neutral His acting as the sixth ligand. Additionally, we found that the substrate homocysteine does not covalently bind to the heme, suggesting that the heme may be playing a regulatory role.

# CHAPTER 1

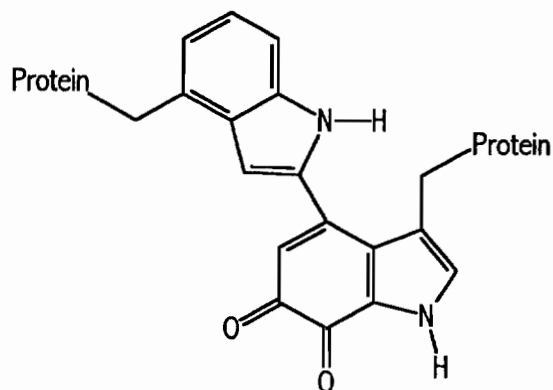
## CHARACTERIZATION OF THE TPQ COFACTOR IN AMINE OXIDASES AND THE HEME COFACTOR IN CYSTATHIONINE B-SYNTHASE BY RESONANCE RAMAN SPECTROSCOPY. IMPLICATIONS FOR CATALYTIC PROPERTIES

### 1.1 Introduction

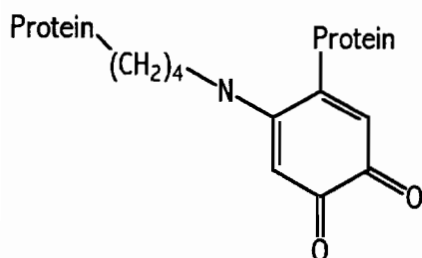
High temperature, high pressure, or very reactive reagents are not available to an organism, so enzymes and coenzymes have evolved to assist in catalyzing essential chemical reactions needed for life. An enzyme catalyzes nearly every reaction that occurs inside an organism, and many enzymes contain organic components (called cofactors) in addition to the protein itself to increase their functionality and capabilities beyond what the polypeptide and the amino acid side chains can perform. One group of organic cofactors includes the quinone cofactors (Fig. 1.1). There are four major quinone cofactors: pyrroloquinolinequinone, a dissociable cofactor discovered in methanotrophic bacteria [McIntire, 1994; Anthony, 1996], tryptophan tryptophylquinone (TTQ) found in methylamine dehydrogenase, lysine tyrosylquinone (LTQ) found in the enzyme lysyl oxidase, and topaquinone (TPQ) found in copper-containing amine oxidases. The amine oxidases are ubiquitous to all living organisms, such as bovine serum amine oxidase, *Escherichia coli* amine oxidase, pea seedling amine oxidase, and amine oxidase in the yeast organism *Hansenula polymorpha* (HPAO). It is interesting to note that the quinone cofactors TTQ, LTQ, and TPQ are all synthesized through a self-processing mechanism in their respective enzyme systems [McIntire et al., 1991; Cai and Klinman, 1994a,b; Matsuzaki et al., 1994; Wang et al., 1996]. Another organic prosthetic group, protoporphyrin IX, binds an iron atom to form the heme cofactor (Fig. 1.2). Heme cofactors have found



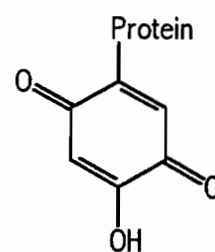
1) pyrroloquinolinequinone, PQQ



2) tryptophan tryptophylquinone, TTQ



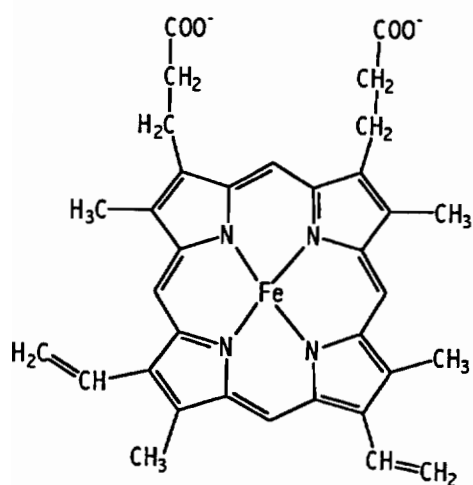
3) lysine tyrosylquinone, LTQ



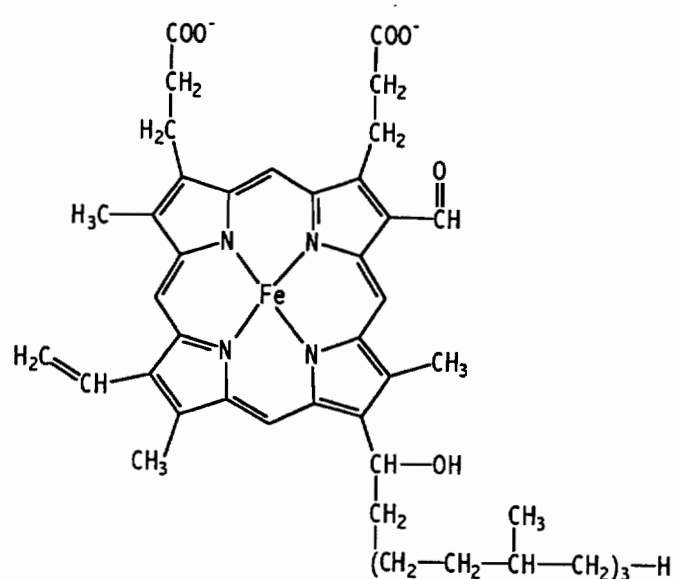
4) topaquinone, TPQ

**Fig. 1.1** Structure diagrams of the four major quinone cofactors.

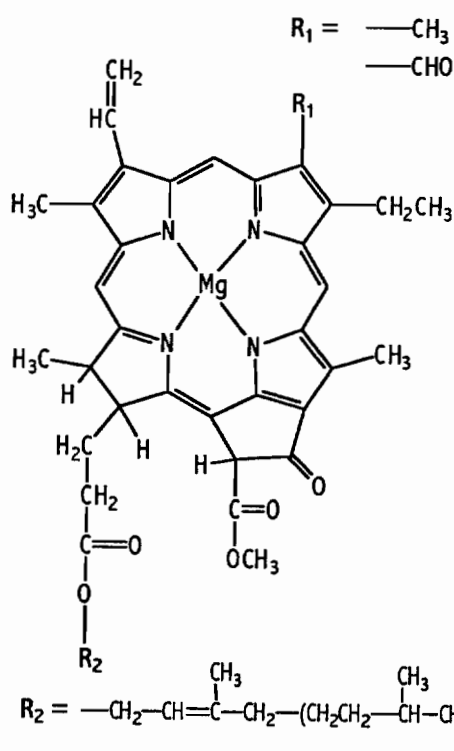




1) Heme (Fe-protoporphyrin IX)



2) Heme A



3) Chlorophyll

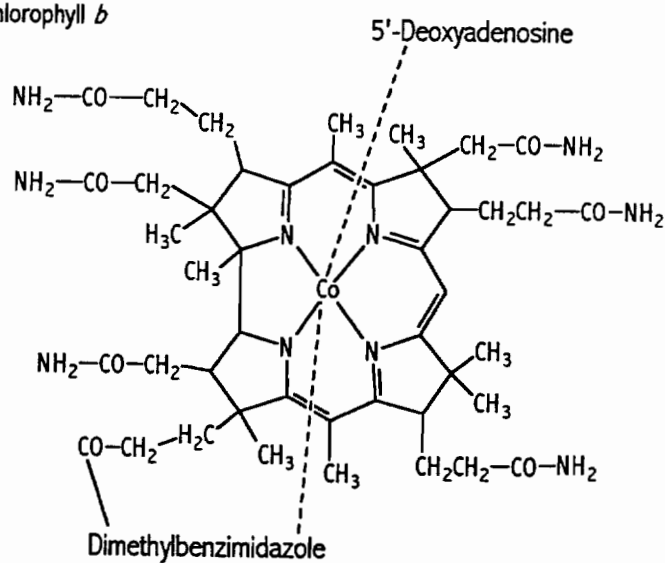
4) Coenzyme B<sub>12</sub>

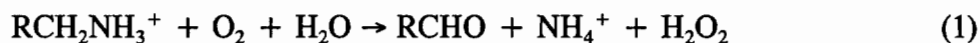
Fig. 1.2 Structural representations of different porphyrin-containing cofactors.

many important uses in enzyme systems ranging from O<sub>2</sub> transport in proteins (such as hemoglobin and myoglobin), to O<sub>2</sub> activation in cytochrome P-450, to single-electron transfer performed by enzymes like cytochrome *c*, and finally functioning as a regulator of protein activity through binding of the small molecules CO and NO as seen in soluble guanylate cyclase, the transcriptional activator CooA, and implicated in cystathionine  $\beta$ -synthase as well as microbial cytochromes *c'* [Shelver et al., 1997; Fan et al., 1998; Vogel et al., 1999a; Lawson et al., 2000; Andrew et al., 2001; Taoka and Banerjee, 2001]. Furthermore, the porphyrinic prosthetic group is essential for photosynthesis through the formation of chlorophyll, where magnesium is bound to the tetrapyrrole ring instead of iron, and vitamin B-12 (cobalamin), which contains cobalt.

Resonance Raman (RR) spectroscopy is a powerful tool for studying the active sites of metalloproteins [Spiro and Li, 1988]. In this thesis, this vibrational technique was used to study the heme cofactor in cystathionine  $\beta$ -synthase (CBS) as well as the quinone cofactor in wild-type and mutant forms of the copper-containing HPAO.

## 1.2 Overview of Copper-Containing Amine Oxidases

Copper-containing amine oxidases (CAO, EC 1.4.3.6) are ubiquitous quinoenzymes (occurring in both prokaryotes and eukaryotes) that catalyze the two-electron oxidative deamination of primary amines by molecular oxygen, producing ammonia, the corresponding aldehyde, and hydrogen peroxide (equation 1) [McIntire et al., 1991; Klinman and Mu, 1994; Knowles and Dooley, 1994].



These enzymes are widely distributed in nature, being found in plants, microorganisms, and animals [Klinman and Mu, 1994; Knowles and Dooley, 1994; Tipping and McPherson, 1995].

### 1.2.1 Active Site Structure

The crystal structures for HPAO [Li et al., 1998], *E. coli* amine oxidase [Parsons et al., 1995], pea seedling amine oxidase [Kumar et al., 1996], and the amine oxidase from *Arthrobacter globiformis* [Wilce et al., 1997] show these enzymes existing as homodimers, each subunit ( $M_r \cong 70\text{--}95$  kDa) containing one tightly bound copper ion and one 2,4,5-trihydroxyphenylalanine (TOPA or TPQ) which arises from a post-translational modification of a specific tyrosine residue within the protein. TPQ has been shown to be the redox cofactor in all CAOs studied to date [Janes et al., 1990; Anthony, 1996; Holt et al., 1998] (Fig. 1.3). Formation of the TPQ cofactor is autocatalytic in the presence of molecular oxygen and the bound copper atom; no additional enzymes or cofactors are necessary for the transformation of protein-bound tyrosine to TPQ [Cai and Klinman, 1994b; Matsuzaki et al., 1994]. In addition to containing TPQ, all known CAOs have the consensus site sequence Asn-Tyr\*-Asp/Glu-Tyr/Asn [Janes et al., 1992]. The copper ion is bound in a square pyramidal geometry and is coordinated by three His side chains and two water molecules,  $W_e$  and  $W_a$  (Fig. 1.3). One of the water ligands, designated  $W_a$ , is further hydrogen bonded to position O2 of TPQ [Li et al., 1998]. An Asp residue located on the opposite side of the TPQ cofactor from the copper atom has been identified as the catalytic base [Wilmot et al., 1997; Li et al., 1998].

### 1.2.2 Biogenesis Mechanism of TPQ

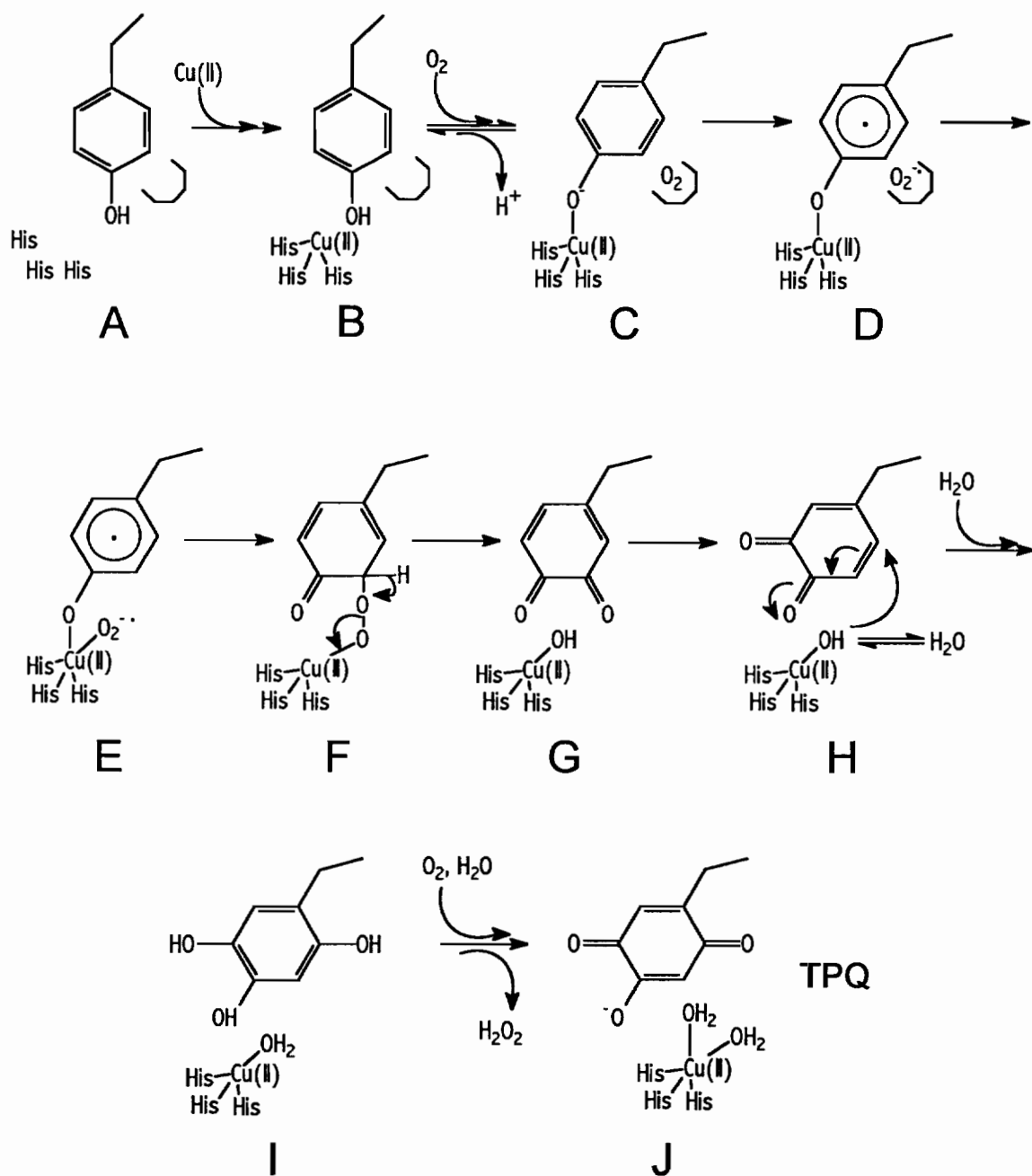
Apo-CAOs are devoid of bound copper and thus contain no TPQ cofactor. The transformation of the precursor tyrosine to TPQ is a six-electron process requiring two molecules of  $O_2$ . The actual mechanism for TPQ biogenesis is still excitedly debated. An initial detailed mechanism was postulated, based largely on inferences drawn from the crystallographic studies and chemical intuition. More recently, spectroscopic techniques have aided in the support and refining of this proposed mechanism. An informative RR experiment identified the origin of the C2 oxygen as coming from solvent [Nakamura et al., 1996]. Recent data indicate that this hydrolysis reaction does not occur readily in simple model compounds and indicates that the active site copper most likely mediates water addition at the C2

Originally published as Figure 6 in:

Used with permission of Elsevier Science and F. Scott Mathews.

position through its proximity to the cofactor or to stereoelectronic features not present in the solution model chemistry [Mandal et al., 2000]. The origin of the C5 oxygen still remains unclear, due to its rapid exchange with solvent, but is believed to be derived from molecular oxygen. To date, the previously proposed  $\text{Cu}^{\text{I}}\text{-Tyr}^\bullet$  species has never been detected by EPR or any other spectroscopic technique under turnover conditions. Recent kinetic data identify a specific oxygen-binding site near the precursor tyrosine, displacing the tyrosine onto the copper atom, and the overall rate-limiting step is concluded to be the electron-transfer reaction between  $\text{O}_2$  and the copper-liganded precursor tyrosine [Schwartz et al., 2000]. A  $\text{Tyr} \rightarrow \text{Cu}^{\text{II}}$  LMCT band has been identified supporting the proposed mechanism in which the active site copper first activates the precursor tyrosine, rather than  $\text{O}_2$  as was initially proposed [Dove et al., 2000]. A recent crystal structure study of zinc-substituted CAO from *H. polymorpha* clearly shows the precursor tyrosine bound to the Zn metal, thus providing the closest analogue to date of an intermediate in TPQ production [Chen et al., 2000].

Scheme 1.1 outlines the newly proposed biogenesis mechanism [Dove et al., 2000].  $\text{Cu}^{\text{II}}$  binds rapidly to apo-enzyme. Copper is liganded by three His residues and two water molecules in a square planar geometry (A,B). Molecular oxygen then binds in a hydrophobic pocket near the precursor tyrosine, displacing it onto the  $\text{Cu}^{\text{II}}$  ion to form the  $\text{Tyr-Cu}^{\text{II}}$  CT species (C), which greatly activates the tyrosine. The activated tyrosine reacts with  $\text{O}_2$  to form tyrosyl radical and superoxide (D), which binds to  $\text{Cu(II)}$  (E) and attacks the tyrosine ring at the C5 position (F). The peroxo intermediate (F) is converted to dihydroxyphenylalanine quinone (G) by homolytic cleavage of the peroxide. Then the cofactor flips to allow access to the C2 position for hydrolytic attack (H). RR evidence firmly supports the origin of the C2 oxygen from solvent [Nakamura et al., 1996]. One final ring oxidation by  $\text{O}_2$  occurs to form active TPQ and hydrogen peroxide (J). Biogenesis of TPQ still occurs in mutants lacking the catalytic base, but not in protein lacking  $\text{Cu(II)}$ .



**Scheme 1.1** Proposed biogenesis mechanism of TPQ [adapted from Dove et al., 2000].

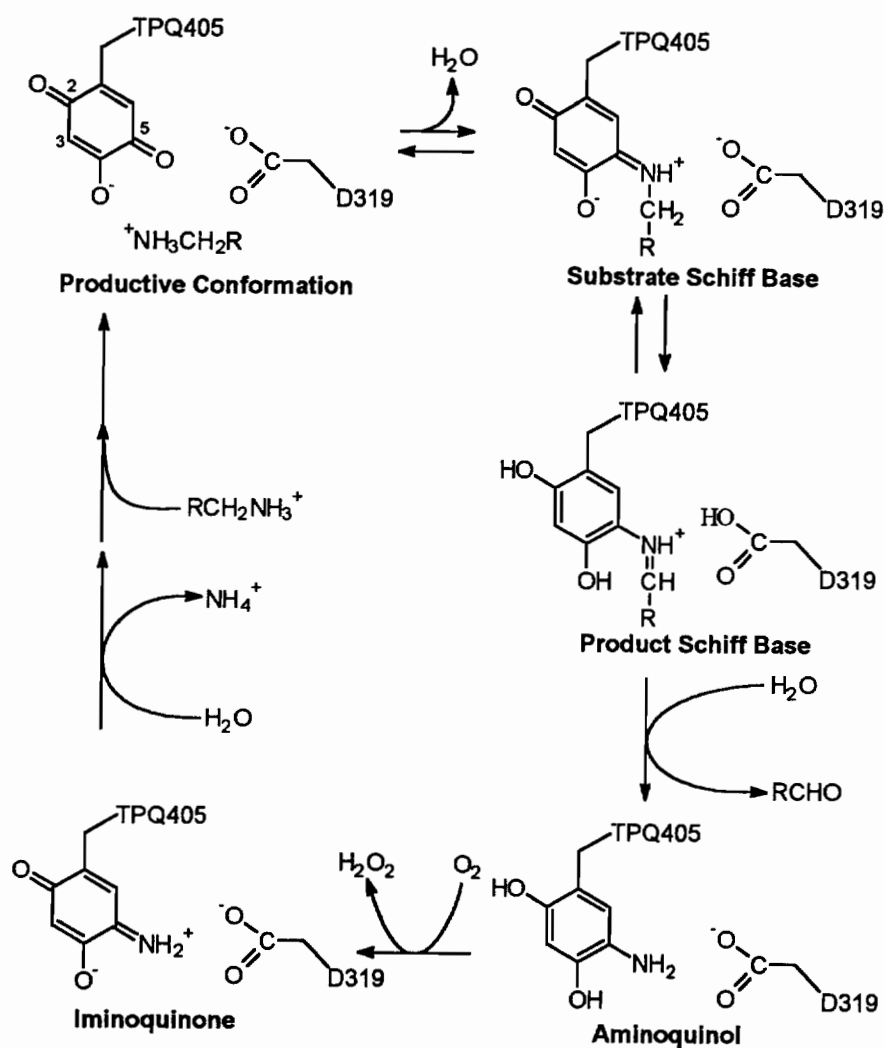
### 1.2.3 Catalytic Mechanism

CAOs catalyze the oxidation of various primary amine substrates to their corresponding aldehydes, with the subsequent release of ammonia and hydrogen peroxide (equation 1). Substrate preference depends on the enzyme source. The proposed catalytic mechanism can be represented by two half-reactions: a reductive half-reaction, leading to reduced enzyme and product aldehyde, and an oxidative half-reaction, in which molecular oxygen is required to reoxidize the enzyme, with production of ammonia and hydrogen peroxide [Klinman and Mu, 1994].

Scheme 1.2 outlines the proposed catalytic mechanism for the turnover of substrate in CAOs [Plastino et al., 1999]. The TPQ cofactor is oriented in a productive conformation, C5=O directed toward the substrate channel and the catalytic base, upon introduction of amine substrate. Substrate reacts at the C5 position, displacing the bound oxygen to produce a substrate Schiff base complex. The active site base then abstracts a proton from the  $\alpha$ -carbon to form a product Schiff base complex. Hydrolysis at the  $\alpha$ -carbon releases the product aldehyde leaving the aminoquinol form of the cofactor. Molecular oxygen oxidizes the aminoquinol to iminoquinone. Hydrolysis of the iminoquinone complex regenerates the active TPQ cofactor.

## 1.3 Overview of Cystathionine $\beta$ -Synthase

Cystathionine  $\beta$ -synthase (CBS, EC 4.2.1.22) is a unique enzyme that requires the cofactors heme and pyridoxal phosphate (PLP) to catalyze the first step in the catabolic removal of homocysteine. The reaction involves the condensation of homocysteine and serine to generate cystathionine. Medicinal importance has been placed upon this enzyme, since it represents one of two major metabolic avenues for the removal of homocysteine in mammalian systems. Homocysteine is a toxic metabolite, formed by the breakdown of S-adenosylhomocysteine, and its elevated levels are correlated with cardiovascular diseases [Refsum et al., 1998], neural tube defects [Mills et al., 1995], and Alzheimer's disease [Clarke et al., 1998]. Catastrophic mutations in CBS result in severe homocystinuria, an inborn error of



**Scheme 1.2** Proposed mechanism for the oxidative deamination of a primary amine [adapted from Plastino et al., 1999].



metabolism that results in very high levels of circulating homocysteine with attendant cardiovascular complications [Mudd et al., 1995].

### 1.3.1 Active Site Structure

To date, no crystal structure has been published for this enzyme. CBS is a tetramer of identical subunits ( $M_r \cong 63$  kDa in human CBS) and is allosterically regulated by S-adenosylmethionine (AdoMet) [Taoka et al., 1998]. Two heme cofactors and four PLP cofactors are bound per tetramer (Fig. 1.4) [Taoka et al., 1998, 1999a]. Purification of the wild-type enzyme from mammalian liver has resulted in the isolation of mixtures of full-length tetrameric enzyme as well as a truncated, but active, dimeric form [Kraus et al., 1978; Kraus and Rosenberg, 1983; Skovby et al., 1984]. The dimeric form is not regulated by AdoMet and binds two hemes and two PLP cofactors per dimer (Fig. 1.4) [Taoka et al., 1999b]. While the  $\beta$ -replacement reaction catalyzed by CBS suggests a role for the PLP cofactor, the role of the heme remains uncertain. No redox reaction is apparent. The sequences of the human, rat, and yeast CBS reveal that they are quite similar. However, the yeast enzyme is devoid of heme [Jhee et al., 2000], suggesting that the heme cofactor is a relatively recent acquisition, and argues against an essential catalytic role for this cofactor. Nonetheless, the activity of human CBS is modulated by oxidation [Taoka et al., 1998], ligation [Taoka et al., 1999b], and coordination [Taoka et al., 2001] state changes in the heme, suggesting a possible regulatory role for the heme cofactor. The heme axial ligands are histidine and cysteine in both the ferric and ferrous states [Taoka et al., 1999a; Ojha et al., 2000; Green et al., 2001]. In the oxidized enzyme, the heme is low-spin six-coordinate and has a Soret peak centered at 428 nm [Taoka et al., 1998]. Reduction of the heme by dithionite results in a large red shift of the Soret peak to 450 nm, consistent with retention of the thiolate ligand in the six-coordinate heme [Dawson and Sono, 1987].

### 1.3.2 Catalytic Mechanism

Substitution of the hydroxyl group of serine with the thiol of homocysteine is a  $\beta$ -replacement reaction catalyzed by CBS. Enzymatic reactions involving either  $\beta$ -

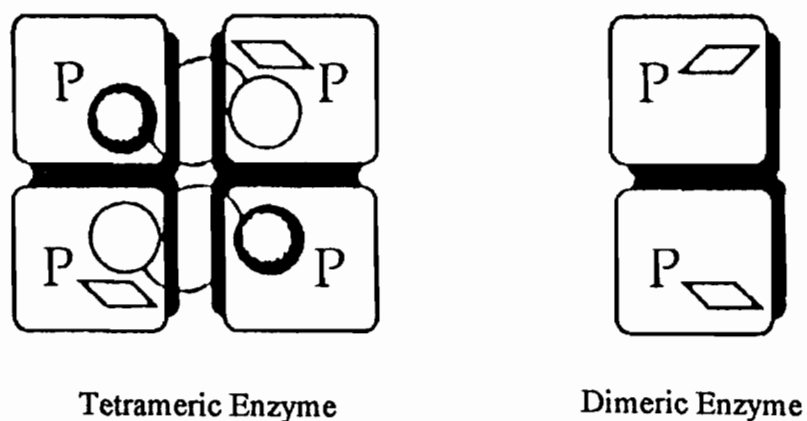


**Fig. 1.4** Postulated organization of the tetrameric and truncated dimer forms of cystathionine  $\beta$ -synthase (CBS). P = pyridoxal phosphate; diamond = heme; circle = AdoMet regulatory site.

Originally published as Scheme 3 in:

Taoka, S., Widjaja, L., and Banerjee, R. (1999b) Assignment of enzymatic functions to specific regions of the PLP-dependent heme protein cystathionine  $\beta$ -synthase. *Biochemistry* 38, 13155–13161.

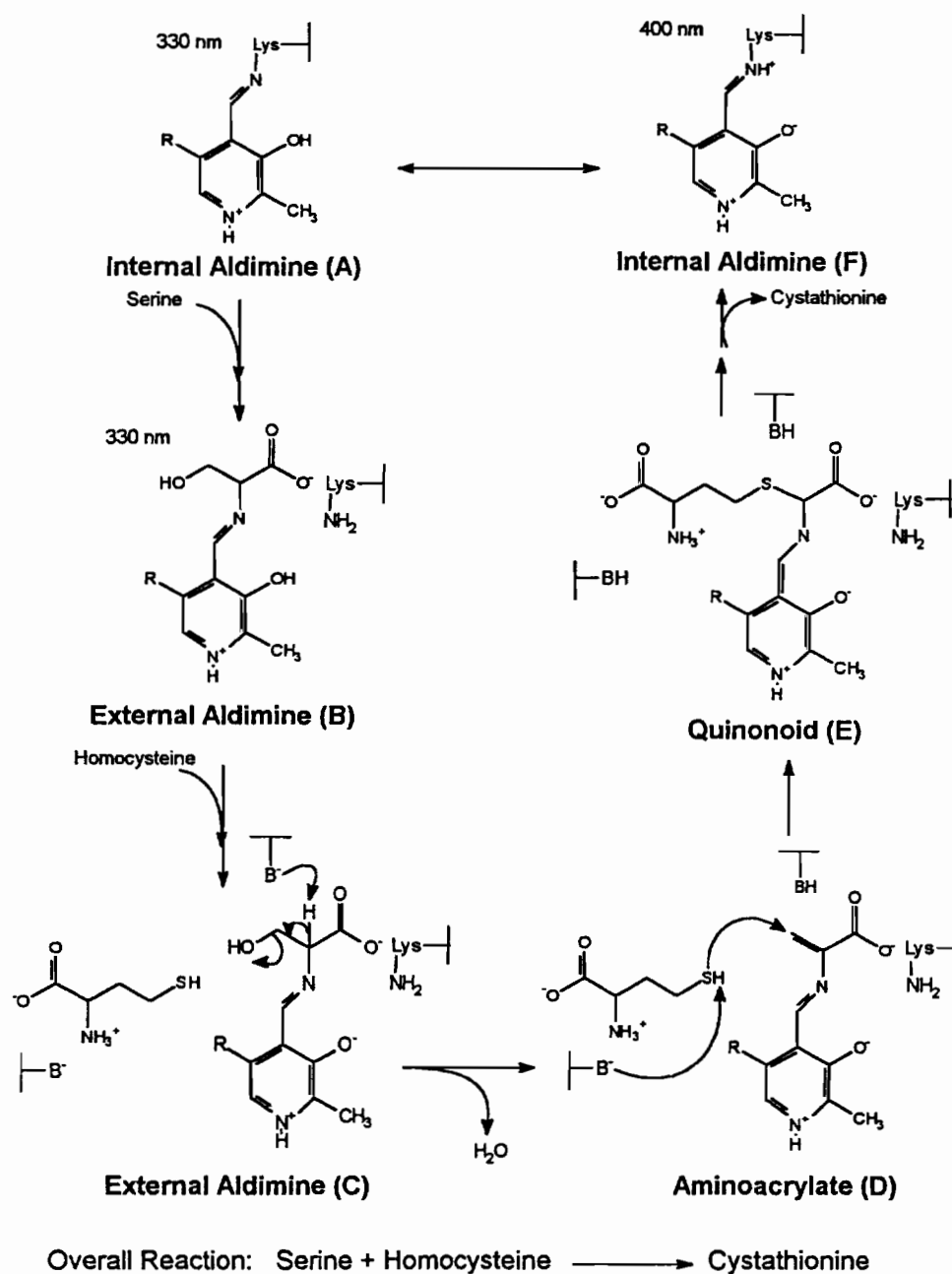
Used with permission of the American Chemical Society.

replacement or  $\beta$ -elimination are characteristically PLP-dependent and generally believed to share a common mechanism. For CBS, it is predicted that an external aldimine is formed between serine and PLP [Borcsok and Abeles, 1982]. The elimination and replacement reactions confer overall retention of configuration at the  $\beta$ -carbon of cystathionine [Borcsok and Abeles, 1982]. This mechanism does not include an obvious role for the heme, and its true function is presently unknown.

Scheme 1.3 outlines a proposed catalytic mechanism for the  $\beta$ -replacement condensation reaction of homocysteine and serine [Taoka et al., 1999a]. The pyridoxal phosphate cofactor forms a Schiff base complex with a protein-derived lysine residue termed an internal aldimine (A). Serine then binds to the protein near the PLP cofactor, displacing the lysine, and forming a Schiff base complex with the PLP cofactor, termed an external aldimine (B). Homocysteine binds to the enzyme and is oriented in such a way as to facilitate a  $\beta$ -replacement reaction with the serine bound to the PLP cofactor (C). Initially it was thought that homocysteine was activated by the heme cofactor, since homocysteine has been shown to bind near the heme [Taoka et al., 1999a], but there is no evidence for homocysteine ligation to the heme [Green et al., 2001]. More likely, an amino acid residue in the active site is acting as a catalytic base to activate the homocysteine for nucleophilic attack at the  $\beta$ -carbon of the aminoacrylate complex (D) to form a quinonoid complex (E). Then the protein-derived lysine residue attacks the quinonoid complex to release cystathionine and reform the internal aldimine complex (F).

#### 1.4 Focus of Present Research

In this thesis, RR spectroscopy was used to study several wild-type and mutant CAOs, including HPAO and active site base mutants of HPAO. Our goals were to obtain structural information about the TPQ active site and to characterize catalytic intermediates in the case of CAOs. In Chapter 2, the use of RR spectroscopy to predict the TPQ conformation in the resting form of the copper-containing amine oxidase enzymes is described. It is shown that the orientation of the TPQ cofactor within the active site is directly correlated to the rates at which the C5 oxygen and the



**Scheme 1.3** Proposed mechanism for cystathionine formation.

Originally published as Fig. 1 in:

Taoka, S., West, M., and Banerjee, R. (1999a) Characterization of the heme and pyridoxal phosphate cofactors of human cystathionine  $\beta$ -synthase reveals nonequivalent active sites. *Biochemistry* **38**, 2738–2744.

Used with permission of the American Chemical Society.

C3 hydrogen exchange with solvent. Fast C5=O exchange coupled with slow C3-H exchange is indicative of the cofactor being stabilized in a productive orientation (Scheme 1.2), whereas slow C5=O coupled with fast C3-H exchange indicates that the TPQ cofactor is in a flipped orientation with the C3-H side of the TPQ ring near the catalytic base. Thus, RR spectroscopy can be used to determine the orientation of the chromophoric TPQ cofactor in the resting form of the copper-amine oxidase enzymes.

Chapter 3 demonstrates that RR spectroscopy is a powerful tool in substantiating the proposed catalytic mechanism for CAOs. Through mutagenesis of specific residues in and near the active site, catalytic intermediates along the reaction pathway build up and can consequently be analyzed using RR spectroscopy. A substrate Schiff base, a product Schiff base, and a deprotonated iminoquinone have all been isolated and characterized by RR spectroscopy.

For the heme-containing enzyme CBS, our goal was to determine the identity of the heme axial ligands, the coordination number and spin state of the cofactor, and whether the substrate homocysteine binds directly to the heme cofactor. As described in Chapter 4, RR spectroscopy was utilized to fully characterize the heme cofactor in CBS. The heme axial ligands were verified to be histidine and cysteine. Furthermore, this study presents the first identification of an Fe-S(Cys) stretching vibration (at  $312\text{ cm}^{-1}$ ) in a six-coordinate, low-spin ferric heme. The His ligand was confirmed through formation of a heme-CO adduct whose Fe-CO vibrational frequency correlated to a histidine-heme-CO complex in a hydrophobic environment. Additionally, homocysteine was shown not to bind directly to the heme cofactor. Finally, addition of thiol-chelators, such as  $\text{HgCl}_2$ , to the ferric heme causes conversion of the 6cLS to a 5cHS heme with loss of the Cys ligand.

Chapter 5 presents conclusions on the significance of the findings in this thesis and directions for future research.

## CHAPTER 2

### RATES OF OXYGEN AND HYDROGEN EXCHANGE AS INDICATORS OF TPQ COFACTOR ORIENTATION IN AMINE OXIDASES<sup>1</sup>

#### 2.1 Introduction

Copper amine oxidases, found in bacteria, fungi, plants, and mammals [McIntire and Hartman, 1993], catalyze the oxidative deamination of a primary amine to its corresponding aldehyde and ammonia, with concomitant reduction of molecular oxygen to hydrogen peroxide. These enzymes allow prokaryotes to use primary amines as a carbon and nitrogen source. The actual function in eukaryotes is unclear, but they are believed to be involved in cell signaling, growth and development, and cell death. A recent study has speculated that in humans, the semicarbazide-sensitive amine oxidase may be linked to carcinogenesis due to the reactive aldehydes and hydrogen peroxides produced by this endogenous enzyme [Ekblom et al., 1999]. Most copper-containing amine oxidases possess the same self-processing organic cofactor, 2,4,5-trihydroxyphenylalanine quinone (TPQ) [Janes et al., 1990; Cai and Klinman, 1994b; Matsuzaki et al., 1994; Choi et al., 1995]. Formation of the TPQ cofactor by the post-translational modification of a tyrosine residue within the active site consensus sequence T-X-X-N-Y\*-D/E involves self-processing events requiring only copper and molecular oxygen [Cai and Klinman, 1994b; Matsuzaki et al., 1994; Ruggiero et al., 1997].

X-ray crystal structures are now available for the copper-containing amine oxidases from yeast, *Hansenula polymorpha* (HPAO) [Li et al., 1998], *Escherichia*

---

<sup>1</sup> This work was performed in collaboration with Dr. Nobu Nakamura at the Oregon Graduate Institute, Dr. David M. Dooley at Montana State University, and Dr. Judith P. Klinman at University of California, Berkeley.

*coli* (ECAO) [Murray et al., 1999], pea seedling (PSAO) [Kumar et al., 1996], and *Arthrobacter globiformis* (AGAO) [Wilce et al., 1997]. Each of these enzymes is a homodimer with subunit molecular weights of approximately 80 kDa. The structure of each subunit is dominated by  $\beta$ -sheets in a large catalytic domain and two or three smaller peripheral domains. In HPAO, the active site pocket contains a square pyramidal  $\text{Cu}^{\text{II}}$  ion bound by three His residues and two water molecules [Li et al., 1998]. The  $\text{Cu}^{\text{II}}$  ion is located near the C2 carbonyl oxygen of the TPQ organic cofactor. An Asp residue at position 319, believed to be the active site base [Janes, 1990; Wilmot et al., 1997], is located on the opposite side of the TPQ cofactor near the C5 carbonyl oxygen. A detailed mechanism has been proposed based on X-ray crystal structures [Kumar et al., 1996; Wilce et al., 1997; Li et al., 1998; Murray et al., 1999] and model studies [Mure and Klinman, 1995a,b] (Fig. 2.1). Substrate oxidation is initiated by covalent addition of amine substrate to the C5 position of the cofactor. After proton abstraction from the substrate Schiff base complex by the catalytic base, the product imine is hydrolyzed to release product aldehyde. Oxidation of aminoquinol cofactor by  $\text{O}_2$  produces the iminoquinone, which is hydrolyzed to release product ammonia.

A wealth of data suggests that the TPQ ring is mobile and can adopt various positions and orientations within the active site, leading to differences in enzyme activity. For example, the crystal structure of the quinone form of HPAO shows the TPQ cofactor in what appears to be a productive conformation, with its C2 carbonyl oxygen directed towards the Cu via a H-bond to a water ligand and the C5 carbonyl oxygen pointed towards the Asp 319 and the substrate-binding pocket [Li et al., 1998]. A bridging water molecule is believed to form hydrogen bonds between the C5 carbonyl oxygen and the catalytic base. In contrast, the PSAO structure at pH 4.6 reveals that the TPQ cofactor rests in a nonproductive (flipped) conformation (Fig. 2.1), with the C5 carbonyl oxygen directed towards the Cu and away from the active site base [Kumar et al., 1996]. Furthermore, mutation of Glu 406, which flanks the cofactor toward the C-terminus, to Asn leads to the accumulation of the product Schiff base intermediate when methylamine is the substrate [Cai et al., 1997]. This phenomenon is attributed to a rotation of the cofactor-product imine complex to a

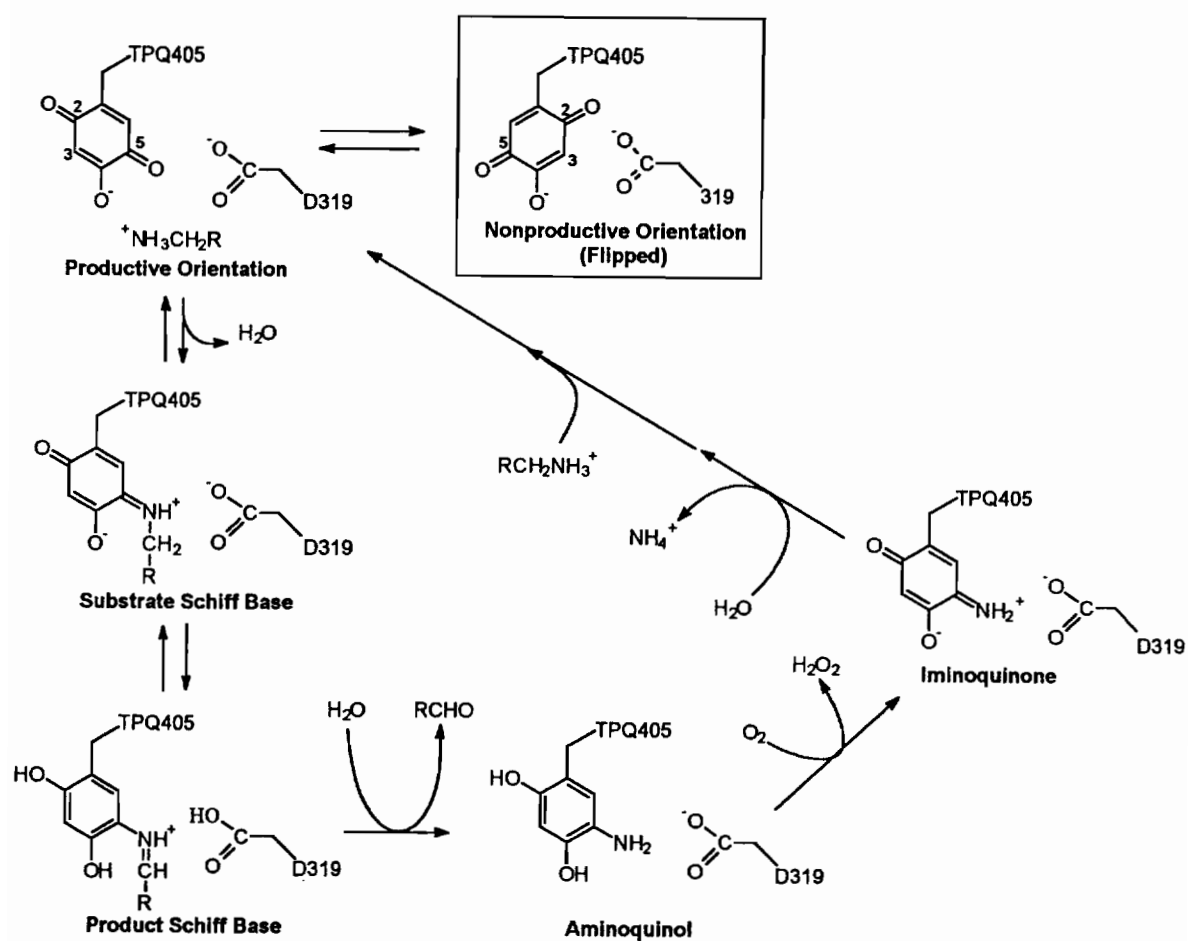


**Fig. 2.1** Proposed reaction cycle for amine oxidation in HPAO [adapted from Plastino et al., 1999].



nonproductive conformation that is incompetent toward hydrolysis. A similar inactivation with methylamine substrate occurs upon mutation of Asn 404, which flanks the cofactor toward the N-terminus, to Ala [Schwartz et al., 1998]. Again, this phenomenon of inactivation is believed to arise from cofactor flipping during turnover, thus shielding the product Schiff base from hydrolysis. Finally, it is also likely that rotation of the TPQ ring occurs during biogenesis of the cofactor [Wilce et al., 1997].

Can we predict the orientation of the TPQ cofactor in the resting form of the enzyme? In previous studies of ECAO and AGAO, we showed that the oxygen at the C5 position and the hydrogen at the C3 position of the TPQ cofactor are capable of exchanging with solvent water [Moënné-Loccoz et al., 1995; Nakamura et al., 1996]. Insertion of heavier isotopes ( $^{18}\text{O}$  or D) causes C=O and C-H vibrational modes to shift to lower energy, thereby affording us the possibility of using resonance Raman (RR) spectroscopy to measure the rates of exchange. Since the substrate-binding channel is likely to be most accessible to solvent, we propose that the TPQ C5 carbonyl oxygen and C3 hydrogen should show different rates of exchange, depending on which edge of the TPQ ring is facing the D319 catalytic base. If the cofactor is in a productive conformation (Fig. 2.1), then the C5 carbonyl exchange rate should be fast and the C3 hydrogen exchange rate should be slow. If the cofactor is in a nonproductive conformation, then the C5 carbonyl exchange rate should be slow and the C3 hydrogen exchange rate should be fast. Finally, fast exchange of both the C5 carbonyl and C3 hydrogen would suggest a dynamic state, with the TPQ ring rapidly flipping between both conformations, corresponding to a disordered TPQ ring in the X-ray crystal structure [Wilmot et al., 1997].

Our present studies of the wild-type forms of HPAO, PSAO, ECAO, and AGAO reveal a strong correlation between the observed rates of C5=O and C3-H exchange and those expected, based on cofactor orientation in crystal structures. We have also analyzed oxygen and hydrogen exchange rates in several mutants of HPAO with altered enzymatic activities: two catalytic-base mutants, D319N and D319E, and two mutants of the residues flanking the TPQ cofactor, N404A and E406Q. Both of the catalytic base mutants generate TPQ, but D319N does not turn over substrates and

D319E turns over substrates at a rate 100-fold slower than in wild-type [Plastino et al., 1999]. For the other two mutants, both E406Q and N404A generate active TPQ cofactors, but the N404A mutant turns over substrate 1000-fold slower than wild-type HPAO (WT-HPAO) [Schwartz et al., 1998]. In each case, we found that the C5=O and C3-H exchange rates measured using RR spectroscopy correlate with differences in enzyme reactivity and, thus, allow us to predict the orientation of the TPQ cofactor.

## 2.2 Experimental Procedures

### 2.2.1 Protein Preparation

WT-HPAO and the HPAO mutants (D319E, D319N, N404A, and E406Q) were prepared as previously described [Schwartz et al., 1998; Plastino et al., 1999; Dove et al., 2000]. The amine oxidase gene from *H. polymorpha* was inserted and expressed in *Saccharomyces cerevisiae* or *E. coli* (E406Q). WT-HPAO in 50 mM potassium phosphate (pH 7.0) was concentrated 3-fold to 0.36 mM TPQ using a Microcon 30 (Amicon) ultrafiltration device. Solutions of mutant enzymes were similarly concentrated to 0.7–0.8 mM. Wild-type ECAO and AGAO (phenethylamine oxidase) were prepared as ~1 mM protein in 0.05 M KPi (pH 7.1) [Moënné-Loccoz et al., 1995; Nakamura et al., 1996]. Wild-type PSAO was purified as described previously [McGuirl et al., 1994] and prepared in 0.1 M KPi (pH 7.2) or 0.01 M sodium acetate (pH 4.6) at a concentration of 1 mM protein.

### 2.2.2 Resonance Raman Spectroscopy

RR spectra were collected on a McPherson 2061 spectrograph (0.67 m, 1800-groove grating) using a Kaiser Optical holographic supernotch filter and a Princeton Instruments (LN-1100PB) liquid N<sub>2</sub>-cooled CCD detector. The excitation source was a Coherent Innova 90-6 Ar laser. Spectra were collected from samples contained in glass capillary tubes and cooled to ice temperature in a copper cold finger [Loehr and Sanders-Loehr, 1993], using 514.5 nm excitation (100 mW), 90° scattering geometry, 4 cm<sup>-1</sup> spectral resolution, and 10-min accumulations (unless otherwise stated). Peak

frequencies were calibrated relative to an indene standard and are accurate to  $\pm 1 \text{ cm}^{-1}$ . In cases where peaks are overlapped, reported peak frequencies and intensities were based on curve resolution. Spectra of samples substituted with isotopes were obtained under identical instrumental conditions such that frequency shifts are accurate to  $\pm 0.5 \text{ cm}^{-1}$  [Loehr and Sanders-Loehr, 1993].

### 2.2.3 Isotope Exchange in WT-HPAO and Mutants

Owing to protein instability under ambient conditions, exchange experiments and Raman spectroscopy were performed on samples at ice temperature. For studying rapid  $^{18}\text{O}$  exchange in WT-HPAO, 10  $\mu\text{L}$  of concentrated HPAO ( $\sim 1 \text{ mM}$  TPQ) was diluted with an equal amount of 50 mM KPi (pH 7.0) in 93%  $\text{H}_2^{18}\text{O}$  and immediately transferred to a capillary tube. This allowed a RR spectrum to be obtained within 1 min of addition of  $\text{H}_2^{18}\text{O}$  buffer. To obtain more complete  $^{18}\text{O}$  exchange at the C5 carbonyl oxygen, concentrated HPAO (0.35 mM TPQ) was diluted 20-fold with 50 mM KPi in 93%  $\text{H}_2^{18}\text{O}$  (pH 7.0) and then reconstituted in a Microcon 30 for 30–60 min to give a final concentration of 0.35 mM TPQ in  $\sim 89\%$   $\text{H}_2^{18}\text{O}$ .  $\text{D}_2\text{O}$  exchange was accomplished by diluting concentrated WT-HPAO (0.35 mM TPQ) 20-fold in 50 mM KPi in 95%  $\text{D}_2\text{O}$  (pH reading 7.0) and then reconstituting in a Microcon 30 to give a final concentration of 0.35 mM TPQ in  $\sim 90\%$   $\text{D}_2\text{O}$ . Oxygen and hydrogen exchange of the D319E, D319N, N404A, and E406Q mutants of HPAO was performed as for WT-HPAO, leading to a final concentration of  $\sim 0.4 \text{ mM}$  TPQ in  $\sim 89\%$   $\text{H}_2^{18}\text{O}$  or  $\sim 90\%$   $\text{D}_2\text{O}$ .

### 2.2.4 Isotope Incorporation during Biogenesis of HPAO

ApoHPAO (0.32 mM in subunits) was prepared from *H. polymorpha* expressed in *E. coli* grown in the absence of copper [Dove et al., 2000] and transferred into  $\text{H}_2^{18}\text{O}$  by diluting 3.5-fold into 50 mM KPi in 93%  $\text{H}_2^{18}\text{O}$  (pH 7.0) and reconstituting two times. Aerobic addition of  $\text{CuCl}_2$  to apoHPAO, followed by mixing and incubation for 30 min at ice temperature, resulted in the formation of holo-HPAO (0.32 mM in TPQ).

### 2.2.5 Isotope Exchange in ECAO, AGAO, PSAO, and Model Compound

Exchange experiments and Raman spectroscopy were performed at room temperature. Slowly exchanging protein samples (> 1 h) were obtained by 20-fold dilution and ultrafiltration, whereas rapidly exchanging samples (< 2 min) were obtained by 2-fold dilution, as described above for HPAO, in H<sub>2</sub><sup>18</sup>O or D<sub>2</sub>O. The ammonium salt of the model compound, 2-hydroxy-5-*tert*-butyl-1,4-benzoquinone (tBQOH), was synthesized according to previously published procedures [Mure and Klinman, 1995a] and dissolved in 25 mM sodium phosphate (pH 7.1) to yield a 20 mM solution. Deuterium exchange was initiated by a 10-fold dilution in 50 mM sodium phosphate (pH reading 7.1) in D<sub>2</sub>O.

### 2.2.6 Exchange Rate Calculation

For the HPAO mutants, 15-min scans were taken repeatedly during the first 2 h of <sup>18</sup>O exchange and then reduced to one scan/h. After 5 h, one scan was taken every 2–4 h until the exchange reached completion. Total elapsed time was calculated to the midpoint (7 min) of each 15-min scan. Interfering vibrational modes from apoprotein and water were subtracted from each spectrum to isolate the C5 carbonyl stretches [Nakamura et al., 1996]. In each case, peak intensities (heights) were calculated for the C5=<sup>18</sup>O stretch at 1650 cm<sup>-1</sup> and the C5=<sup>16</sup>O stretch at 1680 cm<sup>-1</sup>. The fraction exchanged, *F*, was obtained from the ratio of peak intensities:  $[I_{1650} / (I_{1650} + I_{1680})] / [I_{1650} \text{ at completion} / (I_{1650} + I_{1680} \text{ at completion})]$ . The rate of <sup>18</sup>O exchange was obtained by fitting the plot of *F* versus time after <sup>18</sup>O addition to the equation  $F = ae^{-kt}$ , where *a* is a constant, and *k* is the rate constant. This equation is a version of the integrated rate law,  $[A] = [A]_0 e^{-kt}$ . The exchange reaction half-life was calculated using the formula  $t_{1/2} = (\ln 2)/k$ , assuming a first-order reaction. A similar treatment was used for the D- or <sup>18</sup>O-sensitive peaks in the RR spectra of the wild-type amine oxidases.

## 2.3 Results and Discussion

### 2.3.1 Oxygen Exchange in WT-HPAO and ECAO

Excitation of WT-HPAO within its 480-nm absorption band produces a RR spectrum characteristic of the TPQ chromophore (Fig. 2.2B). The large number of vibrational modes between 1200 and 1700  $\text{cm}^{-1}$  are due to a combination of C=C, C-C, and C=O stretching and C-H bending modes of the TPQ cofactor. A similar RR spectral pattern is observed for other copper amine oxidases, including ECAO, PSAO, and AGAO, as well as a TPQ model compound (Fig. 2.2). All of the protein spectra have their most intense vibrational feature near 1400  $\text{cm}^{-1}$ , in addition to other significant features near 1340, 1375, 1580, 1635, and 1680  $\text{cm}^{-1}$ . Upon incubation in  $\text{H}_2^{18}\text{O}$ , the peaks at 1681, 1683, and 1666  $\text{cm}^{-1}$  in ECAO, AGAO, and the tBQO<sup>-</sup> model, respectively, downshift by  $\sim 25 \text{ cm}^{-1}$ , leading to their assignment as the C5=O stretch [Moënne-Loccoz et al., 1995; Nakamura et al., 1996]. The similarity of the RR frequencies and intensities among the amine oxidases suggests that a similar electronic structure and resonance stabilization is common to all of their TPQ moieties. Since this electronic structure is not significantly perturbed by the different TPQ orientations seen in the crystal structures, it seems likely that the marked differences in exchange rates between the C5=O and C3-H (presented below) are mainly a reflection of solvent accessibility.

The C5=O stretching mode in the RR spectra of amine oxidases is obscured by intense protein (amide I) vibrational modes in this region (Fig. 2.2). Subtraction of the Raman spectrum of apo-HPAO, obtained from Cu-deficient organisms prior to TPQ formation [Dove et al., 2000], yields improved definition of the C5=O stretch at 1677  $\text{cm}^{-1}$  in WT-HPAO (Fig. 2.3A). A clear identification of this vibration is obtained by observing its downshift to 1649  $\text{cm}^{-1}$  upon incubation in  $\text{H}_2^{18}\text{O}$  (Fig. 2.3B). The magnitude of the shift ( $-28 \text{ cm}^{-1}$ ) indicates that only one oxygen atom in the TPQ ring has been replaced by  $^{18}\text{O}$ . A similar downshift of  $-23 \text{ cm}^{-1}$  is observed for the 1666  $\text{cm}^{-1}$  peak in the tBQO<sup>-</sup> model in  $\text{H}_2^{18}\text{O}$  and is accompanied by an increase of 2 mass units according to mass spectrometry [Moënne-Loccoz et al., 1995]. A probable pathway for C5=O exchange is shown in Fig. 2.4. Exchange is

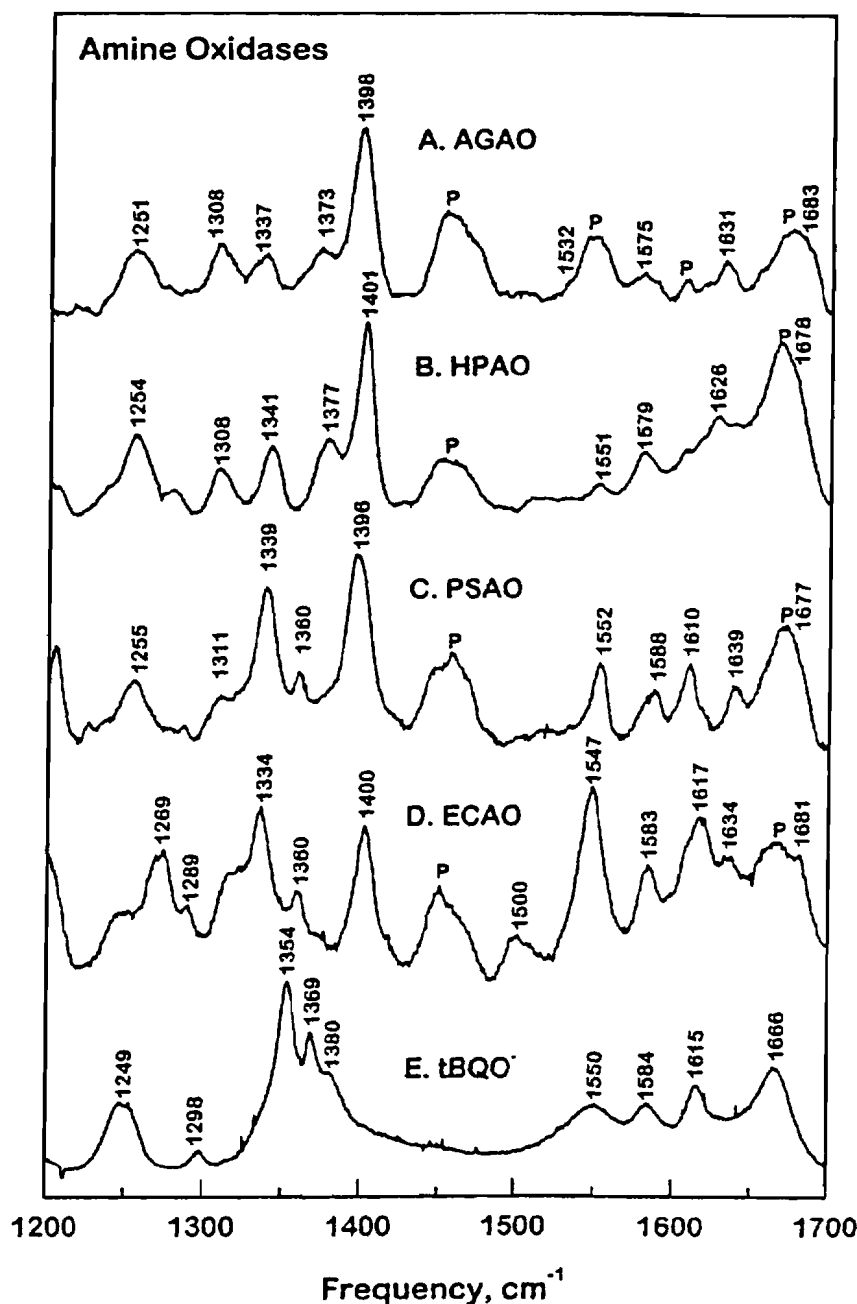


**Fig. 2.2** Resonance Raman spectra of copper-containing amine oxidases and models. (A) Phenethylamine oxidase (1.3 mM) from *A. globiformis* in 50 mM HEPES (pH 6.8). (B) Amine oxidase (1.3 mM) from *H. polymorpha* in 50 mM phosphate (pH 6.8). (C) Pea seedling amine oxidase (1.4 mM) in 100 mM phosphate (pH 7.2). (D) Amine oxidase (0.4 mM) from *E. coli* in 50 mM phosphate (pH 7.0). (E) tBQO<sup>-</sup> model compound (~2 mM) in aqueous solution (pH 9.6). Data for A from Nakamura et al. [1996]; B and C from Wang et al. [1997]; D and E from Moënne-Loccoz et al. [1995]. P denotes protein vibrational mode.

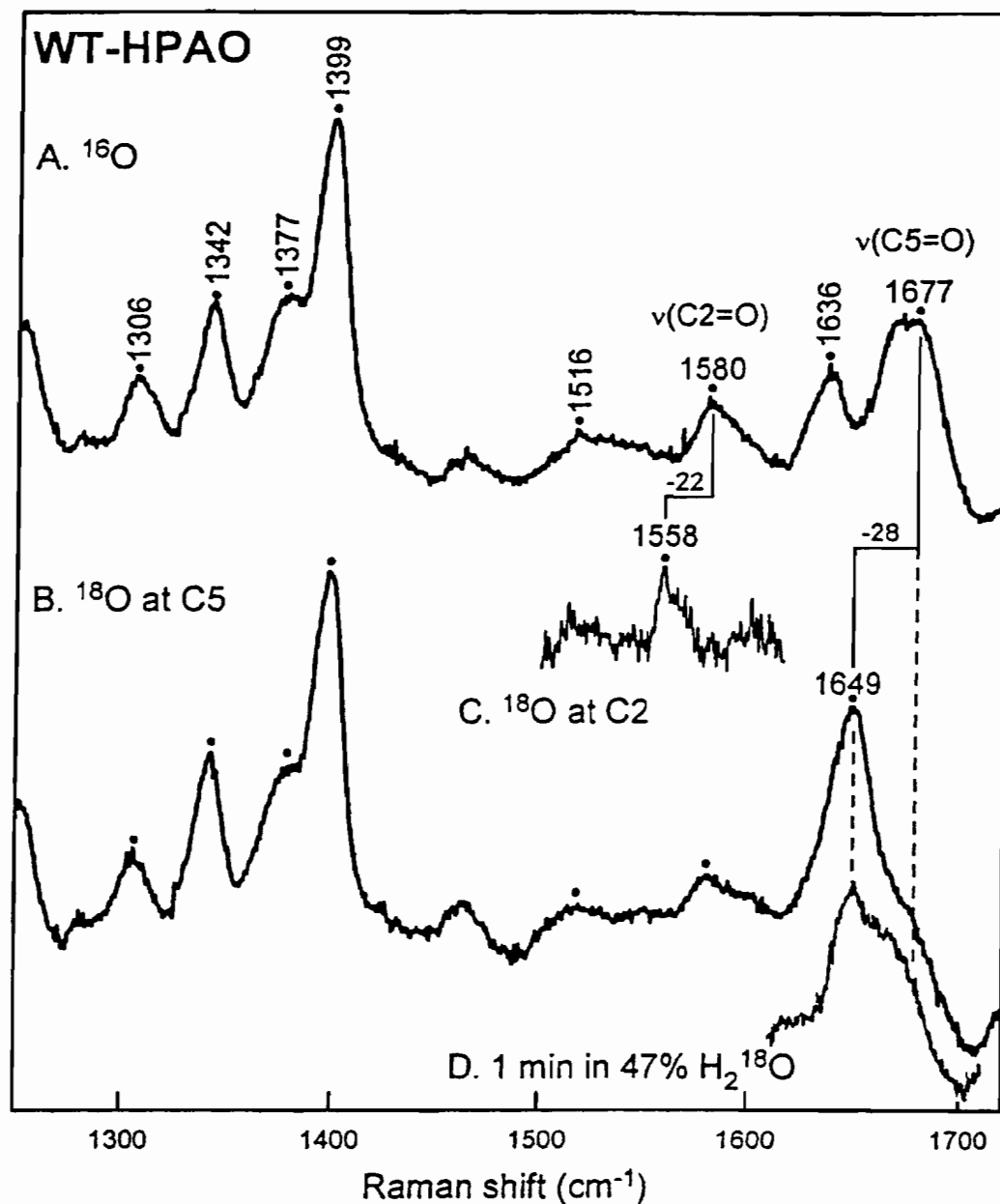


**Fig. 2.3** Effect of oxygen isotopes on Raman spectrum of WT-HPAO. (A) HPAO in  $\text{H}_2^{16}\text{O}$ . (B) HPAO incubated 1 h in 89 atom %  $^{18}\text{O}$ . (C) Biogenesis of HPAO in  $\text{H}_2^{18}\text{O}$ . (D) HPAO in  $\text{H}_2^{16}\text{O}$  diluted with  $\text{H}_2^{18}\text{O}$  to yield 47 atom %  $^{18}\text{O}$ . Spectrum (20-s accumulation) was obtained within 1 min of mixing.

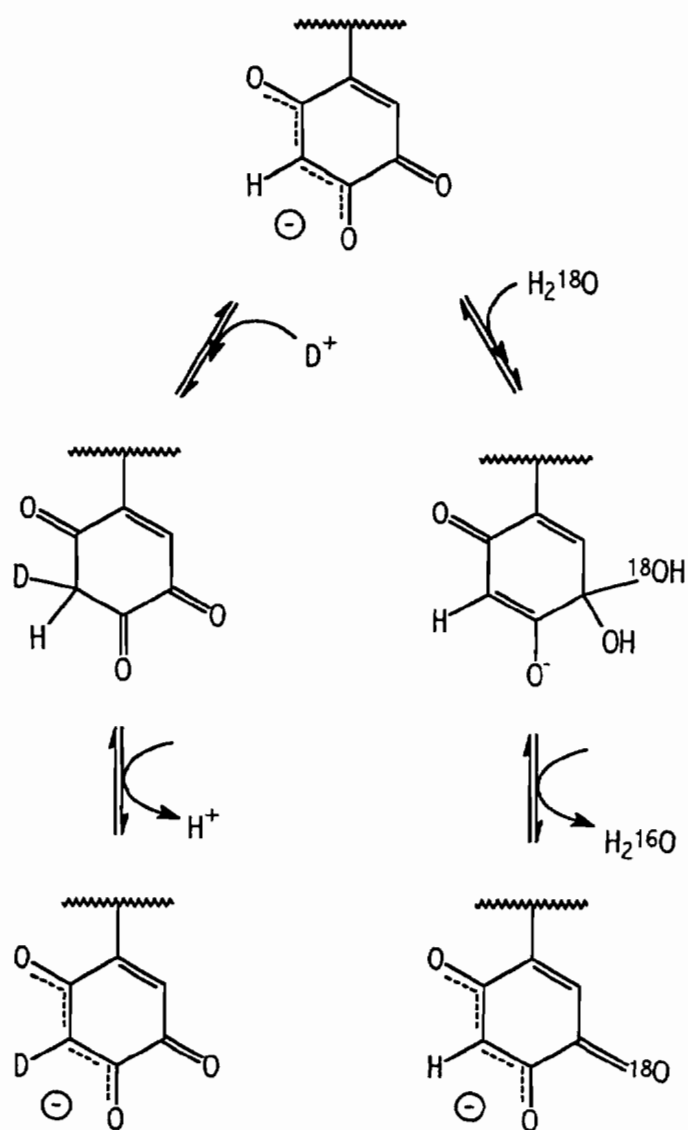


**Fig. 2.4** Proposed mechanisms for H and O exchange on TPQ.



initiated by nucleophilic attack of solvent at C5, similar to reaction of substrate, leading to a dihydroxy intermediate which then reverts back to a carbonyl and accumulates  $C5=^{18}O$  in the presence of excess  $^{18}O$  in the solvent.

In a previous study of AGAO, we showed that the C2 carbonyl is derived from solvent oxygen during cofactor biogenesis and does not exchange with solvent in the fully formed cofactor [Nakamura et al., 1996]. The  $C2=O$  stretch was observed at  $1575\text{ cm}^{-1}$  in the RR spectrum of AGAO and downshifted by  $21\text{ cm}^{-1}$  when the cofactor was generated in  $H_2^{18}O$  [Nakamura et al., 1997]. We have now observed similar results for WT-HPAO. Apo-HPAO in  $H_2^{18}O$  was reacted with  $CuCl_2$  and  $O_2$  to promote cofactor formation. The RR spectrum shows a  $22\text{ cm}^{-1}$  downshift for the peak at  $1580\text{ cm}^{-1}$  (Fig. 2.3C), as well as smaller shifts of  $-3$  to  $-5\text{ cm}^{-1}$  for peaks at  $1252$ ,  $1306$ ,  $1378$ , and  $1398\text{ cm}^{-1}$ , similar to AGAO (Table 2.1). These results establish the  $1580\text{ cm}^{-1}$  mode as the predominant  $C2=O$  stretch and prove that the formation of TPQ involves the insertion of a solvent oxygen at the C2 position in HPAO. The pattern of multiple, small isotope shifts in the  $1200\text{--}1400\text{ cm}^{-1}$  region indicates that the  $C2=O$  stretch in HPAO is coupled with similar ring vibrational modes and, thus, has a similar degree of electron delocalization between the C2 and C4 positions as in AGAO.

Exchange of the  $C5=O$  in WT-HPAO is essentially complete in the 1 h required for dilution and ultrafiltration (Fig. 2.3B). To obtain a closer estimate of the exchange rate, WT-HPAO was diluted 1:1 in  $H_2^{18}O$  buffer and a spectrum was obtained within 1 min (Fig. 2.3D). Exchange was measured by new intensity at  $1649\text{ cm}^{-1}$  and was found to be complete in this time period. The  $t_{1/2}$  for this reaction is  $<1$  min at ice temperature as well as room temperature (Table 2.2). The rapid exchange of the  $C5=O$  in WT-HPAO is in agreement with our prediction, based on the productive orientation of the TPQ ring in the crystal structure [Li et al., 1998]. Since the C5 carbonyl is directed towards the catalytic base and the substrate-binding pocket (Fig. 2.1), it is expected to exchange rapidly with solvent.

**Table 2.1**  
Comparison of Isotopic Shifts due to  $^{18}\text{O}$  Incorporation  
at the C2 and C5 Position of the TPQ Ring in AGAO and HPAO

AGAO <sup>a</sup>			HPAO		
$\nu(\text{cm}^{-1})$	$^{18}\text{O}$ shift		$\nu(\text{cm}^{-1})$	$^{18}\text{O}$ shift	
	C2	C5		C2	C5
1251	-3	-1	1252	-3	0
1308	-4	-1	1306	-5	0
1337	0	0	1342	-1	0
1373	-6	0	1378	-5	0
1398	-4	-1	1398	-5	0
1532	-3	0			
1575	-21	0	1580	-22	0
1631	0	0	1636	0	0
1683	0	-27	1677	0	-28

<sup>a</sup> Data from Nakamura et al. [1997].

**Table 2.2**Raman Frequencies and Half-times for Isotope Exchange in Amine Oxidases<sup>a</sup>

Enzyme	C5=O mode			C3-H mode		
	$\nu$	$[\Delta^{18}\text{O}]$	$t_{1/2}$	$\nu$	$[\Delta\text{D}]$	$t_{1/2}$
<b>Wild-type</b>						
HPAO	1678	-28	< 1 min	n.a.	n.o.	
ECAO	1681	-26	< 5 min	1289	-9	0.5 min
AGAO	1683	-27	< 2 min	1308	-16	6 h
PSAO (pH 7.1)	1677	-26	2 min	n.a.	n.o.	
PSAO (pH 4.6)	1677	-26	4.5 h	n.a.	n.o.	
<b>HPAO mutants</b>						
D319E	1681	-25	3.3 h	1298 <sup>b</sup>		< 30 min
D319N	1674	-22	1.6 h	1298 <sup>b</sup>		< 30 min
N404A	1681	-22	< 30 min	1298 <sup>b</sup>		< 30 min
E406Q	1679	-28	< 30 min	n.a.	n.o.	

<sup>a</sup> Frequencies ( $\nu$ ) and isotope shifts ( $\Delta^{18}\text{O}$  and  $\Delta\text{D}$ ) are in  $\text{cm}^{-1}$ . Half-times ( $t_{1/2}$ ) are based on multiple determinations (3–5) and were calculated by fitting the fraction exchanged,  $F$ , to the equation  $F = ae^{-kt}$ , where  $t_{1/2} = (\ln 2)/k$ . The error range for samples with a half-life greater than 1 h is  $\pm 0.7$  h. Ionic strength was held constant at  $\sim 0.1$ . n.a. = not assigned. n.o. = not observed.

<sup>b</sup> Frequency in  $\text{D}_2\text{O}$ .

### 2.3.2 Hydrogen Exchange in WT-HPAO, ECAO, and Model Compound

In model compounds, exchange of the C3-H of the TPQ ring with solvent deuterium has been amply demonstrated by both NMR and mass spectrometry [Janes et al., 1990; Moënné-Loccoz et al., 1995]. It is likely that reversible proton addition (and D exchange) at the C3 position is facilitated by charge delocalization from the oxygen at C4 into the TPQ ring (Fig. 2.4). The tBQO<sup>-</sup> model compound exhibits substantial RR spectral changes in D<sub>2</sub>O with downshifts of -25 at 1298 cm<sup>-1</sup> and -10 at 1354 cm<sup>-1</sup> [Moënné-Loccoz et al., 1995]. The time course for the D-promoted shift of the 1354-cm<sup>-1</sup> band to 1344 cm<sup>-1</sup> is shown in Fig. 2.5. The reaction is close to completion in 5 min. Curve-resolving the two components and plotting as an exponential leads to a calculated  $t_{1/2}$  of 2 min for D exchange in the tBQO<sup>-</sup> model compound. ECAO exhibits a similar deuterium isotope shift of -9 at 1289 cm<sup>-1</sup>, which has also been ascribed to rapidly exchanging C3 hydrogen [Moënné-Loccoz et al., 1995]. Quantitation of peak intensities reveals an even faster rate of D exchange in ECAO with a  $t_{1/2}$  of 0.5 min (Table 2.2). A similarly rapid rate of <sup>18</sup>O exchange in ECAO suggests that the TPQ ring readily flips between the two orientations, in agreement with its disordered electron density in the crystal structure [Murray et al., 1999].

The RR spectrum of WT-HPAO exhibits a small peak at 1306 cm<sup>-1</sup>, which could be related to the 1289 cm<sup>-1</sup> C3-H vibrational mode in ECAO. However, neither this peak nor any other spectral feature of WT-HPAO changes upon prolonged incubation of hours to days in D<sub>2</sub>O. These results imply that either the C3-H is not exchanging or that vibrations of the C3-H are not resonance-enhanced in WT-HPAO.

### 2.3.3 Oxygen Exchange in PSAO

The X-ray structure of PSAO was determined on material that had crystallized at pH 4.8 [Kumar et al., 1996]. The electron density of the TPQ ring was clearly defined and shown to be in a flipped orientation with the C2=O hydrogen-bonded to Asp 300, the catalytic base. The enzyme is fairly stable at this pH and still exhibits enzymatic activity, albeit 4-fold lower than at neutral pH. The TPQ absorption maximum red shifts from 500 nm at pH 7.2 to 515 nm at pH 5.2 [McGuirl et al.,

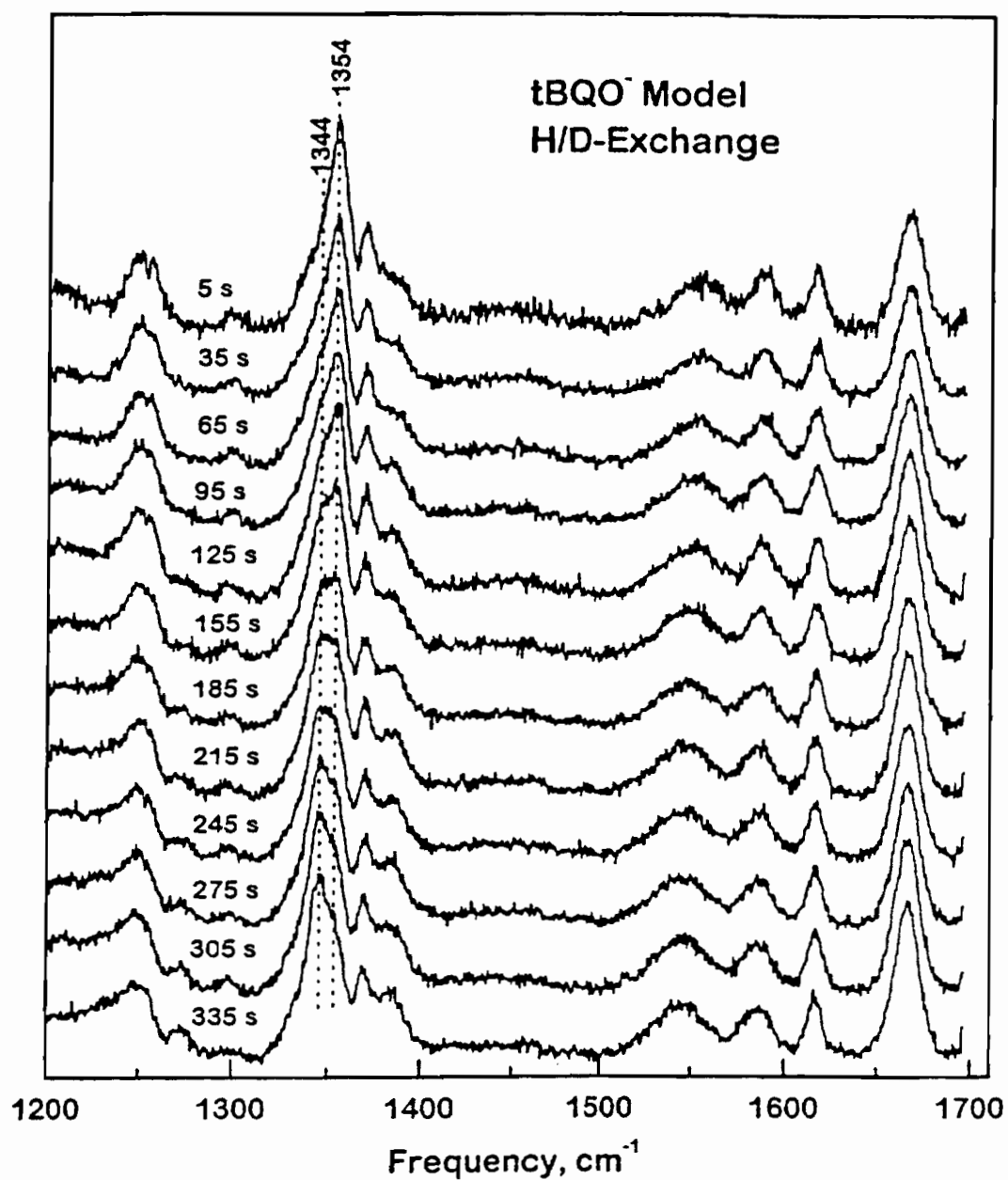


**Fig. 2.5** Raman spectra of  $tBQO^-$  model compound (2 mM) at different times after dilution into  $D_2O$  buffer (90 atom %  $D$ , pH reading 7.1). Each spectrum represents 15-s of data accumulation.

1994]. Studies of the tBQO<sup>-</sup> model compound reveal that protonation of the hydroxyquinone causes the absorption maximum to blue shift from 498 to 372 nm [Mure and Klinman, 1995a]. Thus, the red shift in the PSAO absorption spectrum at low pH is more likely due to an increase in the resonance delocalization of electrons from the C4-oxyanion through the C2=O (Fig. 2.4).

Additional evidence for a change in TPQ electronic structure with pH comes from RR spectroscopy. The RR spectrum of PSAO at pH 7.2 is similar to that of other amine oxidases, with the most intense ring vibrational mode at 1396 cm<sup>-1</sup> (Fig. 2.2). However, at pH 4.6, there is a marked drop in the intensity and slight change in frequency at 1392 cm<sup>-1</sup>, and the peak at 1337 cm<sup>-1</sup> has increased in intensity to become the dominant feature in the RR spectrum (Fig. 2.6B). This RR intensity pattern is actually similar to that seen in the RR spectrum of tBQO<sup>-</sup> at alkaline pH (Fig. 2.2E), a system which has been shown to have strong charge delocalization in the quinone ring [Mure and Klinman, 1995b]. The increase in electron delocalization in PSAO at low pH could be due to the fact that the flipped orientation lacks the (TPQ)C4-O...HO(Tyr) interaction [Kumar et al., 1996] that has been observed in the crystal structures of other amine oxidases at neutral pH [Wilce et al., 1997; Li et al., 1998; Murray et al., 1999].

A dramatic effect of pH is seen in the rates of C5=O exchange in PSAO (Fig. 2.7). At pH 7.1, the reaction is complete in 500 sec ( $t_{1/2}$  = 2 min), whereas complete exchange at pH 4.6 requires 20 h ( $t_{1/2}$  = 4.5 h). In contrast, the tBQO<sup>-</sup> model still undergoes a rapid <sup>18</sup>O exchange at pH 4, indicating that the reaction is not simply limited by the lower concentration of hydroxide. The remarkably slow rate of C5=O exchange in the low pH PSAO can be attributed to two factors: (i) increased electron delocalization away from the C-4 oxyanion makes nucleophilic attack at C5 less favorable, and (ii) the flipped conformation makes C5 less accessible to solvent. The fast rate of <sup>18</sup>O exchange in PSAO at neutral pH indicates that the TPQ cofactor has shifted to the productive orientation where the C5=O is accessible to the solvent. As in the case of WT-HPAO, no D-sensitive ring modes could be detected in PSAO incubated in D<sub>2</sub>O at neutral or low pH. The 135-fold decrease in the rate of C5=O exchange compared to only a 4-fold decrease in enzymatic activity in PSAO at low

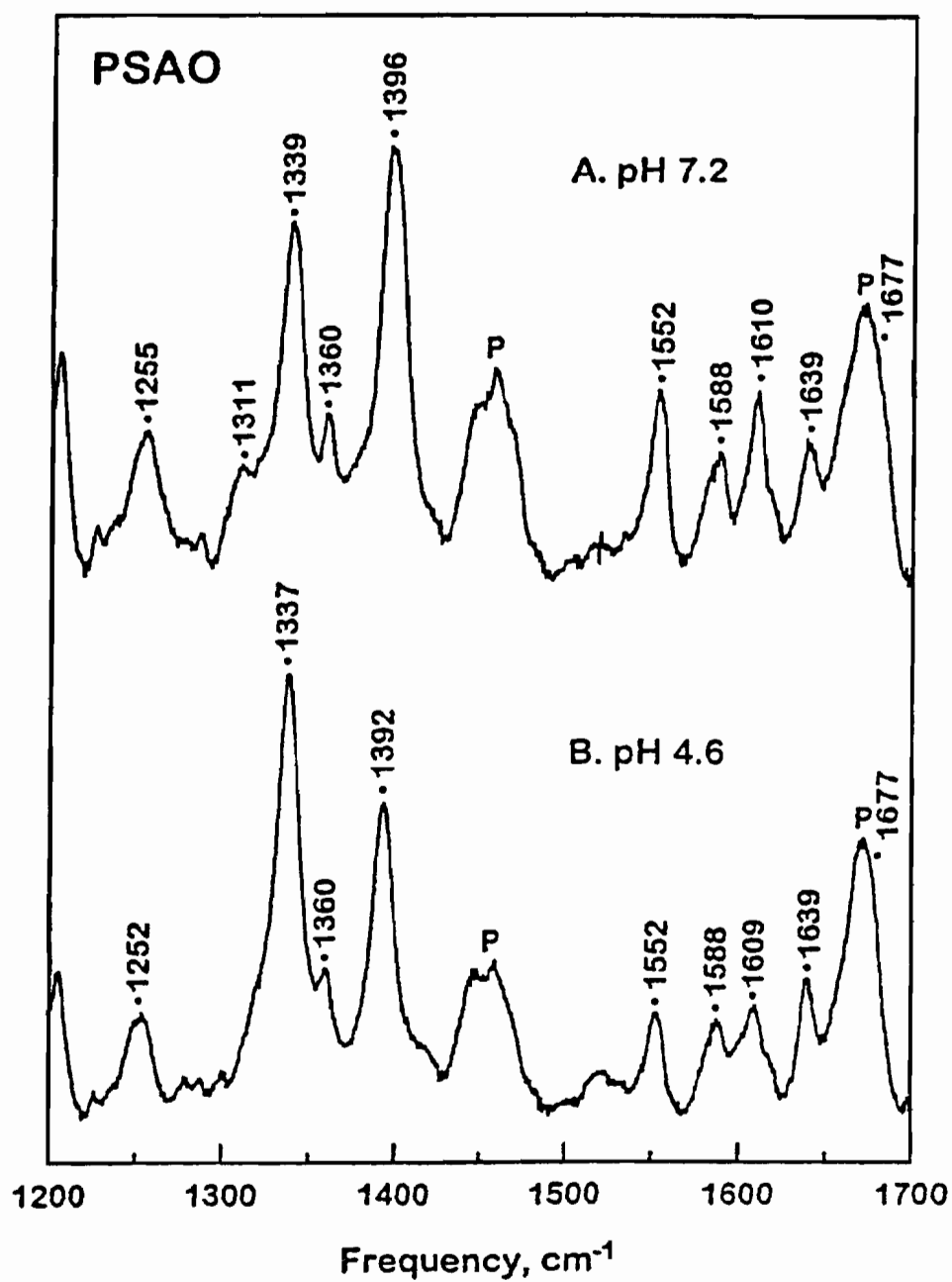


**Fig. 2.6** Effect of pH on the Raman spectrum of PSAO. (A) 1.4 mM enzyme in 0.1 M phosphate (pH 7.2). (B) 1 mM enzyme in 0.01 M acetate (pH 4.6).

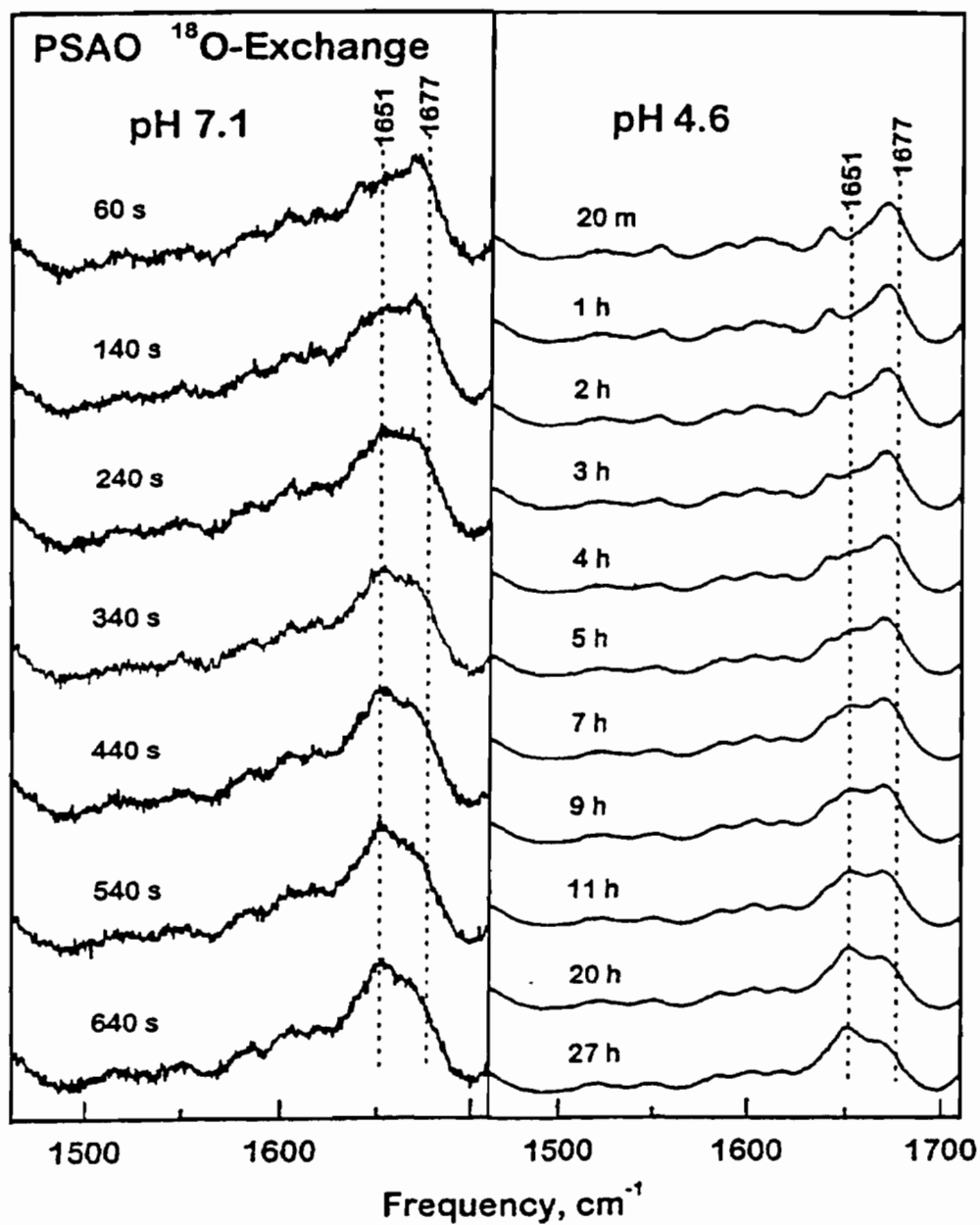


**Fig. 2.7** Raman spectra of PSAO as a function of time of exposure to  $\text{H}_2^{18}\text{O}$ . **(Left)** 0.5 mM enzyme in 0.01 M HEPES (pH 7.1) in 50 atom %  $^{18}\text{O}$ . Spectra are 10-sec accumulations. **(Right)** 1.0 mM enzyme in 0.01 M acetate (pH 4.6) in 81 atom %  $^{18}\text{O}$ .



pH suggests that substrate binding promotes ring flipping to the productive orientation as in HPAO [Plastino et al., 1999].

#### 2.3.4 O and H Exchange in AGAO

The X-ray structure of wild-type AGAO at pH 8.1 and 2.2-Å resolution revealed clear electron density that could be attributed to the entire TPQ ring as well as the oxygens at the C2 and C4 positions, thereby indicating that the ring is in an ordered conformation [Kumar et al., 1996]. However, no density was observed for the oxygen at the C5 position, making it impossible to determine whether the ring is in a productive or flipped orientation. In contrast, the high-resolution X-ray structure of wild-type ECAO at 100 K reveals only partial electron density for the TPQ ring, consistent with rotational motions and a disordered TPQ orientation [Murray et al., 1999]. Our RR findings of fast rates of exchange for both the C5=O and the C3-H in ECAO (Table 2.2) support the crystallographic evidence for a mobile TPQ ring. Similarly, our RR investigation of AGAO points to a more ordered disposition of the TPQ ring, as suggested by the crystal structure.

AGAO is similar to ECAO in that its RR spectrum is affected by incubation in D<sub>2</sub>O, causing a 16-cm<sup>-1</sup> downshift from 1308 to 1292 cm<sup>-1</sup> (Fig. 2.8), compared to the 9-cm<sup>-1</sup> downshift from 1289 to 1280 cm<sup>-1</sup> observed for ECAO. However, the two enzymes differ in the rate of C3-H exchange, which is fast ( $t_{1/2}$  = 0.5 min) for ECAO and slow for AGAO. In 0.05 M HEPES (pH 7.1) at an ionic strength of 0.09, D exchange in AGAO is complete by 20 h with a  $t_{1/2}$  of 6 h (Fig. 2.8). The rate of C3-H exchange in AGAO is inversely proportional to ionic strength, such that a  $t_{1/2}$  of 4 h is achieved at  $I$  = 0.02 (Fig. 2.9). As in the case of HPAO and ECAO, the rate of <sup>18</sup>O exchange in AGAO is much faster ( $t_{1/2}$  < 2 min) (Table 2.2). The slow exchange of the C3-H and rapid exchange of the C5=O in AGAO suggest that the TPQ ring is held in a productive conformation. The ionic strength dependence of the D-exchange rate provides further evidence for the key role of solvent accessibility in the exchange process. Higher ionic strengths decrease the activity of water and thus limit the effective concentration of reactant.

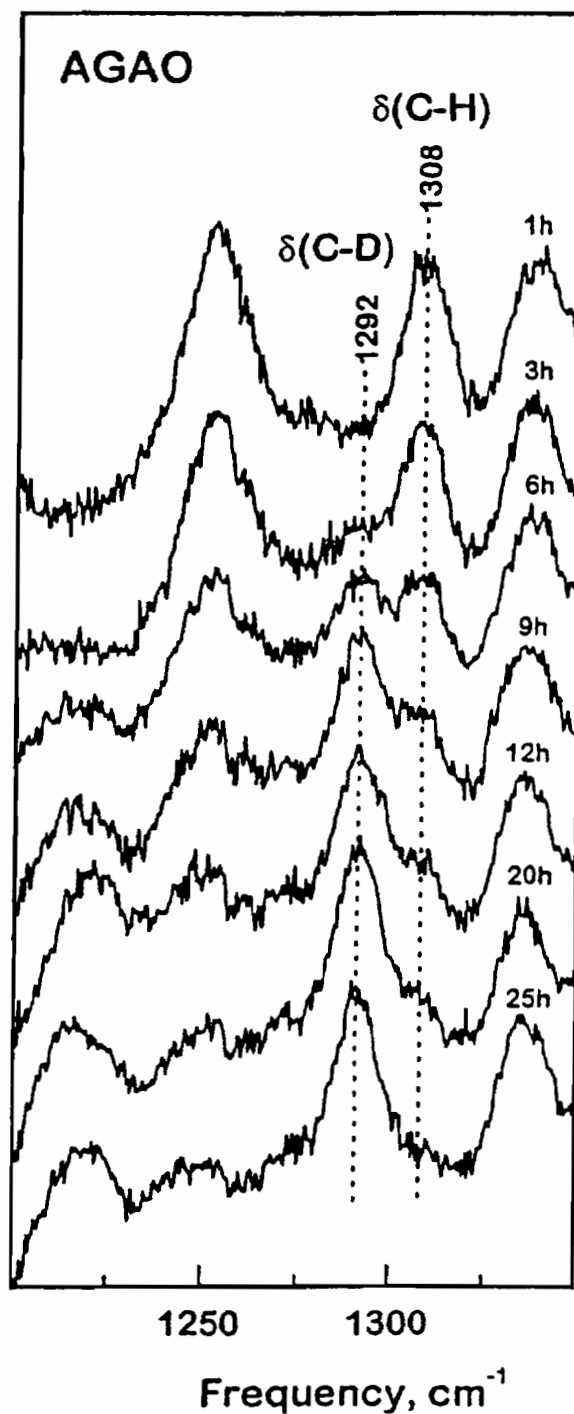


**Fig. 2.8** Raman spectra of AGAO as a function of time of exposure to  $\text{D}_2\text{O}$ . AGAO (1 mM in protein) in 0.05 M HEPES (pH reading 7.1) in 94 atom % D. Spectra are 5-min accumulations.

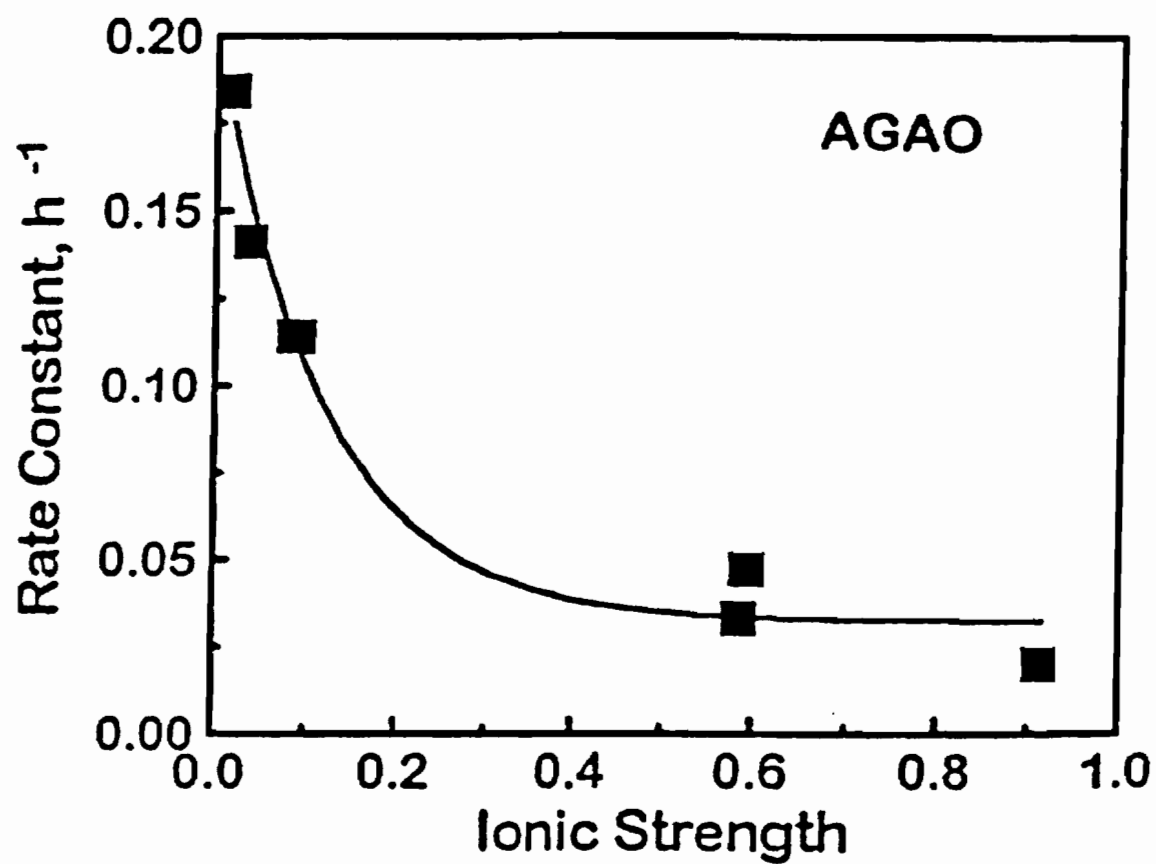
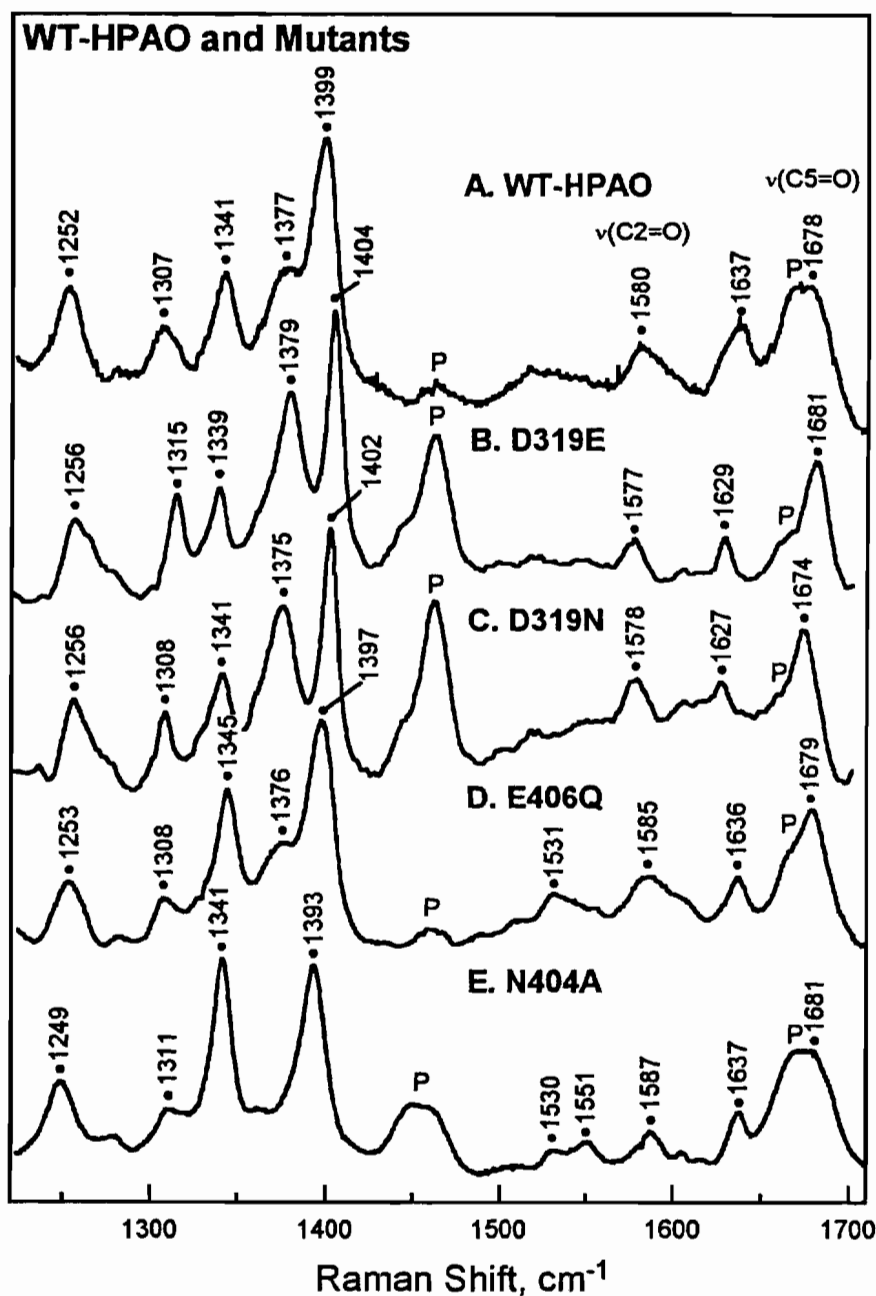


Fig. 2.9 Effect of ionic strength on the rate of D exchange in AGAO at pH 7.1. The ionic strength was altered by varying buffer and salt concentrations.

### 2.3.5 O and H Exchange in the D319 Mutants of HPAO

In the D319E and D319N mutants, the catalytic base has been replaced by a longer chain carboxylate, which behaves as a weaker catalyst, or by an asparagine, which destroys its catalytic activity [Plastino et al., 1999]. These mutants have RR spectra similar to WT-HPAO, with C5=O stretching vibrations at 1681 and 1674  $\text{cm}^{-1}$  (Fig. 2.10) that shift  $-25$  and  $-22$   $\text{cm}^{-1}$  in  $\text{H}_2^{18}\text{O}$  (Table 2.2), respectively. The course of  $^{18}\text{O}$  exchange in D319E was monitored for 28 h to observe the slow appearance of the C5= $^{18}\text{O}$  peak at 1656  $\text{cm}^{-1}$  (Fig. 2.11). A fit of the data for fraction exchanged with time (Fig. 2.12) yielded a  $t_{1/2}$  of 3.3 h for the D319E mutant. A somewhat faster but still slow rate of C5=O exchange was observed for the D319N mutant, yielding a  $t_{1/2}$  of 1.6 h (Table 2.2). Thus, both of these mutants demonstrate a decrease of at least 40-fold in the rate of  $^{18}\text{O}$  exchange relative to WT-HPAO. The RR spectra of the D319E and D319N mutants are still dominated by an intense feature at 1404 and 1402  $\text{cm}^{-1}$ , respectively, with similar peak frequencies and intensities throughout the 1200–1700  $\text{cm}^{-1}$  region, indicating that they have a degree of electron delocalization similar to WT-HPAO (Fig. 2.10). Furthermore, the 480-nm absorption maximum for the D319 mutants [Plastino et al., 1999] is the same as that of WT-HPAO and is not red-shifted as in the case of PSAO at low pH. Thus, the markedly slower rate of C5=O exchange in the D319 mutants compared to WT-HPAO can be mainly ascribed to lower solvent accessibility of the C5=O.

Incubation of the D319E mutant in  $\text{D}_2\text{O}$  results in the appearance of a new peak at 1298  $\text{cm}^{-1}$  (Fig. 2.13), indicative of a C3–D vibrational mode similar to the one observed at 1280  $\text{cm}^{-1}$  in ECAO and at 1344  $\text{cm}^{-1}$  in the tBQO $^-$  model. However, in the case of D319E, there is no corresponding decrease in Raman intensity at higher energy, implying that the C3–H vibration is not resonance enhanced. Typically C–H motions in aromatic systems gain resonance enhancement through coupling to ring vibrations that involve substantial electron delocalization in the electronic excited state. In the case of the D319E mutant, the change in frequency associated with D substitution apparently gives better energy overlap with a TPQ ring mode, thereby allowing the vibration to be observed. The D319N mutant shows the same behavior in  $\text{D}_2\text{O}$ , with a new peak appearing at 1298  $\text{cm}^{-1}$  but no



**Fig. 2.10** Resonance Raman spectra of WT-HPAO and mutants of HPAO. (A) WT-HPAO (0.35 mM) in 50 mM phosphate (pH 7.0). (B) D319E mutant of HPAO (0.7 mM) in 50 mM phosphate (pH 7.0). (C) D319N mutant of HPAO (0.7 mM) in 50 mM phosphate (pH 7.0). (D) E406Q mutant of HPAO (0.75 mM) in 50 mM phosphate (pH 7.0). (E) N404A mutant of HPAO (0.8 mM) in 50 mM phosphate (pH 7.0). P denotes protein vibrational mode. Spectra A and D are corrected for Raman contributions due to protein and solvent. Spectra B, C, and E are corrected for Raman contributions due to solvent.

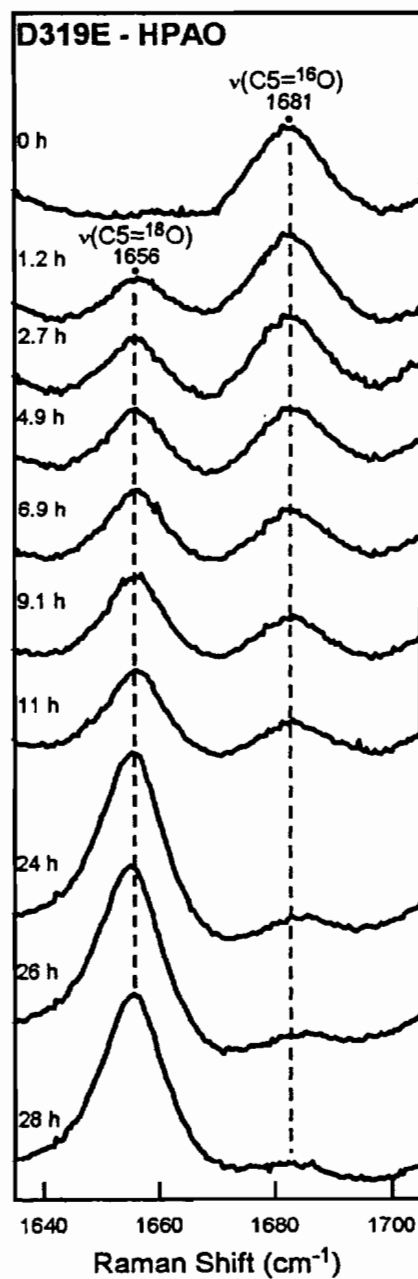


**Fig. 2.11** Raman spectra of D319E mutant of HPAO ( $\sim 0.4$  mM in TPQ) as a function of time of reaction with  $\text{H}_2^{18}\text{O}$  (89 atom %  $^{18}\text{O}$ ). Spectra are 15-min accumulations and have been corrected for Raman contributions of apoHPAO and solvent.

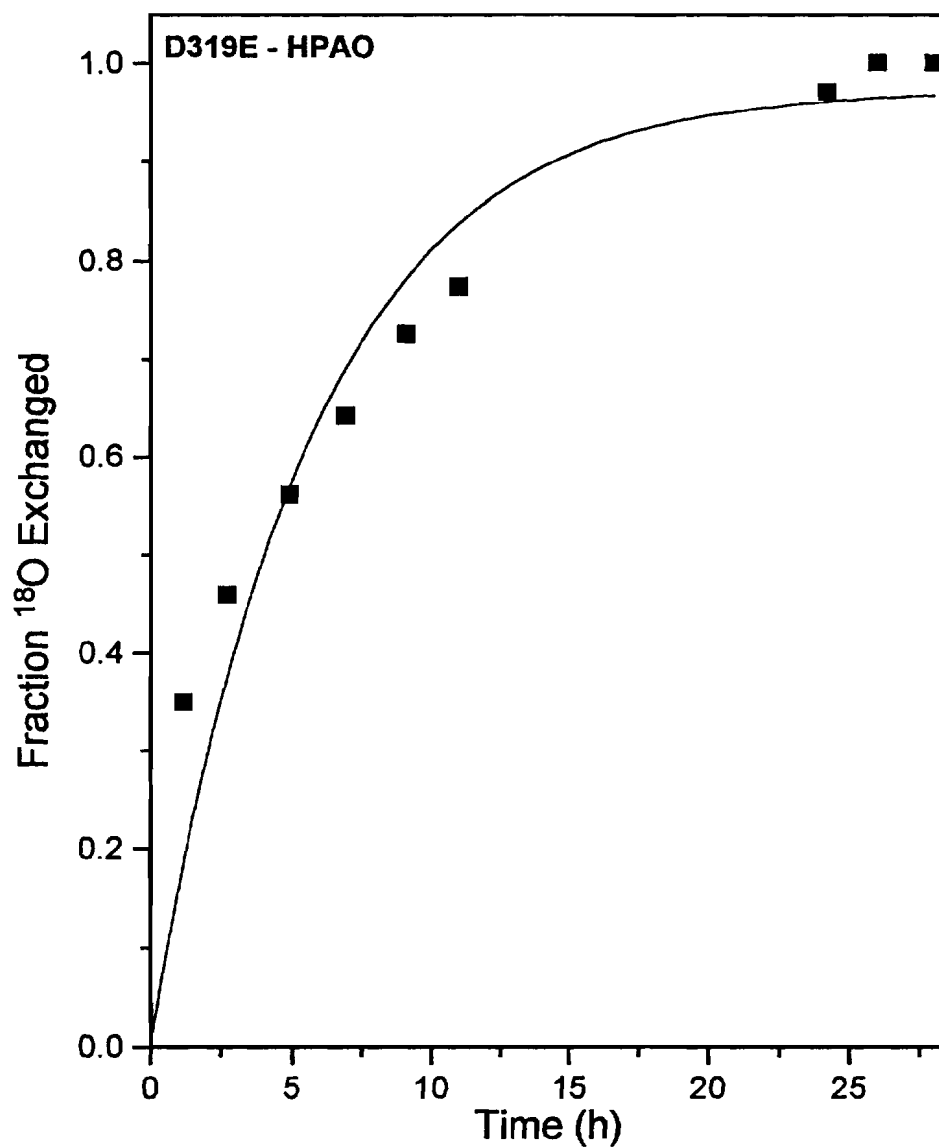


**Fig. 2.12** Fraction of  $\text{C5}=\text{}^{18}\text{O}$  formed as a function of time of incubation of the D319E mutant in  $\text{H}_2\text{}^{18}\text{O}$ . The data obtained from Fig. 2.11 were subject to a nonlinear fit for the relationship  $F=ae^{-kt}$  and yielded a  $k_{\text{obs}}$  of 0.21/h.

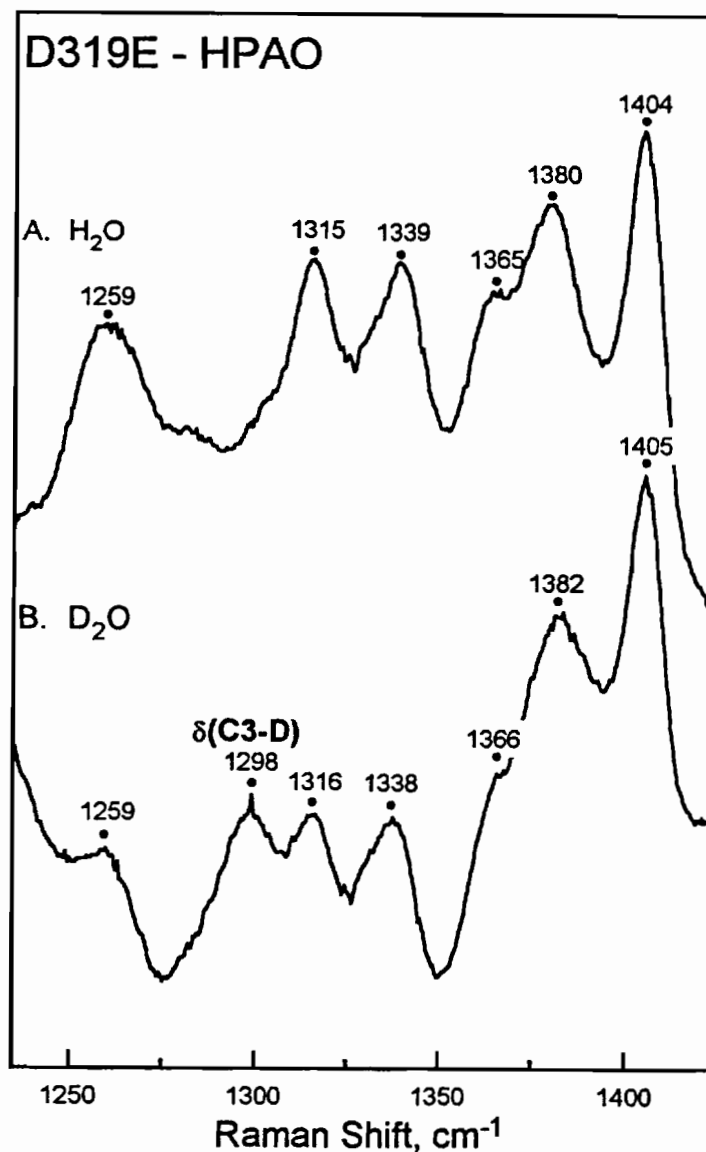


**Fig. 2.13** Effect of D<sub>2</sub>O on Raman spectrum of the D319E mutant of HPAO. (A) D319E in H<sub>2</sub>O. (B) D319E after 86-min incubation in 90% D<sub>2</sub>O. Protein samples are 0.4 mM in TPQ and spectra are 15-min accumulations.



corresponding drop in intensity at higher energy. In both cases, exchange was complete within 60 min, the minimum time for sample preparation by ultrafiltration. The lower stability of the mutant proteins made it impossible to concentrate them to the levels required for RR detection by the dilution method. Thus, earlier reaction times could not be studied. The fact that exchange was complete at the earliest 60-min time point allows us to assign a  $t_{1/2}$  of  $<30$  min for the D319 mutants (Table 2.2).

The pattern of slow exchange for the C5=O and fast exchange for the C3-H in both D319E and D319N suggests that the TPQ cofactor is in the flipped orientation. This interpretation is supported by an enzyme kinetics analysis of the D319E mutant, which found an 80-fold reduction in the  $k_{cat}/K_m$  for methylamine [Plastino et al., 1999]. Since this kinetic parameter was not affected by either substrate or solvent isotopes or viscosity, the rate limitation was best explained as being due to the need for cofactor reorientation. The flipped orientation could be stabilized by hydrogen bonding of C2=O to E319 or N319 in the catalytic base site. However, the fast C3-H exchange in the D319N mutant, which lacks a catalytic base, shows that it is not proximity to residue 319 that is responsible for rapid D exchange but rather the greater accessibility to solvent on that side of the active site.

### 2.3.6 O and H Exchange in E406Q and N404A Mutants of HPAO

Mutations of the residues flanking the TPQ cofactor reveal some interesting differences in  $^{18}\text{O}$  and D exchange rates. The E406Q mutant behaves much like WT-HPAO. The  $\nu(\text{C5}=\text{}^{16}\text{O})$  mode is measured at  $1679\text{ cm}^{-1}$  (Fig. 2.10) and downshifts  $28\text{ cm}^{-1}$  upon  $^{18}\text{O}$  substitution (Table 2.2). The C5 carbonyl oxygen exchange was complete within 1 h, the first time point collected after reconcentration. Also, no observable C3 hydrogen exchange was detected, even after a 24-h incubation in  $\text{D}_2\text{O}$  (Table 2.2). Therefore, we can conclude that the cofactor in the E406Q mutant is in the productive orientation, similar to that of WT-HPAO. This conclusion is in agreement with the similar rates of benzylamine oxidation in E406Q and WT-HPAO [Dove et al., 2000].

In the N404A mutant, the  $\nu(\text{C5}=\text{}^{16}\text{O})$  peak is measured at  $1681\text{ cm}^{-1}$  (Fig. 2.10) and downshifts  $22\text{ cm}^{-1}$  upon  $^{18}\text{O}$  substitution (Table 2.2). The N404A mutant demonstrates a fast  $^{18}\text{O}$  exchange, complete within 1 h ( $t_{1/2} < 30\text{ min}$ ). But, unlike the E406Q mutant, N404A also displays a fast C3 hydrogen exchange, complete within 1 h ( $t_{1/2} < 30\text{ min}$ ) as judged by the appearance of the  $\delta(\text{C3-D})$  peak at  $1298\text{ cm}^{-1}$  upon dilution in  $\text{D}_2\text{O}$  (Table 2.2). These results suggest a fluctuating orientation of the TPQ ring in the N404A mutant, similar to that observed in ECAO. The crystal structure of WT-HPAO shows that one face of the TPQ ring lies against the amide group of Asn404 [Li et al., 1998]. With Ala in place of Asn, this interaction would be lost, thus lowering the kinetic energy barrier for ring flipping, and the active site pocket becomes more open to allow for greater TPQ flexibility. Mobility of the TPQ ring could explain the  $10^3$ -fold lower  $k_{\text{cat}}/K_{\text{m}}$  for substrate in the N404A mutant compared to WT-HPAO [Schwartz et al., 1998]. Furthermore, the inactivation of the N404A mutant by methylamine substrate was found to be due to the formation of a protonated product Schiff base whose stability was attributed to its being in a flipped orientation [Schwartz et al., 1998].

## 2.4 Conclusions

### 2.4.1 Prediction of TPQ Orientation from Exchange Rates

In this study, we have examined the  $\text{C5}=\text{O}$  and  $\text{C3-H}$  exchange rates of the TPQ cofactor for various wild-type copper-containing amine oxidases and mutant forms of HPAO. Examination of the  $\text{tBQO}^-$  model compound indicates that both the C5 carbonyl oxygen and the C3 hydrogen are capable of exchanging rapidly with solvent. However, a number of CAOs exhibit abnormally slow exchange rates ( $t_{1/2} = 1\text{--}6\text{ h}$ ) for either the  $\text{C5}=\text{O}$  or the  $\text{C3-H}$ , and slow exchange on one side of the TPQ ring is generally accompanied by fast exchange ( $t_{1/2} \leq 0.03\text{--}0.5\text{ h}$ ) on the other side of the ring (Table 2.3). These results can be explained by differences in solvent accessibility, suggesting that the edge of the TPQ ring oriented towards the substrate-binding pocket is more exposed to bulk solvent than the edge oriented towards the copper center. Support for this hypothesis comes from the strong correlation between

**Table 2.3**

Rates of Solvent Isotope Exchange as Indicators of Cofactor Orientation

Enzyme	Exchange rate <sup>a</sup>		TPQ orientation <sup>b</sup>	
	C5=O <sup>c</sup>	C3-H <sup>d</sup>	Observed <sup>e</sup> (X-ray)	Predicted (RR)
<b>Wild-type</b>				
HPAO	fast	n.o.	productive	productive
ECAO	fast	fast	disordered	mobile
AGAO	fast	slow	ordered	productive
PSAO (pH 7.1)	fast	n.o.		productive
PSAO (pH 4.6)	slow	n.o.	flipped	flipped
<b>HPAO mutants</b>				
D319E	slow	fast		flipped
D319N	slow	fast		flipped
E406Q	fast	n.o.		productive
N404A	fast	fast		mobile

<sup>a</sup> Fast exchange indicates a half-time of reaction <2 min for wild-type enzymes and <30 min for HPAO mutants. Slow exchange indicates a half-time of reaction of 1–6 h. n.o. = not observed. Exchange was measured at 298 K for the wild-type enzymes and at 278 K for the HPAO mutants.

<sup>b</sup> Productive has C5=O directed towards the catalytic base. Flipped has C5=O directed towards the Cu. Mobile can adopt either conformation.

<sup>c</sup> C5=O exchange in H<sub>2</sub><sup>18</sup>O was measured from the appearance of a new RR peak near 1650 cm<sup>-1</sup>.

<sup>d</sup> C3-H exchange in D<sub>2</sub>O was measured by the appearance of a new RR peak at 1290–1300 cm<sup>-1</sup>.

<sup>e</sup> From crystal structures of HPAO [Li et al., 1998], ECAO [Murray et al., 1999], AGAO [Wilce et al., 1997], and PSAO [Kumar et al., 1996].

the pattern of C5=O/C3-H exchange and the TPQ cofactor orientation observed in the X-ray crystal structure. Thus, the exchange rates determined by RR spectroscopy can be used to differentiate between productive, flipped, and mobile orientations of the TPQ cofactor.

The *productive* orientation of TPQ, with its C5 carbonyl oxygen near the substrate-binding site and its C3 hydrogen near the bound Cu, has been observed in the crystal structure of WT-HPAO [Li et al., 1998]. The resting enzyme exhibits rapid C5=O exchange, as expected, with the C3-H to exchange being either exceedingly slow or not observable due to a lack of resonance enhancement (Table 2.3). The same pattern of fast C5=O exchange and a non-observable C3-H exchange are seen for PSAO at pH 7.1 and for the E406Q mutant of HPAO. Although no crystal structures are available for these proteins, our prediction of a productive orientation is supported by their high enzymatic activities. Finally, AGAO shows the definitive pattern of a productive orientation with fast C5=O exchange and slow C3-H exchange (Table 2.3). Although the orientation of the TPQ ring in AGAO has not been verified by X-ray crystallography because of the difficulty of locating the carbonyl oxygens [Wilce et al., 1997], the ring itself has well-defined electron density, suggestive of an ordered rather than a mobile cofactor.

The *flipped* orientation of TPQ, with its C5 carbonyl oxygen directed towards the Cu-binding site and its C3 hydrogen facing the substrate-binding pocket, has been observed in the crystal structure of PSAO at pH 4.8 [Kumar et al., 1996]. As expected for a flipped orientation, the rate of C5=O exchange in PSAO at pH 4.6 is 135-fold slower than at pH 7.1 (Table 2.2) and is also much slower than that of the tBQO<sup>-</sup> model at pH 4. These results are consistent with a buried environment for the C5=O and flipped designation for TPQ in pH 4.8 PSAO (Table 2.3). The lack of a RR vibrational mode for the C3-H makes it impossible to determine whether the C3-H has the expected fast rate of exchange in pH 4.8 PSAO. However, the D319E and D319N mutants of HPAO do exhibit both of the predicted characteristics of a flipped cofactor orientation: slow C5=O exchange and fast C3-H exchange (Table 2.3). These flipped species, PSAO at pH 4.8 and the D319E mutant of HPAO, also have reduced enzymatic reaction rates consistent with the need for cofactor reorientation.

Kinetic studies for D319E-HPAO reveal that this mutant turns over methylamine and phenethylamine substrates 80-fold and 15-fold more slowly than WT-HPAO, respectively, whereas the D319N-HPAO mutant has no catalytic activity [Plastino et al., 1999]. The fact that D319E is still active towards substrates and that the reaction is faster than the rate of C5=O exchange in the resting enzyme implies that the TPQ cofactor must flip back to a productive conformation in the presence of substrate to initiate substrate turnover [Plastino et al., 1999]. The need for TPQ to flip back to a productive conformation, as well as the altered active site base providing more steric hindrance (glutamate versus aspartate), could lead to the decreased rate of reaction with substrate in the D319E mutant. Additionally, D319N was shown to form a covalent adduct with ammonium chloride similar to the adduct formed with D319E reacted with methylamine. Both of these adducts were identified as deprotonated iminoquinones by RR spectroscopy [Plastino et al., 1999]. We ascribed the deprotonation of this complex to be a result of TPQ cofactor flipping. A flipped iminoquinone complex would be expected to hydrolyze slowly, due to lack of solvent accessibility to the back side of the TPQ ring; in fact, a large solvent isotope effect was observed for  $k_{cat}$  for the oxidation of methylamine by D319E and was attributed to a rate-limiting hydrolytic step [Plastino et al., 1999]. These kinetic results support our conclusion that the TPQ cofactor in the D319E and D319N mutants of HPAO has a tendency to be stable in the flipped orientation. Finally, the similarity of the solvent exchange rates for D319E and D319N rules out the possibility that the catalytic base is playing a significant role in either C3-H or C5=O exchange, and is consistent with the fast rates observed for uncatalyzed exchange in the tBQO<sup>-</sup> model compound [Moënné-Loccoz et al., 1995].

A *mobile* cofactor, with the TPQ ring adopting a multitude of conformations, is suggested by the crystal structure of ECAO with its lack of electron density for TPQ, suggesting a disordered structure [Murray et al., 1999]. The fast exchange rates for both the C5=O and C3-H in ECAO are consistent with a mobile TPQ (Table 2.3). The N404A mutant of HPAO shows a similar pattern of rapid C5=O and C3-H exchange, indicating that it too has a mobile cofactor. Since the Asn404 side chain lies against one face of the TPQ ring in WT-HPAO [Li et al., 1998], it is understandable why conversion of this Asn to Ala would increase cofactor mobility.

There are limitations to X-ray crystallography, which include the difficulty in observing an accurate electron density in large molecular structures and the potential difference between enzyme conformational states in the crystal versus the enzyme in solution. However, the high-resolution (2.0 Å) structure for ECAO showed well-defined electron densities for other aromatic rings and amino acid residues, but the TPQ cofactor ring was disordered [Murray et al., 1999]. This would indicate that the resolution was sufficiently good to distinguish the full electron density for the TPQ ring, but they were unable to see an ordered cofactor due to cofactor mobility rather than limitations of the technique. Additionally, the crystals were shown to be catalytically competent [Parsons et al., 1995], consistent with the crystals being in the same conformation as in solution.

#### **2.4.2 Structural Basis for Differences in Exchange Rates**

The crystal structure of HPAO identifies a large substrate channel leading from the solvent-accessible surface to the active site base (Fig. 2.14) [Li et al., 1998]. A bridging water molecule, W4, between the C5 carbonyl oxygen and the aspartate base is very near to the edge of the substrate channel, whereas the immobilized water molecules W5 and W6 are contained within the identified substrate channel and all are expected to be displaceable by substrate binding. The fact that these water molecules have defined and identical locations in the six independent subunits that comprise the asymmetric unit [Li et al., 1998] suggests that they can be considered as part of the protein structure in the resting enzyme. Nevertheless, the disordered solvent that comprises the bulk of the substrate channel comes within close proximity of the C5=O. Therefore, for the edge of the TPQ ring oriented towards the substrate-binding site, water would be expected to exchange easily and rapidly.

On the Cu side of the active site in HPAO, the crystal structure identified a chain of five immobilized water molecules (Fig. 2.14). This chain begins with the axial copper ligand Wa and continues through W2, W3, and Wx. The fifth water (Wy) is hydrogen bonded to a cluster of solvent molecules in another solvent-accessible cavity [Li et al., 1998]. This chain of water molecules is conserved for subunit B of the 2-hydrazinopyridine complex of ECAO [Wilmot et al., 1997] and is

### Solvent Accessible Channel

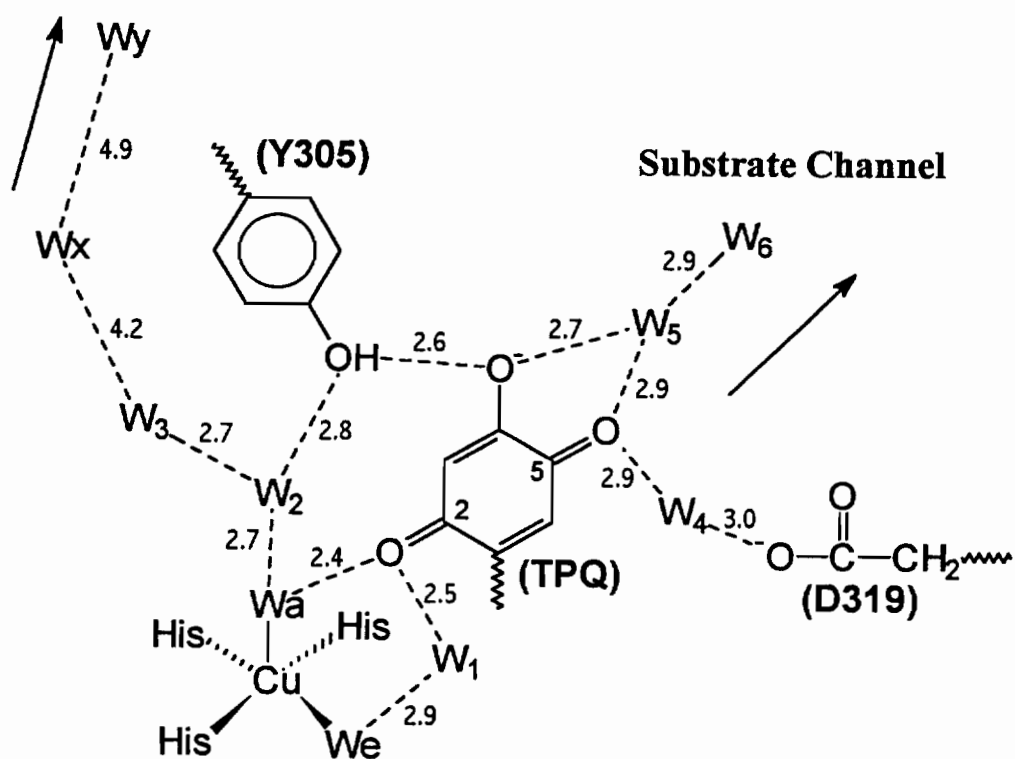


**Fig. 2.14** Immobilized water molecules in the active site of HPAO as detected in the crystal structure at 2.4 Å resolution [adapted from Li et al. 1998].

conserved from the W2 position on for the zinc-substituted copper amine oxidase of *H. polymorpha* [Chen et al., 2000]. The distance to this other solvent-accessible channel is quite large, on the order of 15-Å from the TPQ ring. Although the immobilized waters are potentially solvent exchangeable, the extensive and conserved nature of the H-bonding chain suggests that it is stabilized by the protein environment. Such environmental effects have been well documented for bovine pancreatic trypsin inhibitor, where the rate of amine NH exchange with solvent was found to decrease as much as  $10^5$ -fold for buried amides due to hydrogen-bonding and/or lack of solvent accessibility [Wagner and Wüthrich, 1982]. Thus, it is possible that the slow exchange rates for C3-H or C5=O when they are located on the Cu side of the active site (see also Fig. 1.3) could be due to this site having reduced accessibility to bulk solvent.

#### 2.4.3 Functional Significance of Cofactor Mobility

The ability of the TPQ cofactor to thermodynamically access catalytically nonproductive orientations would appear to be counterproductive for normal enzyme activity. However, copper amine oxidases are unique enzymes in that they self-catalyze the biogenesis of their own organic cofactor as well as providing catalytic activity for the oxidative deamination of primary amine substrates. Cofactor biogenesis has been proposed to begin with a copper-facilitated oxygenation at the C5 position, followed by ring flipping and a copper-facilitated hydroxylation at the C2 position (Scheme 1.1) [Ruggiero et al., 1997; Dove et al., 2000]. Thus, the TPQ precursor ring must be able to rotate through 180° to allow access of both sides of the ring to the Cu site. The ability to incorporate  $^{18}\text{O}$  at the C2 position [Nakamura et al., 1997; Table 2.1] shows that the Cu-binding site is fully accessible to solvent in the apoenzyme. Since only the productive TPQ orientation is expected to promote catalysis, a tightening up of the active site presumably accompanies TPQ formation. This explains why mutations within the active site that lead to increased cofactor mobility (e.g., N404A in HPAO) do not necessarily affect biogenesis but markedly affect catalysis.



## CHAPTER 3

### DETECTION AND CHARACTERIZATION OF REACTION INTERMEDIATES IN AMINE OXIDASE<sup>1</sup>

#### 3.1 Introduction

The redox-active organic cofactor of all known copper-containing amine oxidases (CAOs) has been identified as 2,4,5-trihydroxyphenylalanine (topa) in the reduced form of the enzyme and topaquinone (TPQ) in the oxidized enzyme [Janes et al., 1990]. Recent studies show that this quinone cofactor is derived by the post-translational modification of an active site tyrosine residue by enzyme-bound copper and oxygen [Cai and Klinman, 1994b; Matsuzaki et al., 1994]. The X-ray crystal structures of the amine oxidases from various sources reveal that the TPQ cofactor is situated next to a copper ion and that a cavity on the opposite side of the cofactor is the substrate-binding site [Parsons et al., 1995; Kumar et al., 1996; Wilce et al., 1997; Li et al., 1998]. Covalent adduct formation is known to occur at the C5 carbonyl of TPQ from the reaction of the enzyme and model compounds with substrate analogs such as hydrazines [Janes et al., 1992; Mure and Klinman, 1993, 1995b].

---

<sup>1</sup> Material in this chapter has been published in this or similar form in *Biochemistry* and is used here with permission of the American Chemical Society.

Schwartz, B., Green, E. L., Sanders-Loehr, J., and Klinman, J. P. (1998) Relationship between conserved consensus site residues and the productive conformation for the TPQ cofactor in a copper-containing amine oxidase from yeast. *Biochemistry* **37**, 16591-16600.

Plastino, J., Green, E. L., Sanders-Loehr, J. and Klinman, J. P. (1999) An unexpected role for the active site base in cofactor orientation and flexibility in the copper amine oxidase from *Hansenula polymorpha*. *Biochemistry* **38**, 8204-8216.

CAOs catalyze the oxidative conversion of amine substrates to form the corresponding aldehyde and ammonia, concomitant with a two-electron reduction of molecular oxygen to hydrogen peroxide, to regenerate the oxidized enzyme. There is strong evidence for the reaction to proceed by a pyridoxal-like transamination mechanism (Scheme 1.1) [Klinman and Mu, 1994]. Substrate activation occurs through the covalent addition of amine substrate to cofactor, resulting in the labelization of the hydrogen  $\alpha$  to the nitrogen. This substrate Schiff base intermediate has been detected by rapid scanning spectroscopy [Hartman et al., 1993]. Base-catalyzed abstraction of a methylene proton results in the formation of the product Schiff base that is rapidly hydrolyzed to yield the aminoquinol form of the reduced cofactor and product aldehyde. The cofactor is then reoxidized by molecular oxygen, producing hydrogen peroxide, ammonia, and the oxidized cofactor. Anaerobic single turnover results in release of aldehyde product, whereas  $\text{NH}_3$  is released only upon  $\text{O}_2$ -dependent reoxidation of the reduced cofactor [Janes and Klinman, 1991]. This reaction sequence is supported by extensive studies on model compounds [Mure and Klinman, 1993, 1995a,b; Wang et al., 1994; Lee and Sayre 1995a,b; Lee et al., 1996]. Resonance Raman (RR) spectroscopy has proved to be a valuable technique for both the detection of different reaction intermediates and for providing additional information about their structures.

Utilizing modified enzyme or substrate has led to the formation of various dead-end complexes along the reaction pathway [Cai et al., 1997; Schwartz et al., 1998; Plastino et al., 1999]. Use of a substrate mimic, aniline, leads to the formation of substrate Schiff base [Nakamura et al., 1997]. Mutations of the amino acids flanking the tyrosine precursor leads to the formation of a product Schiff base complex with methylamine as substrate [Cai et al., 1997; Schwartz et al., 1998]. Mutation of the catalytic base allows for the detection of the deprotonated iminoquinone complex [Plastino et al., 1999]. Characterization and detection of all three of these intermediates have strengthened the proposed catalytic mechanism. In this chapter, the enzyme mutations that lead to the buildup of these complexes and the RR characterization of each is discussed in detail.

### 3.1.1 Catalytic-Base Mutants

The role of the active site aspartate in the catalytic mechanism of the copper amine oxidase from *Hansenula polymorpha* (HPAO) has been examined by site-directed mutagenesis. Altering the active site base to an asparagine results in an enzyme that does not turn over substrate [Plastino et al., 1999]. Introduction of a glutamic acid in place of aspartate leads to an enzyme that catalyzes the oxidation of smaller substrates such as methylamine and phenethylamine, but not larger substrates like benzylamine, at a rate approximately 80-fold slower than wild-type HPAO [Plastino et al., 1999]. This dramatic decrease in the catalytic rate of D319E has been attributed to a flipped (nonproductive) orientation of the TPQ cofactor in the absence of substrate, based on RR evidence that the C5 carbonyl is less solvent accessible and the C3 hydrogen is more solvent accessible than seen in wild-type [Chapter 2]. The enzymatic reaction is initiated by flipping of the cofactor into a productive orientation upon substrate binding [Plastino et al., 1999].

Under conditions of saturating methylamine and oxygen, the D319E mutant of HPAO accumulates a new species with a 428-nm absorption maximum. The D319N mutant produces a similar absorbance at 430 nm when treated with ammonia, despite the fact that this mutant has no observable amine oxidase activity. RR spectroscopic examinations of the ammonia adduct of D319N and the steady-state species of D319E methylamine oxidation indicate that the observed species in both cases is the deprotonated iminoquinone with a flipped TPQ orientation (Fig. 3.1). These results, together with the cofactor solvent exchange data, indicate a central role for the catalytic base in positioning the free cofactor and enzyme intermediates for optimal activity.

### 3.1.2 Flanking Residue Mutations

All known CAOs have the consensus site sequence **Asn-Tyr\*-Asp/Glu-Tyr-Asn** (residues 404–407 in HPAO) [Janes et al., 1992]. A post-translational modification of the Tyr405 residue results in the formation of the TPQ cofactor. The highly conserved asparagine residue at position 404 in HPAO has its side chain residing proximal to the TPQ ring in X-ray crystal structures [Parsons et al., 1995;

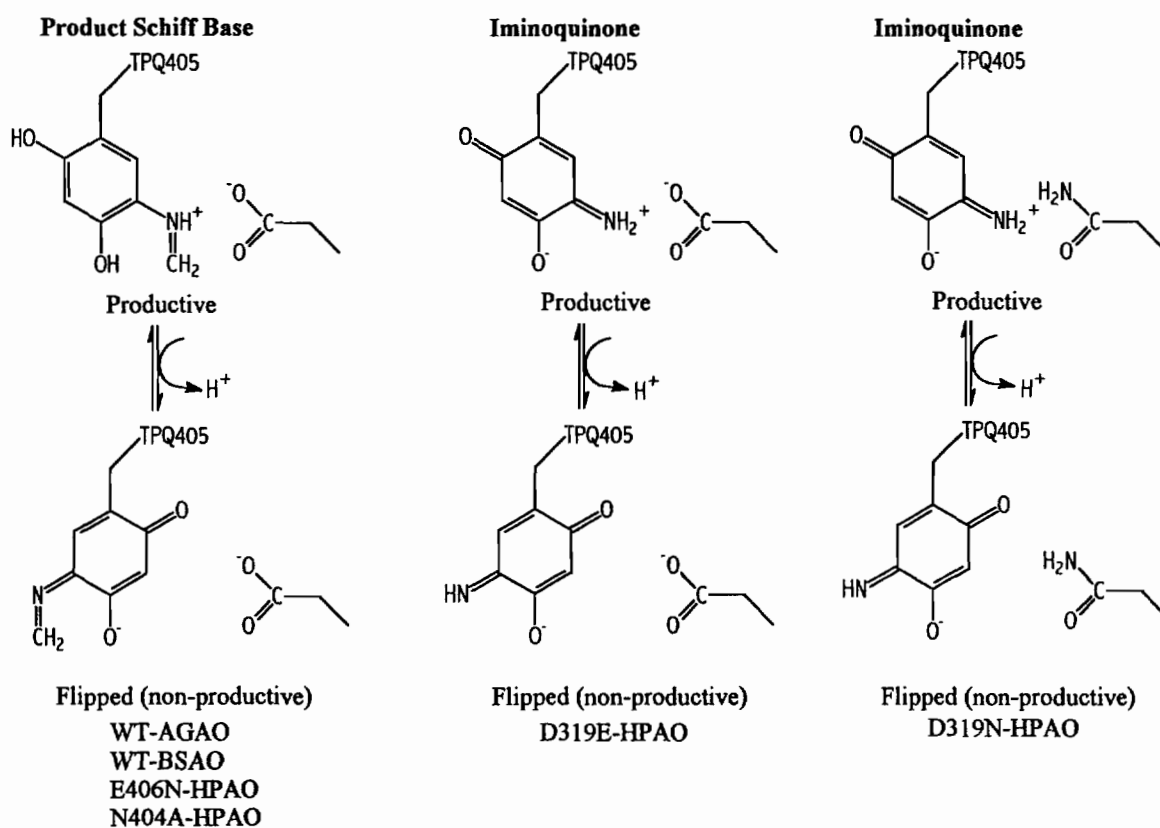


**Fig. 3.1** Flipped (nonproductive) intermediates observed during reaction of amine oxidases with methylamine or ammonia.

Kumar et al., 1996; Wilce et al., 1997; Li et al., 1998]. In this study, the conserved asparagine was mutated to an alanine, and the mutant's catalytic properties were characterized using electronic absorption and RR spectroscopy. Accumulation of an inactive product Schiff base complex upon incubation with methylamine substrate leads to the conclusion that the TPQ cofactor exists in a nonproductive, flipped orientation in this form of the enzyme (Fig. 3.1). Previously, a similar product Schiff base complex with methylamine substrate was observed following mutation of another flanking conserved consensus site residue, a glutamate to an asparagine at position 406 in HPAO [Cai et al., 1997]. The results of these studies suggest that these two flanking residues are crucial in maintaining the proper orientation of the TPQ cofactor during catalysis.

## 3.2 Experimental Procedures

### 3.2.1 Sample Preparation

Mutagenesis and protein purification were performed as described previously [Schwartz et al., 1998; Plastino et al., 1999]. For RR studies, a stock solution of the D319N mutant (1.25 mM in protein monomer,  $\sim 0.75$  in TPQ) was prepared in 50 mM potassium pyrophosphate (pH 9.0). Adducts were prepared by the addition of 3 M ammonium chloride which yielded final concentrations of 0.5 M ammonium chloride and 0.6 mM TPQ. Isotopic labeling was performed by the addition of [ $^{15}\text{N}$ ]ammonium chloride (99 atom %  $^{15}\text{N}$ , Cambridge Isotope Laboratories) prepared in  $\text{H}_2\text{O}$  or  $\text{D}_2\text{O}$ , as needed. The  $\text{D}_2\text{O}$  sample was prepared by diluting the 1.25 mM protein 10-fold in  $\text{D}_2\text{O}$  buffer (pH reading 9.0) and allowed to incubate for 22 h at  $4^\circ\text{C}$  before reconcentration back to 1.25 mM protein by ultrafiltration (Microcon-30, Amicon).

A stock solution of D319E (1.0 mM protein monomer,  $\sim 0.45$  mM TPQ) was prepared in 50 mM potassium pyrophosphate (pH 7.0). Formation of the methylamine adduct was initiated by the addition of 250 mM methylamine, yielding final concentrations of 42 mM methylamine and 0.38 mM TPQ. The protein and methylamine solutions were flushed with  $\text{O}_2$  gas for 10 min to ensure  $\text{O}_2$  saturation

for the reaction. These solutions were transferred in gastight syringes to a preflushed sample holder, a modified Pasteur pipet that was flame-sealed at the capillary end and fitted with a rubber serum stopper on the other [Loehr and Sanders-Loehr, 1993]. Raman spectra were collected immediately after mixing as a series of 1-min scans. Isotopic labeling was performed by the addition of [ $^{15}\text{N}$ ]methylamine (98 atom %  $^{15}\text{N}$ , Cambridge Isotope Laboratories), or [ $^2\text{H}_3$ ]methylamine (98 atom % D, Aldrich), or by preparation of the protein and substrate in  $\text{D}_2\text{O}$ , as described above.

A stock solution of N404A (0.88 mM protein monomer,  $\sim 0.50$  mM TPQ) was prepared in potassium pyrophosphate buffer (pH 9.0). The methylamine adduct was formed by the addition of methylamine to yield final concentrations of 0.17 M methylamine and 0.42 mM TPQ. Isotopic labeling was performed by the addition of [ $^2\text{H}_3$ ]methylamine (98 atom % D). A  $\text{D}_2\text{O}$  protein sample was prepared by diluting the 0.88 mM protein 10-fold in  $\text{D}_2\text{O}$  buffer (pH reading 9.0) and reconcentrating back to 0.88 mM protein by ultrafiltration, followed by exchange for 20 h at  $4^\circ\text{C}$ . Then, deuterated methylamine ( $\text{ND}_2\text{CH}_3$ ) was added to yield final concentrations of 0.17 M amine and 0.42 mM TPQ.

### 3.2.2 Resonance Raman Spectroscopy

Raman spectra were collected on a McPherson 2061 spectrograph (0.67 m, 1800-groove grating for the D319 samples, 2400-groove grating for N404A) using Kaiser Optical holographic supernotch filters and a Princeton Instruments (LN-1100PB) liquid  $\text{N}_2$ -cooled CCD detector. The excitation source was a Coherent Innova 90-6 Ar $^+$  laser (D319N and D319E) or a Coherent Innova 302 Kr laser (N404A). Spectra were collected from samples in capillary tubes, cooled to ice temperature in a copper coldfinger, using 514.5 nm excitation (30 mW) (D319 samples) or 413.1 nm excitation (20 mW) (N404A),  $90^\circ$  scattering geometry, and a  $4\text{ cm}^{-1}$  spectral resolution. Peak frequencies were calibrated relative to an indene standard and are accurate to  $\pm 1\text{ cm}^{-1}$ . Spectra of samples substituted with isotopes were obtained under identical instrumental conditions such that frequency shifts are accurate to  $\pm 0.5\text{ cm}^{-1}$  [Loehr and Sanders-Loehr, 1993]. Spectral data were accumulated for 15 min.

### 3.3 Results and Discussion

#### 3.3.1 Ammonia Adduct of D319N and Methylamine Adduct of D319E

The ammonium ion complex of D319N and the steady-state species formed with D319E during methylamine turnover exhibit similar absorption maxima at 430 and 428 nm, respectively (Fig. 3.2). RR spectroscopy of the complexes was undertaken to determine if they represent covalent adducts of the TPQ cofactor. The ammonium complex of D319N offers a simplified system, since the only possible adducts are the carbinolamine and iminoquinone species. As shown in Fig. 3.3, the C5 carbonyl stretch of TPQ at  $1675\text{ cm}^{-1}$  is no longer present in the ammonium ion complex of D319N. Instead, two new peaks are observed at  $1643$  and  $1603\text{ cm}^{-1}$ . Previously, a  $1603\text{ cm}^{-1}$  peak was identified as the substrate imine C=N stretch in the aniline adduct of AGAO [Nakamura et al., 1997]. Isotopic replacement of  $[^{14}\text{N}]$ ammonium chloride with  $[^{15}\text{N}]$ ammonium chloride in the D319N adduct results in a shift of the  $1603\text{ cm}^{-1}$  peak by  $-11\text{ cm}^{-1}$ , positively identifying this peak as the imine species (Fig. 3.3). This is the expected shift for a change of 1 mass unit, given that the change of 2 mass units in the substitution of  $^{18}\text{O}$  for  $^{16}\text{O}$  at C5 produces a shift of approximately  $-25\text{ cm}^{-1}$ . Solvent  $\text{D}_2\text{O}$  had little effect on the  $[^{14}\text{N}]$ ammonia adduct, but shifted the imine stretch  $-9\text{ cm}^{-1}$  further in the  $[^{15}\text{N}]$ ammonia adduct (Fig. 3.3). This shift is most consistent with a change of 1 mass unit, indicating the presence of one deuterium on the imine nitrogen. These data suggest that the ammonia adduct of D319N is the deprotonated iminoquinone (Fig. 3.1).

The RR study of the methylamine adduct of D319E was complicated by the fact that D319E turns over methylamine. Since diffusion of oxygen into the capillary was poor, the oxygen in the sample was rapidly depleted and the steady-state 430 nm species was quickly replaced by the reduced cofactor. The data shown in Fig. 3.4 indicate the initial formation of a species highly analogous to the ammonia adduct of D319N, with a small peak at  $1607\text{ cm}^{-1}$  and a larger peak at  $1648\text{ cm}^{-1}$ . The differences in peak frequency between the D319E and D319N data may be indicative of slightly altered active site environments in the two enzymes. The  $1607\text{ cm}^{-1}$  peak of the D319E methylamine adduct shifts  $-12\text{ cm}^{-1}$  with  $[^{15}\text{N}]$ methylamine, similar to

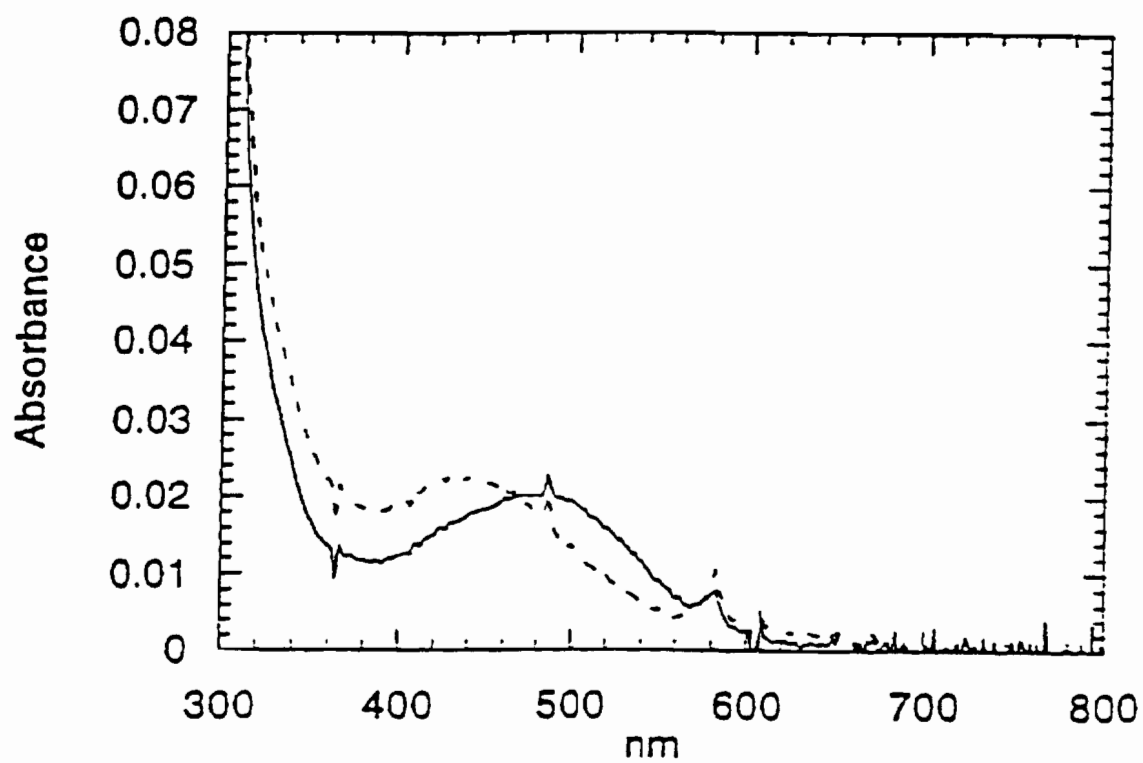


**Fig. 3.2** Reaction of D319E with methylamine: (—) D319E alone; (---) D319E reaction with methylamine. The conditions were 18  $\mu$ M D319E, 12 mM methylamine, 50 mM phosphate, pH 7.2, and 20°C.



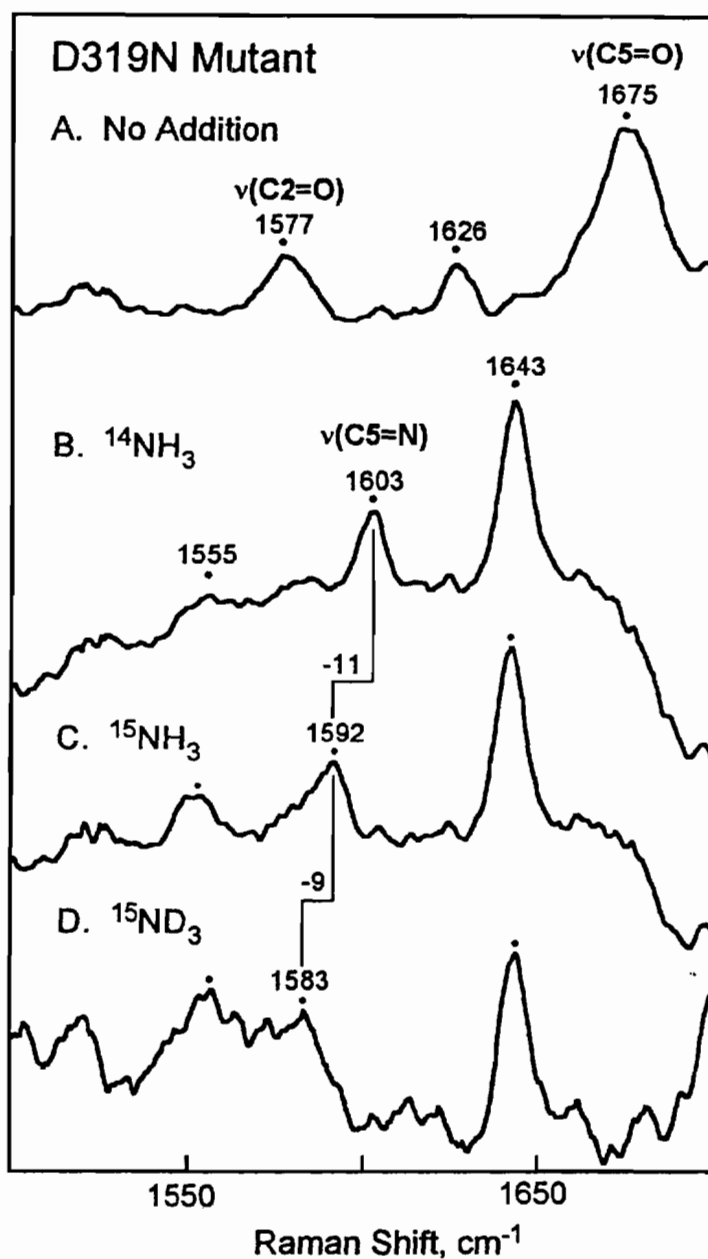


**Fig. 3.3** Resonance Raman spectra of the ammonia adduct of D319N. Samples were prepared with (B)  $^{14}\text{NH}_4\text{Cl}$  in  $\text{H}_2\text{O}$ , (C)  $^{15}\text{NH}_4\text{Cl}$  in  $\text{H}_2\text{O}$ , (D)  $^{15}\text{NH}_4\text{Cl}$  in  $\text{D}_2\text{O}$ , and with (A) no added  $\text{NH}_4\text{Cl}$ . Data were obtained using 15-min data accumulation, and spectra were corrected for water and protein bands by subtraction of the apoprotein spectrum. Frequency shifts relative to spectrum A are indicated above peaks, and peaks with frequencies identical to those of spectrum A are unlabeled.

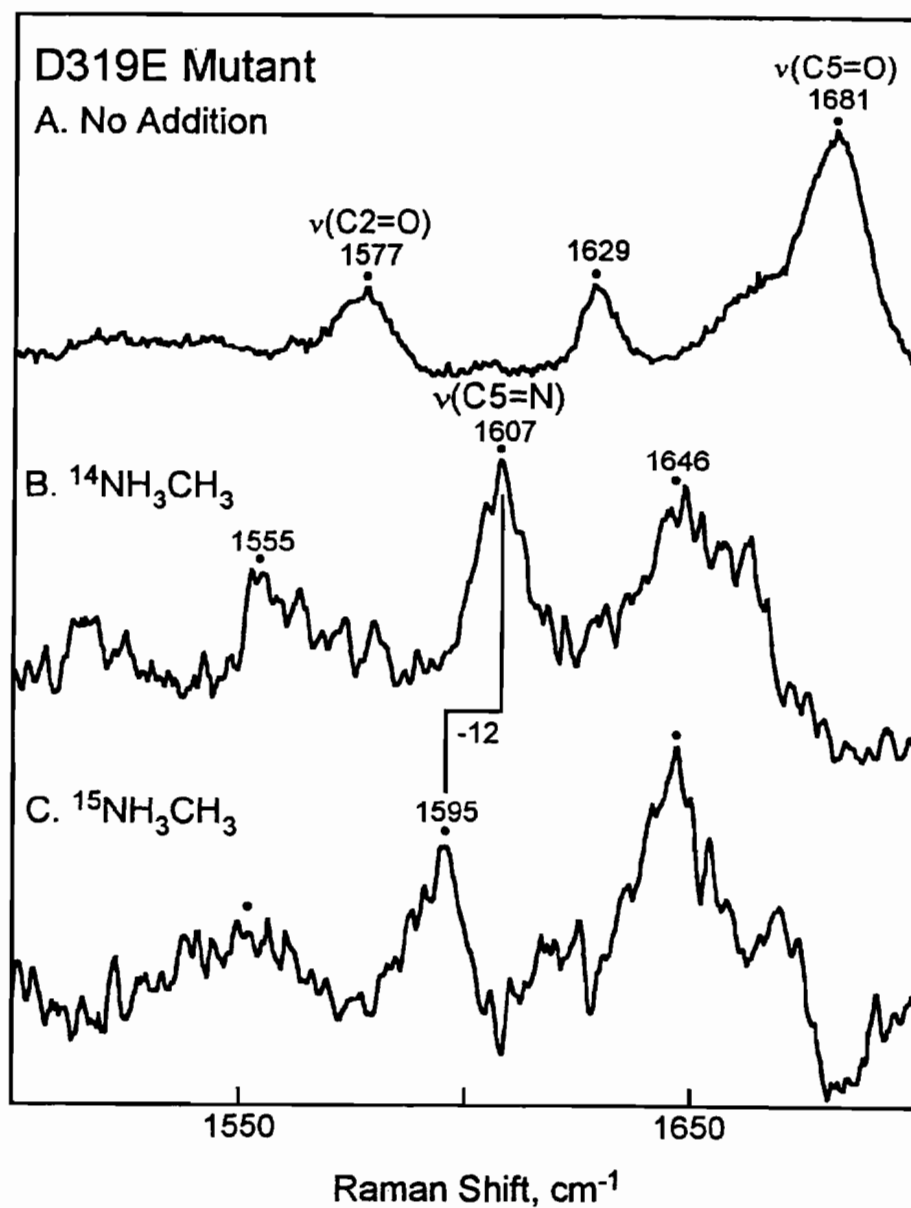


**Fig. 3.4** Resonance Raman spectra of the methylamine adduct of D319E. Samples were prepared with (B)  $^{14}\text{NH}_3\text{CH}_3$  in  $\text{H}_2\text{O}$ , (C)  $^{15}\text{NH}_3\text{CH}_3$  in  $\text{H}_2\text{O}$ , and with (A) no added methylamine. Data were obtained using 2-min data accumulations, and spectra were corrected for water and protein bands by subtraction of the apoprotein spectrum. Frequency shifts relative to spectrum A are indicated above peaks, and peaks with frequencies identical to those of spectrum A are unlabeled.

the shift observed with [ $^{15}\text{N}$ ]-ammonium chloride and D319N (Figs. 3.3 and 3.4). The  $1607\text{ cm}^{-1}$  peak does not shift to lower energy in  $\text{D}_2\text{O}$ ; however, we note that while there is a further shift of  $-9\text{ cm}^{-1}$  with  $\text{D}_2\text{O}$  for the [ $^{15}\text{N}$ ]methylamine complex of D319N, there is no effect of  $\text{D}_2\text{O}$  on the [ $^{14}\text{N}$ ]methylamine sample (Fig. 3.3). This could mean that the  $\text{C}=\text{}^{14}\text{N}$  is more coupled to other modes than the  $\text{C}=\text{}^{15}\text{N}$  stretch. No shifts are apparent upon adduct formation with [ $^2\text{H}_3$ ]methylamine, which indicates that the methyl group of the substrate is no longer present in the methylamine adduct of D319E. This helps to rule out the possibility that the 430 nm species is the substrate Schiff base, although the signal-to-noise ratio in this experiment is such that a small isotopic shift could have gone undetected. However, the similarity of the RR data for the methylamine adduct of D319E and the ammonia adduct of D319N strongly suggests that the species accumulating during methylamine turnover by D319E is the deprotonated iminoquinone.

Further evidence for the assignment of a deprotonated iminoquinone rests in the UV/Vis characterization of the ammonia adduct of D319N and the methylamine adduct of D319E. The reaction of BSAO and ammonia at pH 9.13 produced a 450 nm absorbance [Mure and Klinman, 1993], and 448–450 nm absorbances have been observed for iminoquinone model compounds [Mure and Klinman, 1993, 1995b]. The only adduct formed by reaction of the D319N mutant with ammonium ion at pH 9.0 is the iminoquinone with an absorption maximum at 430 nm (Fig. 3.2). The blue shift of the absorbance band from 450 nm in the model compounds and BSAO complex to 430 nm in the D319N mutant is consistent with deprotonation of the iminoquinone.

The substrate Schiff base (Scheme 1.1) has an iminoquinone structure similar to that formed from the reaction of the D319N mutant with ammonia, and a deprotonated substrate Schiff base model compound was found to have a 454-nm absorption maximum [Mure and Klinman, 1995b]. The deprotonated substrate Schiff base formed by the reaction of AGAO with aniline has its absorption maximum at 450 nm and its  $\text{C5}=\text{N}$  stretch at  $1603\text{ cm}^{-1}$  [Nakamura et al., 1997], close to the  $\nu(\text{C5}=\text{N})$  values for the D319 mutants (Figs. 3.3 and 3.4). Thus, the question arises whether the 428-nm absorption in the D319E mutant reacted with methylamine could

be due to a substrate Schiff base rather than the postulated iminoquinone (Fig. 3.1). The major arguments in favor of the deprotonated iminoquinone are the  $\sim 20$  nm lower value for the absorption maximum and the absence of a shift with  $[^2\text{H}_3]\text{methylamine}$  in the RR spectrum of the D319E product.

### 3.3.2 Methylamine Adduct of N404A

A previous flanking residue mutant of HPAO (E406N) displayed rapid, reversible inhibition when incubated with methylamine substrate [Cai et al., 1997]. The methylamine adduct exhibited a characteristic absorbance at 380 nm that was shown by RR spectroscopy to be due to the deprotonated product Schiff base complex (Fig. 3.1). The flanking residue on the other side of the cofactor, the asparagine at position 404 in HPAO, has now been mutated to an alanine [Schwartz et al., 1998]. Incubation of N404A with methylamine results in the appearance of a similar absorbance at 380 nm. As with E406N, this species is not formed when N404A is incubated with larger substrates such as ethylamine or phenethylamine [Cai et al., 1997; Schwartz et al., 1998].

In the earlier study of E406N reacted with methylamine [Cai et al., 1997], the RR spectrum was dominated by an intense  $\text{C}=\text{N}$  stretch at  $1622\text{ cm}^{-1}$  (Fig. 3.5A) that shifted  $-59\text{ cm}^{-1}$  upon deuteration of the substrate methyl group (Fig. 3.5C) and was unaffected by deuteration of the amino group (Fig. 3.5B). Using a simple two-body approximation to calculate expected isotopic shifts with deuterated methylamine ( $\text{CD}_3\text{NH}_2$ ), the expected shift for the substrate and product Schiff base complexes would be  $-22$  and  $-52\text{ cm}^{-1}$ , respectively [Nakamura et al., 1997]. The observed isotopic shift of  $-59\text{ cm}^{-1}$  supported the product Schiff base assignment. A lack of isotopic sensitivity of the  $1622\text{ cm}^{-1}$  peak in  $\text{D}_2\text{O}$  indicated that the product Schiff base nitrogen was deprotonated. Similar deprotonated product Schiff base species have been observed by RR spectroscopy for methylamine adducts of wild-type AGAO and BSAO, where the  $\text{C}=\text{N}$  stretching assignment was further verified by a  $-19\text{ cm}^{-1}$  shift with  $\text{CH}_3^{15}\text{NH}_2$  [Nakamura et al., 1997].

The Raman spectrum of the N404A methylamine adduct is similarly dominated by an intense peak at  $1622\text{ cm}^{-1}$  (Fig. 3.5D) that undergoes a similar shift of  $-58\text{ cm}^{-1}$

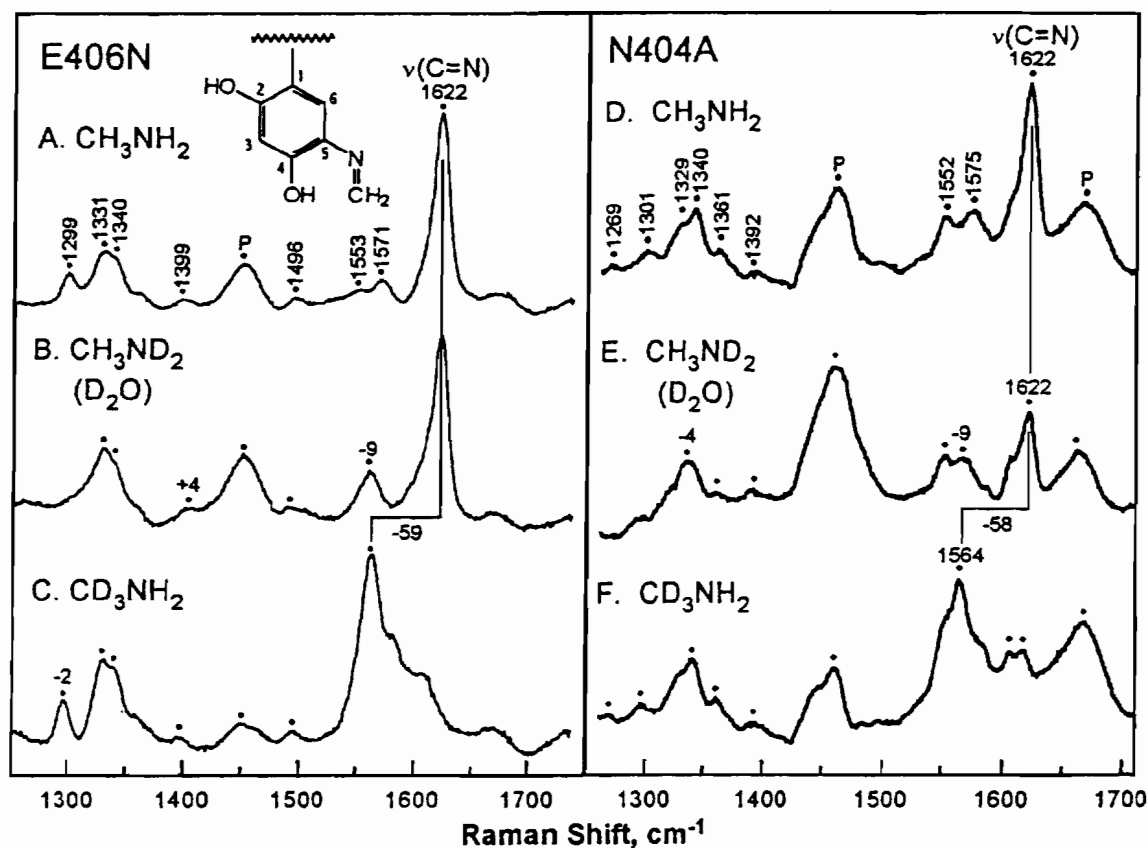


**Fig. 3.5** Resonance Raman spectra of methylamine adducts. Samples of E406N were prepared with (A) CH<sub>3</sub>NH<sub>2</sub> in H<sub>2</sub>O, (B) CH<sub>3</sub>NH<sub>2</sub> in D<sub>2</sub>O, and (C) CD<sub>3</sub>NH<sub>2</sub> in H<sub>2</sub>O [data from Cai et al., 1997]. Samples of H404A (0.42 mM in TPQ) were prepared with (D) CH<sub>3</sub>NH<sub>2</sub> in H<sub>2</sub>O, (E) CH<sub>3</sub>NH<sub>2</sub> in D<sub>2</sub>O, and (F) CD<sub>3</sub>NH<sub>2</sub> in H<sub>2</sub>O. P indicates residual peaks from the apoprotein. Frequency shifts relative to spectrum A are indicated above peaks, and peaks with frequencies identical to those of spectrum A are unlabeled.

with  $\text{CD}_3\text{NH}_2$  (Fig. 3.5F), thereby positively identifying this peak as the  $\text{C}=\text{N}$  stretch of the product Schiff base complex. As in the case of E406N, the N404A adduct failed to exhibit any shift in the  $\text{C}=\text{N}$  stretch with  $\text{CH}_3\text{ND}_2$  in  $\text{D}_2\text{O}$  (Fig. 3.5E), thereby indicating a lack of exchangeable proton on the  $\text{C}=\text{N}$  moiety. The  $\text{D}_2\text{O}$ -dependent shifts of  $-4$  and  $-9\text{ cm}^{-1}$  for the peaks at  $1340$  and  $1575\text{ cm}^{-1}$ , respectively, were observed previously for the methylamine adduct of BSAO [Nakamura et al., 1997] and are ascribed to exchange of the C3 hydrogen of the TPQ cofactor. This would indicate that the C3 hydrogen is more solvent accessible than in wild-type HPAO, lending further proof that the TPQ ring adduct is in a flipped conformation.

### 3.4 Conclusions

The crystal structure of wild-type HPAO shows the cofactor to be properly oriented in the active site with the C5 carbonyl bridged to the active site aspartate, position 319 in HPAO, through a conserved water molecule (Fig. 2.14) [Li et al., 1998]. This interaction may serve to hold the cofactor in a productive conformation in the wild-type HPAO protein. When the aspartate is mutated to either a glutamate or an asparagine, the hydrogen bonding network holding the cofactor in place is expected to be altered, allowing the cofactor to adopt a nonproductive orientation in the resting form of the mutant enzyme. This is supported by the solvent exchange data for the C5 carbonyl and the C3 hydrogen of the TPQ cofactor (Chapter 2). Incorporating what we know about the flexibility of the underivatized cofactor in the active site base mutant enzymes, we propose that the accumulation of the iminoquinone complex with the mutant enzyme results from a rapid rotation of this intermediate into a similar flipped nonproductive orientation which is less accessible to hydrolysis. Deprotonation, as indicated from RR and electronic absorption studies, occurs as a consequence of cofactor rotation away from the active site base counterion and its removal from the environment of the substrate-binding site. The outcome of the analysis of the catalytic base mutants is that, in addition to catalysis of proton abstraction from substrate, the aspartate also helps to maintain the resting cofactor and enzyme intermediates in a reactive orientation. However, the tendency of other

species of wild-type and mutant amine oxidases to have flipped cofactor orientations, despite the presence of aspartate as the catalytic base, shows that other factors are also involved in cofactor orientation.

Residing proximal to the aromatic face of the TPQ ring in the crystal structure of wild-type HPAO, the amide side chain of N404 could likely form a hydrogen bond between the amide nitrogen and the  $\pi$  face of the TPQ ring [Li et al., 1998]. This type of amide/aromatic hydrogen bond is well documented in crystal structures and can contribute a considerable amount of stabilization energy to the TPQ ring to hold it in a particular conformation [Mitchell et al., 1994]. This interaction may be additionally strengthened by means of an unusual hydrogen bond found between the N404 amide side-chain oxygen and its own backbone amide nitrogen, which would make the side chain amide nitrogen less electronegative, therefore increasing its hydrogen-donating ability [Li et al., 1998; Schwartz et al., 1998]. Thus, the asparagine flanking residue at position 404 in HPAO is important for maintaining the integrity of the active site. Mutation of this residue to alanine leads to a more mobile cofactor. In the resting form of the N404A mutant, this increased mobility compared to wild-type is seen in the rapid exchange of both the C5 carbonyl and the C3 hydrogen with solvent (Chapter 2). The product Schiff base formed upon reaction of N404A with methylamine (Fig. 3.5) shows an even greater tendency to remain flipped in the nonproductive orientation, as evidenced by its deprotonation and lack of reactivity. Similar deprotonated product Schiff bases have been identified by RR spectroscopy for the reaction of methylamine with wild-type BSAO, wild-type AGAO, as well as the E406N flanking-residue mutant of HPAO [Nakamura et al., 1996; Cai et al., 1997]. The accumulation of the dead-end complex in wild-type enzymes is an indication that these enzymes are not designed to utilize small substrates like methylamine and that additional active site structural features are involved in determining substrate specificity.

The crystal structure of wild-type HPAO shows the TPQ cofactor to be in a catalytically productive conformation, stabilized by hydrogen bonds to a network of water molecules throughout the active site pocket [Li et al., 1998]. This structure raises the possibility that any mutation within the active site pocket could disrupt this

hydrogen bonding network and thus allow the cofactor to adopt alternate conformations that are quite different from the optimal configuration for catalysis. It is believed that multiple conformational states arise during biogenesis [Wilce et al., 1997], whereas only one active conformation is expected during substrate catalysis; thus, the active site in this class of enzymes represents a careful balance between these conflicting requirements. D319 and N404 have been shown herein to be essential elements in maintaining this balance, and mutations of these residues result in the cofactor readily displaying biogenesis-like characteristics of cofactor mobility during catalysis. Interestingly, neither the flanking residue mutations (N404A and E406Q) nor the catalytic base mutations (D319E or D319N) inhibit cofactor biogenesis, suggesting that the autocatalytic oxidation of Tyr405 to TPQ has less stringent environmental requirements.



## CHAPTER 4

### RESONANCE RAMAN CHARACTERIZATION OF THE HEME COFACTOR IN CYSTATHIONINE $\beta$ -SYNTHASE. IDENTIFICATION OF THE Fe-S(Cys) VIBRATION IN THE SIX-COORDINATE LOW-SPIN HEME<sup>1</sup>

#### 4.1 Introduction

Human cystathionine  $\beta$ -synthase (CBS) is a unique heme protein that catalyzes a pyridoxal phosphate-dependent condensation of serine and homocysteine to generate cystathionine. This enzyme is clinically important since it represents one of two major metabolic avenues for the removal of homocysteine in humans. Elevated levels of homocysteine are correlated with cardiovascular diseases [Refsum et al., 1998], neural tube defects [Mills et al., 1995], and Alzheimer's disease [Clarke et al., 1998]. Mutations in CBS are the single most common cause of homocystinuria, an inborn error of metabolism that results in very high levels of circulating homocysteine with attendant cardiovascular complications [Mudd et al., 1995].

The sequences of the human, rat, and yeast cystathionine  $\beta$ -synthase reveal that they are quite similar. However, the yeast enzyme is devoid of heme [Jhee et al., 2000]. This suggests that evolutionarily, the heme is a relatively recent acquisition, and argues against an essential catalytic role for this cofactor. However, the activity of human CBS is modulated by oxidation [Taoka et al., 1998], ligation

---

<sup>1</sup> This material has been published in this or similar form in *Biochemistry* and is used here with permission of the American Chemical Society.

Green, E. L., Taoka, S., Banerjee, R., and Loehr, T. M. (2001) Resonance Raman characterization of the heme cofactor in cystathionine  $\beta$ -synthase. Identification of the Fe-S(Cys) vibration in the six-coordinate low-spin heme. *Biochemistry* **40**, 459-463.

[Taoka et al., 1999a], and coordination state [Taoka and Banerjee, 2001] changes in the heme, suggesting a possible regulatory role for the heme cofactor.

To define the role of the heme in this enzyme, experiments are underway to characterize its properties. Recent electron paramagnetic resonance (EPR) and X-ray absorption spectroscopic studies of the human enzyme implicated histidine and cysteine as the axial heme ligands in both the ferric and ferrous states [Ojha et al., 2000]. In the oxidized enzyme, the heme is low spin and six-coordinate and exhibits a Soret peak at 428 nm [Taoka et al., 1998]. Treatment of the enzyme with the thiol chelator  $\text{HgCl}_2$  results in conversion of the low-spin heme to a high-spin species [Ojha et al., 2000]. Reduction of the heme results in a large red shift of the Soret peak to 450 nm, consistent with retention of the thiolate ligand in the six-coordinate heme [Dawson and Sono, 1987].

In this study, we have used resonance Raman (RR) spectroscopy to characterize the heme in human cystathionine  $\beta$ -synthase. The Fe-S(Cys) vibration in the ferric enzyme has been observed at  $312\text{ cm}^{-1}$  and verified by global  $^{34}\text{S}$  labeling of the enzyme. This is the first detection of an iron-sulfur stretching frequency ( $\nu(\text{Fe-S})$ ) in a six-coordinate low-spin (6cLS) heme. This identification has permitted us to evaluate directly whether or not the thiolate substrate, homocysteine, coordinates to the heme in CBS by displacement of the active site cysteine ligand, as had been postulated [Taoka et al., 1998]. Our results indicate that homocysteine does *not* replace cysteine as a ligand in the binary complex. Further studies of the ferric and ferrous enzymes in the presence of  $\text{HgCl}_2$  and of the ferrous-CO complex confirm the presence of cysteine and histidine as the axial ligands to the heme in human cystathionine  $\beta$ -synthase.

## 4.2 Materials and Methods

### 4.2.1 Chemicals

The following materials were obtained from Sigma Chemical Co.: L-homocysteine thiolactone,  $\delta$ -aminolevulinic acid, sodium dithionite, IPTG, and  $\text{HgCl}_2$ . Homocysteine was prepared from L-homocysteine thiolactone as described previously

[Drummond et al., 1995]. Sodium [ $^{34}\text{S}$ ]sulfate (93%  $^{34}\text{S}$ ) was from ICON (Marion, NY).

#### 4.2.2 Enzyme Labeling and Purification

The truncated and highly active form of human CBS lacking 143 amino acids at the C-terminus was purified from *E. coli* containing the expression vector pGEXCBSN [Shan and Kruger, 1998] provided by Warren Kruger (Fox Chase Cancer Center, Philadelphia). The cells were cultured, and the protein was purified as described previously [Taoka et al., 1999b]. For global  $^{34}\text{S}$ -labeling of CBS, 10 mL of an overnight culture (in LB medium at 25°C) was used to inoculate 1 L of M9 minimal medium containing 75 mg of ampicillin. The minimal medium was supplemented with 10 mL of modified mineral salt solution (in which the sulfate salts were replaced with chloride salts in the original recipe [Jeter and Ingraham, 1984], 4 mL of a nitrogen stock solution [Jeter and Ingraham, 1984], 284 mg of sodium [ $^{34}\text{S}$ ]sulfate, and 40 mg of each of the amino acids except methionine. The cells were grown at 25°C and, at an  $\text{OD}_{600}$  of 0.5, 75 mg of  $\delta$ -aminolevulinic acid and 0.1 mM IPTG (final concentration) were added. The cells were harvested after 21 h when the  $\text{OD}_{600}$  was  $\sim 1.8$ . Approximately 6 g of cell paste (wet weight) were obtained from a 1 L culture and yielded 13 mg of  $^{34}\text{S}$ -labeled cystathionine  $\beta$ -synthase after purification.

#### 4.2.3 Resonance Raman Samples

Stock solutions of oxidized CBS (native unlabeled and globally  $^{34}\text{S}$ -labeled) were in 100 mM Tris buffer (pH 8.6) at a concentration of  $\sim 200\ \mu\text{M}$  ferric heme. For RR measurements, these solutions were diluted 2-fold with 50 mM Tris buffer (pH 8.6), and aliquots of these  $\sim 100\ \mu\text{M}$  heme solutions were transferred to glass capillaries. Samples of reduced CBS were prepared in a Coy anaerobic glovebox. First, oxidized CBS was equilibrated with the anoxic atmosphere ( $\text{N}_2$ ,  $\text{CO}_2$ ,  $\text{H}_2\text{O}$ , and  $\text{H}_2$ ) over several hours to exchange the dissolved oxygen. Two microliters of freshly prepared 40 mM sodium dithionite was then added to a 15  $\mu\text{L}$  aliquot of the deaerated solution to give a final concentration of  $\sim 90\ \mu\text{M}$  ferrous heme. The reduced CBS

solution was transferred to sealed Pasteur pipets, and capped with rubber septa to maintain anaerobicity. Reduction of the heme was monitored by UV/Vis spectroscopy on samples in the Pasteur pipettes [Loehr and Sanders-Loehr, 1993], with the shift of the Soret peak from 428 to 450 nm indicating the extent of reduction (Fig. 4.1). Samples of the oxidized enzyme were also treated with  $\text{HgCl}_2$  to give final concentrations of  $\sim 90 \mu\text{M}$  heme and 1 mM  $\text{HgCl}_2$  resulting in a shift in the sharp Soret band at 428 nm to a broad band at 390 nm. The  $\text{HgCl}_2$ -treated sample was then made anaerobic by placing the solution in the glovebox for several hours and reduced with dithionite to give a final concentration of  $\sim 80 \mu\text{M}$  heme and  $\sim 0.9 \text{ mM}$   $\text{HgCl}_2$ . CO binding to reduced cystathionine  $\beta$ -synthase is indicated by a shift of the Soret peak from 450 to 422 nm (Fig. 4.1). CO adducts of CBS were prepared by injection of 2 mL of gas ( $^{12}\text{CO}$ , CP grade, Air Products; or  $^{13}\text{CO}$ , 99%  $^{13}\text{C}$ , Cambridge Isotope Laboratories) into sealed Pasteur pipets containing the ferrous enzyme at a concentration of  $\sim 90 \mu\text{M}$  heme. All RR experiments were performed at least in duplicate on separate days to confirm all vibrational frequencies and intensities. Optical absorbance spectra were collected on a Perkin-Elmer Lambda 9 UV/Vis spectrophotometer.

#### 4.2.4 Resonance Raman Spectroscopy

Resonance Raman spectra were collected on a custom McPherson 2061/207 spectrograph set to a focal length of 0.67 m, fitted with a 2400 groove/mm grating, a Kaiser Optical holographic supernotch filter, and a Princeton Instruments (LN-1100PB) liquid- $\text{N}_2$ -cooled CCD detector. The excitation sources were an Innova 302 Kr laser (413.1 nm) and a LiConix 4240NB HeCd laser (441.6 nm). Spectra were collected from samples contained in glass capillary tubes or Pasteur pipets fitted with rubber septa, in a  $90^\circ$  scattering geometry, and a  $4 \text{ cm}^{-1}$  spectral resolution. Data were accumulated at 5–10 min intervals for all samples. Frequencies were calibrated relative to indene,  $\text{CCl}_4$ ,  $\text{CD}_3\text{CN}$ , aspirin, and  $^{14}\text{NO}$  as standards and are accurate to  $\pm 1 \text{ cm}^{-1}$ . Spectra of samples substituted with isotopes were obtained under identical instrumental conditions such that frequency shifts are accurate to  $\pm 0.5 \text{ cm}^{-1}$ .

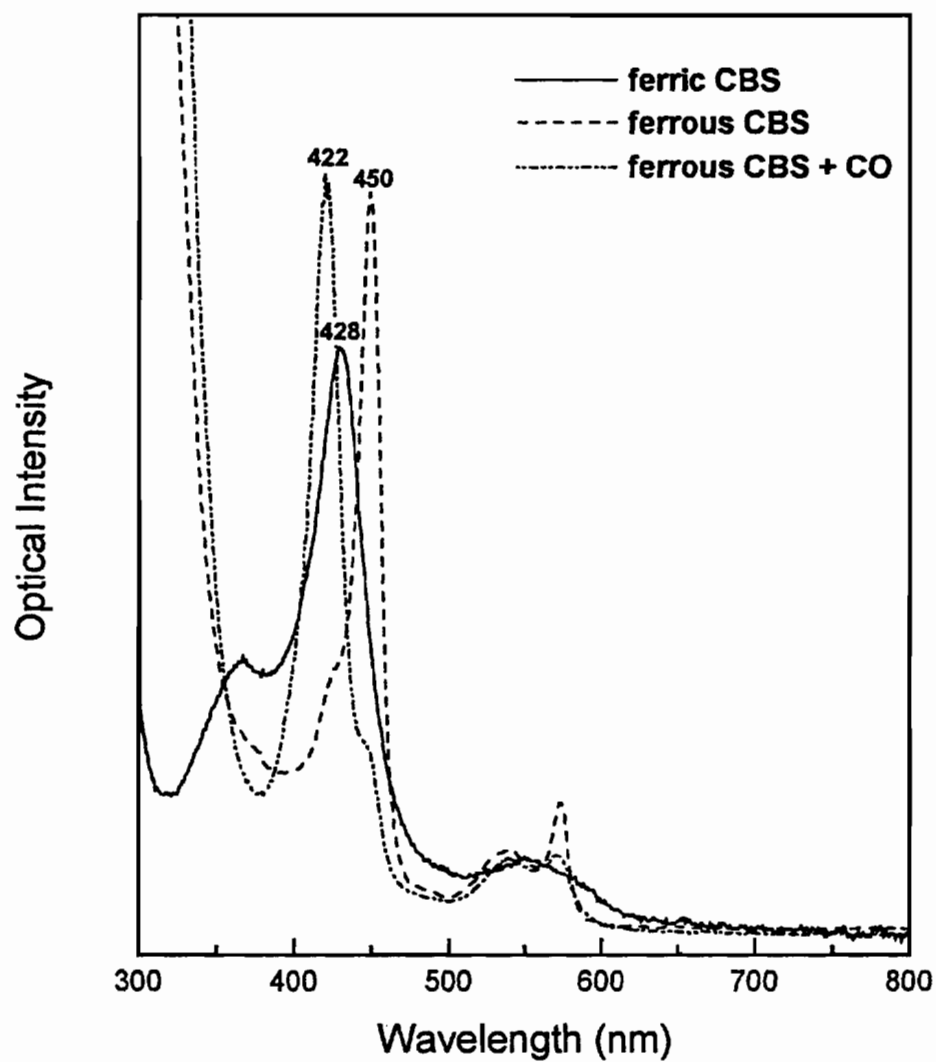


**Fig. 4.1** Electronic absorption spectra of cystathionine  $\beta$ -synthase in oxidized, reduced, and reduced + CO forms. Similar data have been previously reported [Taoka et al., 1998].

### 4.3 Results and Discussion

#### 4.3.1 Resonance Raman of Oxidized Cystathionine $\beta$ -Synthase

We have used resonance Raman spectroscopy to characterize the heme in human cystathionine  $\beta$ -synthase and establish that the axial ligands of the heme cofactor are cysteine and histidine as had been previously suggested [Ojha et al., 2000]. Excitation of oxidized CBS within the Soret band at 428 nm produces a RR spectrum dominated by porphyrin modes (Fig. 4.2). Bands in the high-frequency region (1200–1700  $\text{cm}^{-1}$ ) are sensitive indicators of the oxidation state ( $\nu_4$ ) and spin and coordination states ( $\nu_2$ ,  $\nu_3$ , and  $\nu_{10}$ ) of the heme iron [Spiro and Li, 1988]. The RR spectrum of oxidized CBS in Fig. 4.2 is dominated by the oxidation state marker,  $\nu_4$ , at 1372  $\text{cm}^{-1}$ , while higher frequency porphyrin skeletal modes are at the positions expected for a 6cLS *b*-type heme. These frequencies are consistent with the heme in cystathionine  $\beta$ -synthase being coordinated to histidine and cysteine residues as suggested by EPR [Omura et al., 1984; Ojha et al., 2000], X-ray absorption [Ojha et al., 2000], and MCD (magnetic circular dichroism) [Svastits et al., 1989] spectroscopic studies. There are no isotope-sensitive peaks that result from global  $^{34}\text{S}$  substitution in this spectral region [data not shown].

The low-frequency RR spectrum also exhibits signals characteristic of the heme cofactor, with intense peaks at 676 and 371  $\text{cm}^{-1}$  (Fig. 4.3). We have identified the peak at 312  $\text{cm}^{-1}$  as the Fe–S(Cys) stretching frequency by its 3  $\text{cm}^{-1}$  downshift that is observed in the RR spectrum of the globally  $^{34}\text{S}$ -labeled enzyme (Fig. 4.3, inset). No other bands in the RR spectrum were sensitive to the isotopic substitution. The observation of the Fe–S(Cys) stretch in CBS is unique in that it is the first detection of this vibration in a 6cLS heme species. Fe–S(Cys) vibrations have been seen previously only in five-coordinate high-spin (5cHS) species. In cytochrome P450<sub>cam</sub> [Champion et al., 1982], chloroperoxidase [Bangcharoenpaorong et al., 1986], and the His25Cys mutant of heme oxygenase [Liu et al., 1999],  $\nu(\text{Fe–S})$  occurs at  $\sim 350 \text{ cm}^{-1}$ . The lower frequency in cystathionine  $\beta$ -synthase suggests that the Fe–S bond is weaker than in the 5cHS species found in the other heme enzymes, the difference being consistent with its six-coordinate state.

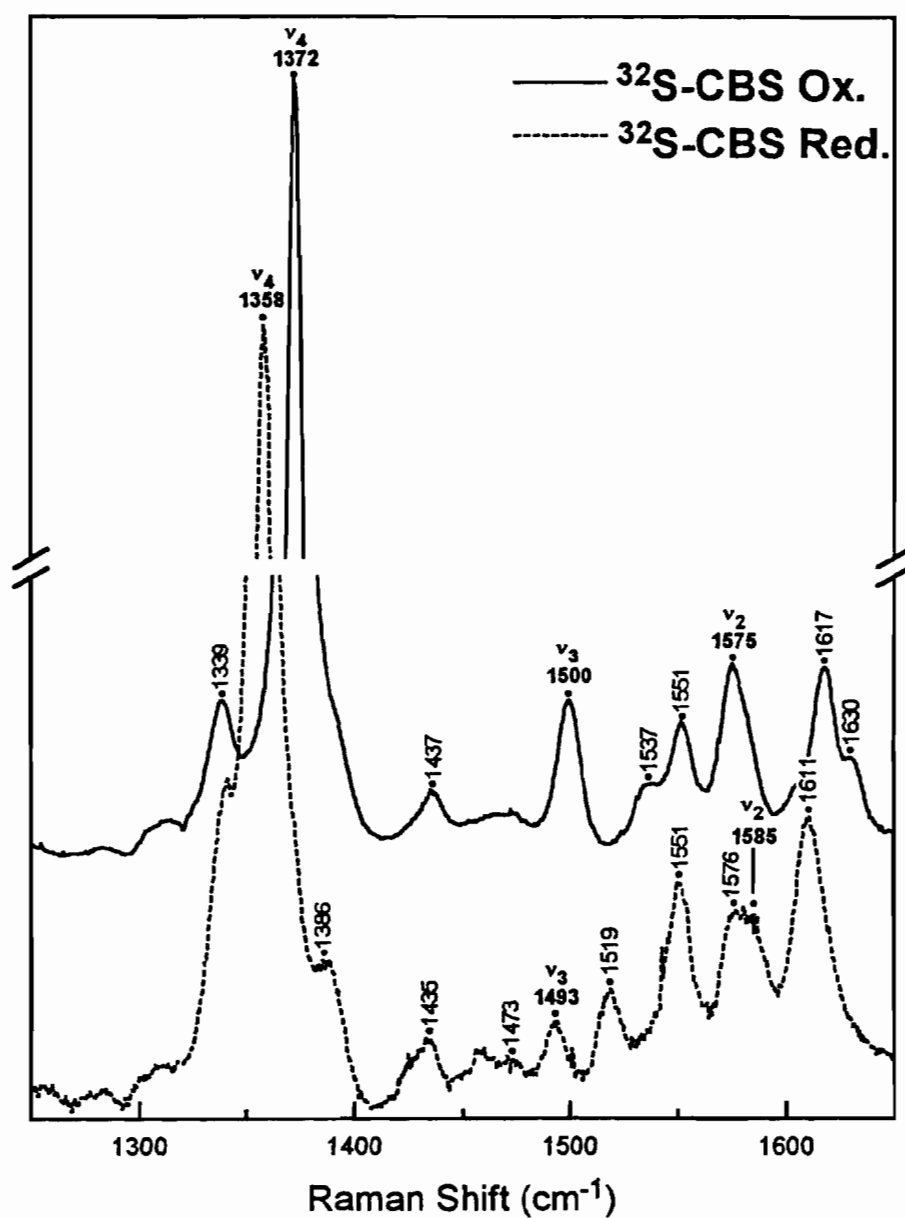


**Fig. 4.2** High-frequency Raman spectra of nonlabeled ferric cystathionine  $\beta$ -synthase ( $\lambda_{\text{ex}} = 413 \text{ nm}$ ) and nonlabeled ferrous cystathionine  $\beta$ -synthase ( $\lambda_{\text{ex}} = 442 \text{ nm}$ ). The heme cofactor is 6cLS for both oxidized and reduced cystathionine  $\beta$ -synthase as indicated by the heme marker bands  $\nu_4$ ,  $\nu_3$ , and  $\nu_2$ .

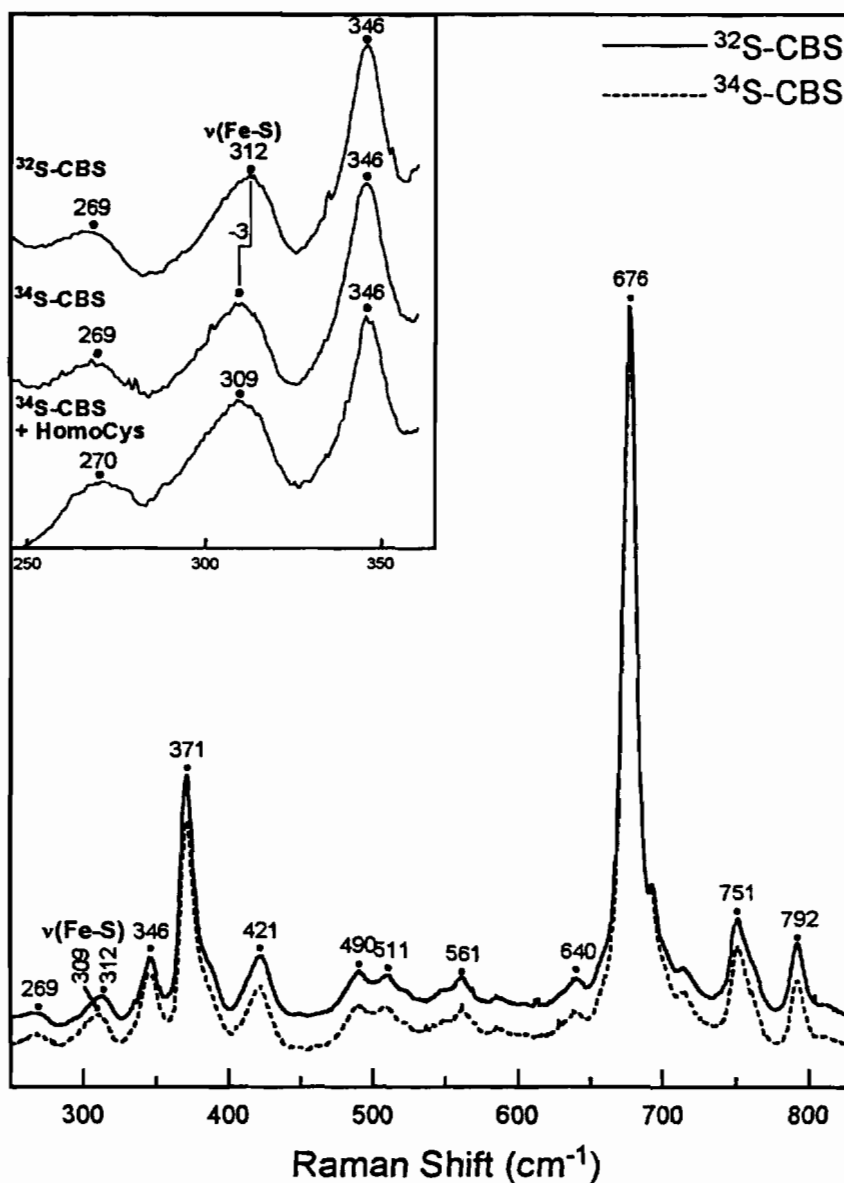


**Fig. 4.3** Low-frequency Raman spectra of unlabeled ferric cystathionine  $\beta$ -synthase and global  $^{34}\text{S}$ -labeled ferric cystathionine  $\beta$ -synthase. Isotopic substitution allows for the identification of the Fe-S(Cys) vibrational peak at  $312\text{ cm}^{-1}$  ( $\lambda_{\text{ex}} = 413\text{ nm}$ ). **Inset:** Resonance Raman spectrum of unlabeled versus uniformly  $^{34}\text{S}$ -labeled cystathionine  $\beta$ -synthase after addition of excess homocysteine substrate. The position of the Fe-S(Cys) vibrational peak is unchanged, indicating that the substrate does not bind directly to the heme cofactor by displacement of the cysteine ligand.



#### 4.3.2 Homocysteine Binding to Cystathionine $\beta$ -Synthase

We have examined the effect of the thiolate substrate, homocysteine, on the RR spectrum of CBS. It has been postulated that the heme may function to activate the substrate *via* direct coordination to the heme [Taoka et al., 1998]. If homocysteine were to displace the coordinated cysteine residue, then the 309  $\text{cm}^{-1}$  Fe-S peak of the  $^{34}\text{S}$ -labeled enzyme would be expected to shift back to 312  $\text{cm}^{-1}$  provided that the Fe-S(Cys) and Fe-S(homocysteine) bonds were of comparable strengths. However, addition of homocysteine, even in large excess over the enzyme, resulted in no significant changes in the Fe-S peak frequency and intensity in both the unlabeled and, more importantly, the  $^{34}\text{S}$ -labeled protein (Fig. 4.3, inset). Furthermore, no new peaks appeared in the low-frequency region that would be expected if Fe-S(homocysteine) ligation had occurred. In fact, no changes were detectable in any region of the RR spectrum in the presence of homocysteine. These data indicate that homocysteine does not displace the cysteine ligand of the heme cofactor in the binary enzyme-homocysteine complex.

#### 4.3.3 Resonance Raman of Reduced Cystathionine $\beta$ -Synthase

Formation of ferrous heme in CBS results in the Soret band shifting from 428 to  $\sim 450$  nm [Kim and Deal, 1976; Omura et al., 1984] (Fig. 4.1). Excitation at 442 nm within the Soret band gives a RR spectrum characteristic of a 6cLS ferrous heme, identified by the  $\nu_4$ ,  $\nu_3$ , and  $\nu_2$  markers at 1358, 1493, and 1585  $\text{cm}^{-1}$ , respectively (Fig. 4.2). As with oxidized CBS, the ferrous heme spectrum also exhibits no observable shifts upon global  $^{34}\text{S}$  substitution in this region [data not shown].

The low-frequency region of the resonance Raman spectrum displays several changes including the disappearance of the Fe-S(Cys) vibrational peak at 312  $\text{cm}^{-1}$ . In the ferrous heme, the Fe-S(Cys) bond is expected to be weaker due to the lower positive charge on the iron atom, and, therefore,  $\nu[\text{Fe-S(Cys)}]$  should be at a lower frequency than in the oxidized enzyme. However, no isotope-sensitive peaks were observed in the spectrum of the reduced enzyme [data not shown], suggesting that the Fe-S(Cys) vibration has fallen out of resonance in the ferrous heme complex. The high-frequency RR spectrum clearly shows that the ferrous heme is in a 6cLS state

(Fig. 4.2), a result consistent with histidine and cysteine residues still ligated in the reduced enzyme. The 450 nm Soret band also supports the presence of a thiolate ligand in a six-coordinate ferrous heme [Dawson and Sono, 1987]. In contrast, in CooA, the CO-sensing transcriptional activator from *Rhodospirillum rubrum*, the ferric heme is also coordinated by a cysteine ligand, but reduction leads to replacement of the ligating residue Cys75 by His77 [Aono et al., 1998; Shelper et al., 1999].

#### 4.3.4 Spectrum of Oxidized Cystathionine $\beta$ -Synthase Treated with $\text{HgCl}_2$

Addition of  $\text{HgCl}_2$  to oxidized enzyme results in loss of the sharp Soret absorbance at 428 nm and the appearance of a broad band at  $\sim 390$  nm [Ojha et al., 2000]. The RR spectrum of  $\text{HgCl}_2$ -treated CBS reveals the presence of a 5cHS ferric heme with  $\nu_2$  at 1570,  $\nu_3$  at 1492, and  $\nu_4$  at 1373  $\text{cm}^{-1}$  (Fig. 4.4). This finding is consistent with recent EPR data that have identified a spin-state conversion of the ferric heme on treatment of the enzyme with  $\text{HgCl}_2$  [Ojha et al., 2000].

The low-frequency RR spectrum of the  $\text{HgCl}_2$ -treated sample displays several other changes compared to that of oxidized enzyme (Figs. 4.3 and 4.4). The three peaks at 346, 371, and 421  $\text{cm}^{-1}$  have greatly changed in relative intensities and, to a smaller degree, in frequencies and are now seen at 347, 379, and 415  $\text{cm}^{-1}$ , respectively. The prominent peak at 676  $\text{cm}^{-1}$  has also decreased in intensity. We propose that the cysteine ligand dissociates when cystathionine  $\beta$ -synthase is treated with  $\text{HgCl}_2$ . This is supported by the loss of the Fe-S(Cys) vibration at 312  $\text{cm}^{-1}$ . There are no observable frequency shifts upon global  $^{34}\text{S}$  isotopic substitution [data not shown].

#### 4.3.5 Spectrum of Reduced Cystathionine $\beta$ -Synthase Treated with $\text{HgCl}_2$

Very different results are obtained when oxidized CBS, treated with  $\text{HgCl}_2$ , is then reduced. The broad Soret band shifts from  $\sim 390$  to  $\sim 422$  nm. The RR spectrum of the  $\text{HgCl}_2$ -treated ferrous CBS indicates a 6cLS species, as identified by  $\nu_4$ ,  $\nu_3$ , and  $\nu_2$  at 1359, 1493, and 1581  $\text{cm}^{-1}$ , respectively (Fig. 4.4), showing that the heme converts back to a 6cLS species upon reduction. The position of the absorbance

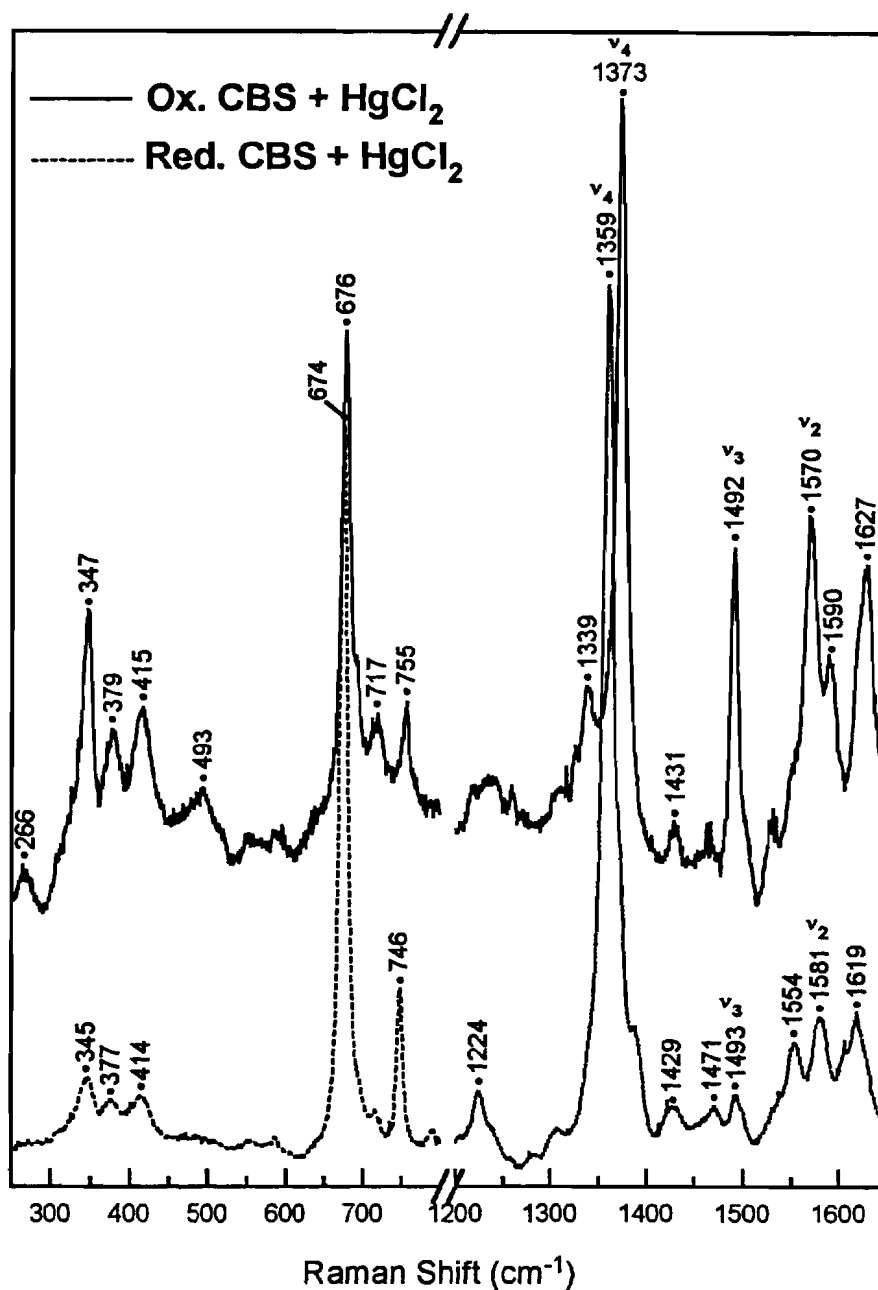


Fig. 4.4 Resonance Raman spectra of unlabeled ferric and ferrous CBS after treatment with  $\text{HgCl}_2$  ( $\lambda_{\text{ex}} = 413 \text{ nm}$ ). The spectra demonstrates conversion of 6cLS to 5cHS heme as indicated by the heme marker bands  $\nu_4$ ,  $\nu_3$ , and  $\nu_2$  at 1373, 1492, and 1570  $\text{cm}^{-1}$ , respectively, for the oxidized treated sample. Upon reduction of the oxidized treated sample, the heme marker bands clearly demonstrate a conversion back to 6cLS as identified by  $\nu_4$ ,  $\nu_3$ , and  $\nu_2$  at 1359, 1493, and 1581  $\text{cm}^{-1}$ , respectively.

band at  $\sim 422$  nm also supports a six-coordinate ferrous heme in which the Cys ligand has been replaced [Reynolds et al., 2000]. It is unclear as to which amino acid could displace the Cys ligand as there is no analogous His residue as seen in CooA [Aono et al., 1998; Shelper et al., 1999]. Global  $^{34}\text{S}$ -isotope substitution resulted in no observable shifts in either the low- or high-frequency regions [data not shown].

#### 4.3.6 CO Adduct of Cystathionine $\beta$ -Synthase

Addition of CO to ferrous heme results in a blue shift of the Soret peak from 450 to 422 nm [Omura et al., 1984] (Fig. 4.1). The appearance of  $\nu(\text{CO})$  and  $\nu(\text{Fe-CO})$  modes in the RR spectrum confirms that CO binds to the heme by displacement of one of the original axial ligands. The vibrational modes of the CO complex were identified by  $^{12}\text{CO}/^{13}\text{CO}$  isotopic substitution (Fig. 4.5), with  $\nu(\text{Fe-CO})$  observed at  $497\text{ cm}^{-1}$  (downshifts  $4\text{ cm}^{-1}$  with  $^{13}\text{CO}$ ) and  $\nu(\text{C=O})$  at  $1961\text{ cm}^{-1}$  (downshifts  $\sim 45\text{ cm}^{-1}$  with  $^{13}\text{CO}$ ). These frequencies are similar to those seen for other 6cLS CO complexes having a hydrophobic distal pocket and, furthermore, are characteristic of a heme-CO complex with histidine as the sixth heme ligand [Ray et al., 1994; Sun et al., 1997]. Thus, the present RR data indicate that the cysteine ligand is displaced by CO, a result supporting the recent assignment of histidine as the sixth ligand in the ferrous-CO heme complex of cystathionine  $\beta$ -synthase by Taoka et al. [1999a]. Carbon monoxide is a competitive inhibitor with respect to homocysteine, and CO binding results in complete loss of enzyme activity [Taoka et al., 1999a]. Since our data indicate that homocysteine does not displace the cysteine ligand, they suggest that CO interferes with homocysteine binding by affecting the heme microenvironment resulting from displacement of the cysteine ligand.

#### 4.3.7 Summary

In summary, characterization of human cystathionine  $\beta$ -synthase by resonance Raman spectroscopy has led to the first detection of the  $\nu(\text{Fe-S})$  mode in a 6cLS ferric heme and provides supporting evidence for the assignment of cysteine and histidine as the axial ligands. Addition of unlabeled homocysteine to the isotopically labeled enzyme does not perturb the heme spectrum and, in particular, the  $\nu(\text{Fe-S})$

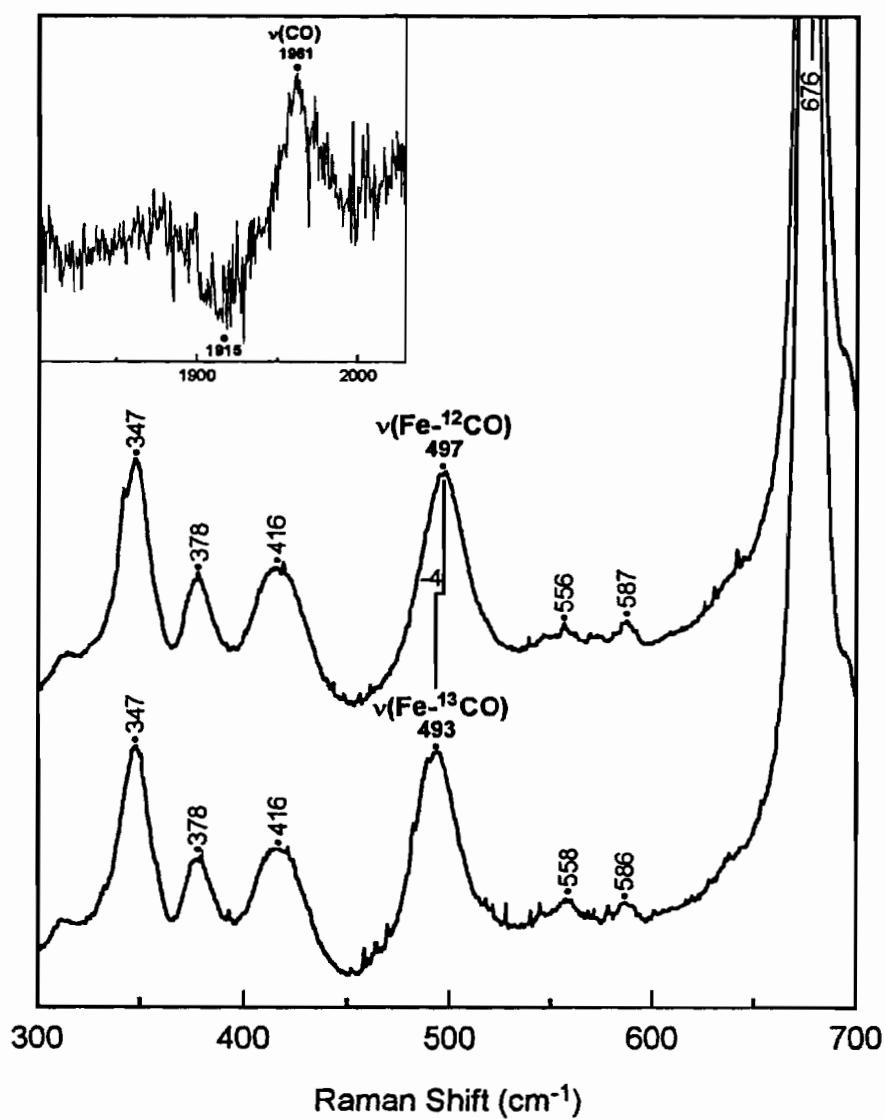


**Fig. 4.5** Resonance Raman spectrum of the CO adduct of ferrous cystathionine  $\beta$ -synthase ( $\lambda_{\text{ex}} = 413 \text{ nm}$ ). Isotopic substitution with  $^{13}\text{C}$  allows for the identification of the  $\nu(\text{Fe-CO})$  stretch at  $497 \text{ cm}^{-1}$  and the  $\nu(\text{CO})$  stretch at  $1961 \text{ cm}^{-1}$  (inset).

peak, indicating that homocysteine does not replace cysteine as an axial ligand as had been proposed. In the ferrous state, the heme retains its 6cLS electronic configuration. CO binds to the ferrous heme by displacement of the cysteine ligand, and the  $\nu(\text{Fe-CO})/\nu(\text{CO})$  correlation supports a His/CO axial ligand set. Addition of the thiol chelator  $\text{HgCl}_2$  to the ferric enzyme results in a spin-state conversion that is readily detected by RR spectroscopy. However, addition of  $\text{HgCl}_2$  to the ferrous enzyme results in a 6cLS heme, indicating substitution of the coordinating cysteine by another, and as yet unidentified, residue in the active site.

## CHAPTER 5

### CONCLUSIONS AND FUTURE DIRECTIONS

As described in Chapter 1, copper-containing amine oxidases (CAOs) catalyze two separate reactions: the biogenesis of the 2,4,5-trihydroxyphenylalanine quinone (TPQ) cofactor and the degradation of primary amine substrates to form ammonia, aldehyde, and peroxide. In Chapters 2 and 3, we described the use of resonance Raman (RR) spectroscopy to further characterize the TPQ cofactor and reaction intermediates. Cystathionine  $\beta$ -synthase (CBS), containing heme and pyridoxal phosphate (PLP) cofactors, catalyzes the first step in the catabolic removal of homocysteine. In Chapter 4, we demonstrated the utility of RR spectroscopy to characterize the heme cofactor in CBS. In this final chapter, I will briefly summarize our new contributions to the copper amine oxidases and CBS, and conclude with suggestions for future research directions.

#### 5.1 Characterization of Biogenesis in Amine Oxidases

CAOs have been extensively studied for over two decades, but it wasn't until 1990 that the true nature of the organic cofactor was revealed to be TPQ and not PQQ as previously proposed [Janes et al., 1990]. In earlier studies of ECAO and AGAO, we showed that the oxygen at the C5 position and the hydrogen at the C3 position of the TPQ cofactor are capable of exchanging with solvent water [Moënnelocoz et al., 1995; Nakamura et al., 1996]. A study of cofactor biogenesis revealed that the origin of the C2 oxygen is from solvent [Nakamura et al., 1996]. The C5 and C2 carbonyl stretching frequencies have been assigned by heavy atom replacement. Upon incubation in  $\text{H}_2^{18}\text{O}$ , the peaks at 1681, 1683, 1678, and 1666  $\text{cm}^{-1}$  in *E. coli* amine oxidase (ECAO), the amine oxidase from *Arthrobacter*

*globiformis* (AGAO), bovine serum amine oxidase (BSAO), and the tBQO<sup>-</sup> model compound, respectively, downshift by  $\sim 25\text{ cm}^{-1}$ , leading to their assignment as the C5=O stretch [Moënne-Loccoz et al., 1995; Nakamura et al., 1996, 1997]. The  $\nu(\text{C5=O})$  is a fairly pure vibration with little coupling to other modes indicated by shifts no greater than  $-1\text{ cm}^{-1}$  of other peaks in the high-frequency region. Cofactor biogenesis in the presence of  $\text{H}_2^{18}\text{O}$  results in the peak at  $1575\text{ cm}^{-1}$  downshifting by  $\sim 21\text{ cm}^{-1}$ , leading to its assignment as the C2=O stretch [Nakamura et al., 1997]. The frequency of the C2=O stretch suggests that it has some single-bond character arising from the delocalization of electron density from the phenyl ring. Additional  $^{18}\text{O}$  shifts of  $-3$  to  $-6\text{ cm}^{-1}$  in several features in the  $1200\text{--}1500\text{ cm}^{-1}$  region, which arise from coupling of the C2=O stretch with lower energy vibrational motions, further support this interpretation. The C3-H bending vibration was identified in BSAO at  $1310\text{ cm}^{-1}$  ( $-23\text{ cm}^{-1}$  in  $\text{D}_2\text{O}$ ) and in ECAO at  $1289\text{ cm}^{-1}$  ( $-9\text{ cm}^{-1}$  in  $\text{D}_2\text{O}$ ) by deuterium exchange [Moënne-Loccoz et al., 1995; Nakamura et al., 1997]. It is likely that the difference in frequency downshift in  $\text{D}_2\text{O}$  is due to the variability in their coupling with ring vibrational modes.

In Chapter 2, we characterized the biogenesis of the TPQ cofactor in the amine oxidase from the yeast *Hansenula polymorpha* (HPAO). The RR spectrum of wild-type (WT) HPAO is dominated by an intense peak at  $1401\text{ cm}^{-1}$ , with other significant features in the  $1200\text{--}1700\text{ cm}^{-1}$  region, characteristic of TPQ-containing enzymes as well as a TPQ model (Fig. 2.2). Upon incubation in  $\text{H}_2^{18}\text{O}$ , only the peak at  $1678\text{ cm}^{-1}$  ( $-28\text{ cm}^{-1}$  in  $\text{H}_2^{18}\text{O}$ ) demonstrates any significant shifting, thus identifying it as the C5=O carbonyl stretching frequency (Fig. 2.3B). Biogenesis in  $\text{H}_2^{18}\text{O}$  results in the stretching vibration at  $1580\text{ cm}^{-1}$ , downshifting by  $22\text{ cm}^{-1}$  (Fig. 2.3C), thus identifying this band as the C2=O carbonyl stretch with smaller shifts of  $-3$  to  $-5\text{ cm}^{-1}$  in the vibrational bands in the  $1200\text{--}1400\text{ cm}^{-1}$  region (Table 2.2). This pattern is similar to that observed for AGAO, indicating that cofactor biogenesis in HPAO also involves insertion of solvent oxygen at the C2 position, with a similar degree of electron delocalization between the C2 and C4 position on the phenyl ring.



## 5.2 Determination of TPQ Orientation

In Chapter 2, we analyzed the exchange rates for the C5 oxygen and the C3-H in WT-HPAO, WT-PSAO at pH 7.2 and 4.6, WT-AGAO, WT-ECAO, TPQ model tBQO<sup>-</sup>, and HPAO mutants to determine the cofactor orientation in the resting form of these enzymes. We classify the TPQ cofactor as adopting one of three possible orientations: productive, flipped, or mobile.

### 5.2.1 Productive Orientation

A productive orientation is characterized by the C5=O directed towards the substrate-binding pocket and the C3-H directed towards the Cu cofactor. Positioned in this orientation, the C5 position would be more accessible to solvent and, thus, would demonstrate a much more rapid rate of exchange than the C3-H. Our data support a productive orientation for the TPQ cofactor in WT-HPAO, WT-AGAO, WT-PSAO at neutral pH, and the E406Q-HPAO mutant. Each of these enzymes displayed a rapid rate of solvent exchange for the C5 carbonyl oxygen (Table 2.2). Furthermore, C3-H exchange was not observed, even after 24-h incubation in D<sub>2</sub>O, for WT-HPAO, WT-PSAO (pH 7.1), and the E406Q-HPAO mutant. However, for WT-AGAO, we observed a slow rate of exchange for the C3-H ( $t_{1/2} = 6$  h). A non-observable or slow rate of C3-H exchange, coupled with a rapid rate of C5=O exchange, supports a productive orientation for the TPQ cofactor in each of these enzymes. These results are in agreement with the published crystal structure data for WT-HPAO, which clearly shows the cofactor resting in a productive conformation [Li et al., 1998] and for WT-AGAO in which the crystal structure data clearly shows an ordered TPQ ring. The unresolved electron density for the C2 carbonyl and lack of observed electron density for the C5 carbonyl could support either a productive or flipped orientation. However, our data clearly indicate that the ring is in an ordered conformation, most consistent with a productive orientation.

### 5.2.2 Flipped Orientation

A flipped orientation is characteristic of the TPQ cofactor, with the C5=O directed towards the Cu(II) and the C3-H near the active site base. In this orientation, the C5 carbonyl oxygen is less solvent accessible and would be expected to exchange much more slowly. However, the C3-H is now more solvent accessible and would be expected to exchange rapidly. The RR spectrum of WT-PSAO at pH 7.2 is similar to that observed for other amine oxidases with the most intense ring vibrational modes at  $1396\text{ cm}^{-1}$  (Fig. 2.6A). However, lowering the pH to 4.6 causes this peak to drop in intensity and shift to  $1392\text{ cm}^{-1}$ , and the peak at  $1339\text{ cm}^{-1}$  to increase in intensity and shift to  $1337\text{ cm}^{-1}$ . A red shifting of the TPQ absorption band from 500 nm at pH 7.2 to 515 nm at pH 5.2 is also observed. We attribute this effect to a change in the charge delocalization in the quinone ring. The increase in electron delocalization at low pH could be due to flipping of the ring and loss of a hydrogen bonding interaction of the C4 oxyanion with a nearby Tyr-OH moiety observed in the crystal structure [Kumar et al., 1996]. This interaction is observed in all of the active, neutral pH crystal structures [Wilce et al., 1997; Li et al., 1998; Murray et al., 1999].

Changing of the pH has a dramatic effect on the observed rate of C5=O exchange in PSAO as well. At pH 7.1, exchange is complete in 500 sec ( $t_{1/2} = 2$  min), whereas at pH 4.6 complete exchange requires 20 h ( $t_{1/2} = 4.5$  h) (Fig. 2.7). Rapid  $^{18}\text{O}$  exchange of the model compound (tBQO<sup>-</sup>) at pH 4 indicates that the exchange reaction is not limited by the lower concentration of hydroxide. The slow rate of exchange in PSAO at pH 4.6 is most consistent with a flipped orientation, thus making the C5 carbonyl less accessible to solvent. Additionally, at low pH, PSAO shows only a 4-fold lower activity towards substrates, whereas the  $^{18}\text{O}$  exchange is decreased over 100-fold. If it were just a matter of increased charge delocalization, the lower activity and the decreased rate of exchange should be similar. In contrast, with the cofactor in a flipped conformation, the C5=O is much less accessible to solvent, thus dramatically decreasing the rate of  $^{18}\text{O}$  exchange; whereas binding of substrate is proposed to induce a ring reorientation back to the productive conformation [Plastino et al., 1999]. The flipping of the ring back to a productive

conformation in the presence of substrate would result in a much less decreased rate of activity and could account for the marked difference in the observed rate of activity versus the rate of exchange. The rapid rate of  $^{18}\text{O}$  exchange at neutral pH suggests that the cofactor has shifted to the productive conformation.

The active site base mutants of HPAO, D319E and D319N, were observed to behave quite differently from the other mutants. Both of the D319 mutants demonstrated slow  $^{18}\text{O}$  exchange at the C5 carbonyl position. The average half-life for  $^{18}\text{O}$  exchange was determined to be 3.3 h for D319E and 1.6 h for D319N. Furthermore, both of these mutants displayed a fast C3-H exchange, complete within 1 h. These data are most consistent with the TPQ cofactor in both of the D319 mutants resting in a flipped orientation, much like that observed in the PSAO crystal structure at low pH. We further conclude that the active site base does not catalyze the solvent exchange at the C5 carbonyl, owing to the fact that the exchange rates for the D319E-HPAO and D319N-HPAO mutants were relatively equal; whereas, if the hydrolysis were base catalyzed, the D319N-HPAO mutant would be expected to display a much slower rate of exchange due to asparagine-lacking catalytic base properties.

### 5.2.3 Mobile Orientation

A mobile orientation is characteristic of a TPQ cofactor that could readily adopt multiple orientations between a productive and a flipped orientation. This would result in a rapid rate of exchange for both the C5 carbonyl oxygen and the C3 hydrogen due to increased solvent accessibility for both sides of the TPQ ring. Our RR findings for WT-ECAO demonstrate rapid rates of exchange for both the C5=O and C3-H. These results support a mobile orientation for the cofactor in the resting form of the enzyme and are supported by the crystal structure of WT-ECAO, which shows only partial electron density for the TPQ ring, consistent with a disordered conformation [Murray et al., 1999]. A bridging water molecule between the active site base of the C5=O of the TPQ ring, observed in the crystal structure of WT-HPAO but not observed in half of the subunits in the crystal structure of WT-ECAO,

supports the increased flexibility of the TPQ ring in WT-ECAO [Li et al., 1998; Murray et al., 1999].

Mutation of a conserved residue flanking the TPQ cofactor in HPAO, the N404A-HPAO mutant, displayed a rapid C5=O exchange, complete within 1 h. However, the C3-H exchange was observed to be equally rapid. Our results indicate a mobile orientation for the TPQ cofactor in the N404A mutant of HPAO. Mutation of the asparagine residue at position 404 (on the catalytic-base side of the active site) disrupts an important hydrogen-bonding interaction with the TPQ ring. With the kinetic energy barrier for ring flipping lowered and the active site pocket becoming more open, this would allow the TPQ ring greater flexibility for movement within the active site pocket.

### 5.3 Characterization of Reaction Intermediates

CAOs catalyze the oxidative deamination of primary amine substrates, producing the corresponding aldehyde and ammonia, with the side reaction of formation of hydrogen peroxide. Evidence is strong for the reaction to proceed by a pyridoxal-like transamination mechanism (Scheme 1.2) [Klinman and Mu, 1994]. Anaerobic single turnover results in release of aldehyde product, whereas  $\text{NH}_3$  is released only upon  $\text{O}_2$ -dependent reoxidation of the reduced cofactor [Janes and Klinman, 1991]. As described in Chapter 1, amine substrate is activated through covalent addition to the TPQ cofactor. Labilization of the hydrogen atom  $\alpha$  to the nitrogen group results in formation of the substrate Schiff base. The product Schiff base is formed by abstraction of a methylene proton by the active site base. This complex is rapidly hydrolyzed to yield the aminoquinol and product aldehyde. Molecular oxygen reoxidizes the reduced cofactor, producing hydrogen peroxide, ammonia, and the active oxidized cofactor.

Extensive model studies and rapid scanning spectroscopy support the proposed catalytic mechanism [Mure and Klinman, 1993, 1995a,b; Hartman et al., 1993; Wang et al., 1994; Lee and Sayre, 1995a,b; Lee et al., 1996]. Additionally, earlier studies have shown that RR spectroscopy is particularly valuable for the detection and

characterization of reaction intermediates along this reaction pathway [Cai et al., 1997; Nakamura et al., 1997]. In Chapter 3, we described the application of this technique to three mutant enzymes of HPAO (D319N, D319E, and N404A) to characterize intermediates along this reaction pathway and to further test the proposed catalytic mechanism.

### 5.3.1 Identification of Deprotonated Iminoquinone

Incubation of the D319E mutant of HPAO with methylamine or the D319N mutant with ammonium chloride results in the buildup of a species absorbing at  $\sim 430$  nm. With 413-nm excitation, we have detected the deprotonated iminoquinone species for both the methylamine adduct of D319E and the ammonia adduct of D319N. As shown in Fig. 3.2, upon addition of ammonium chloride to D319N, the C5 carbonyl stretch at  $1675\text{ cm}^{-1}$  disappears and is replaced by a new peak at  $1603\text{ cm}^{-1}$  ( $-11\text{ cm}^{-1}$  in  $^{15}\text{NH}_4\text{Cl}$ ), identified by heavy atom replacement as the C=N stretch of the imine species. The imine stretch downshifted an additional  $9\text{ cm}^{-1}$  in  $^{15}\text{ND}_4\text{Cl}$ , consistent with the presence of one deuterium atom on the imine nitrogen. These data suggest that the ammonia adduct of D319N is the deprotonated iminoquinone species.

Similar results were obtained for the methylamine adduct of the D319E mutant. Upon incubation with methylamine, a new peak at  $1607\text{ cm}^{-1}$  appears ( $-12\text{ cm}^{-1}$  with  $^{15}\text{NH}_2\text{CH}_3$ ), corresponding to the peak observed at  $1603\text{ cm}^{-1}$  for the ammonium adduct of the D319N mutant (Fig. 3.3). Substitution with  $^{15}\text{ND}_2\text{CH}_3$  leads to a further shift of  $-9\text{ cm}^{-1}$ , consistent with the presence of only one deuterium on the imine nitrogen. Furthermore, no shifts are observed upon adduct formation with  $\text{NH}_2\text{CD}_3$ , indicating that the methyl group of the substrate is no longer present and unambiguously ruling out either the substrate or product Schiff base species. The similarity in peak frequencies and intensities with the D319N ammonia adduct support that the species accumulating during methylamine turnover by D319E is the deprotonated iminoquinone.

Crystal structure and exchange rate studies described in Chapter 2 indicate that the TPQ cofactor can adopt various conformations that alter cofactor accessibility. When the aspartate base is mutated to either a glutamate or an asparagine, the

hydrogen-bonding network holding the cofactor in a productive orientation is altered, allowing the TPQ ring to flip to a less accessible conformation. This is supported by the solvent exchange data for these mutants, which indicate that the TPQ ring in both mutants is in a flipped orientation in the resting enzyme. We propose that the accumulation of the iminoquinone species with these mutant enzymes results from a rotation of this intermediate into a flipped orientation that is less accessible to hydrolysis. Deprotonation, as indicated by RR and electronic absorption studies, occurs as a consequence of cofactor flipping away from the substrate-binding pocket. Thus, the active site base not only orients the cofactor in the resting form through the bridging water molecule between C5=O and the catalytic base, but also plays a key role in maintaining the orientation of the catalytic intermediates to facilitate rapid hydrolysis back to an active TPQ cofactor.

### 5.3.2 Identification of Product Schiff Base

A previous conserved flanking residue mutant of HPAO (E406N) displayed rapid, reversible inhibition when incubated with methylamine substrate [Cai et al., 1997]. Mutation of the opposite flanking residue asparagine to an alanine (N404A) results in the formation of a similar species (absorption maximum at 380 nm), when reacted with methylamine substrate. The RR spectrum of N404A inactivated with methylamine was similarly dominated by an intense C=N stretch at  $1622\text{ cm}^{-1}$  that shifted  $-58\text{ cm}^{-1}$  upon incubation with  $\text{CD}_3\text{NH}_2$  (Fig. 3.5). The observed isotopic shift of  $-58\text{ cm}^{-1}$  supports the product Schiff base species. A flipped orientation for the adduct is supported by the lack of any observable shift with  $\text{CH}_3\text{ND}_2$  in  $\text{D}_2\text{O}$ , thus indicating a lack of an exchangeable proton on the C=N moiety. Furthermore, the  $\text{D}_2\text{O}$ -dependent shifts of  $-4$  and  $-9\text{ cm}^{-1}$  for the peaks at  $1340$  and  $1575\text{ cm}^{-1}$ , respectively, are ascribed to the exchange of the C3 hydrogen of the TPQ cofactor [Nakamura et al., 1997]. This would indicate that the C3-H is more solvent accessible than in WT-HPAO, supporting a flipped conformation. Exchange rate studies of the resting enzyme also support a more mobile cofactor, indicated by rapid C3-H and C5=O exchange [Chapter 2].

The N404A mutant of HPAO has decreased activity with all substrates compared to wild type, with a 450-fold decrease in activity for either ethylamine or phenethylamine as substrate [Schwartz et al., 1998]. However, the rate of reaction of methylamine with N404A is decreased 1000-fold relative to that with wild type. The formation of a dead-end complex is not observed when N404A is reacted with other larger substrates such as phenethylamine or ethylamine. Since the chemical reactivities are expected to be similar among these amines, the inhibitory differences observed among the three substrates are likely due to the differing steric constraints on the abilities of the respective product Schiff base complexes to adopt nonproductive orientations.

#### **5.4 Future Copper Amine Oxidase Work**

Much is understood about the catalytic mechanism of CAOs. Focus is now being placed on the biogenesis mechanism of the TPQ cofactor. Importantly, isolation of intermediates along the biogenesis pathway would provide clear indication of the step-by-step mechanism of biogenesis. Our lab previously showed that RR spectroscopy could identify the origin of the C2 carbonyl oxygen as from solvent [Nakamura et al., 1996]. A key step to substantiating the proposed biogenesis mechanism is to identify the origin of the C5 carbonyl oxygen.

We have undertaken some preliminary RR studies, but have been so far unsuccessful, due to the rapid exchange of the C5 carbonyl oxygen with solvent. One possible way to perform this experiment would be to perform a rapid freeze quench at different times directly after the initiation of biogenesis. Unfortunately, these experiments would most likely be hampered by the high fluorescence of the protein when frozen. Furthermore, the extinction coefficients of intermediates along the biogenesis pathway are very low, leading to the need for very concentrated protein samples, which are difficult to obtain.

Another biogenesis intermediate that has received attention lately is the Cu(II)-Tyr species. Recent crystallographic analysis of a zinc-substituted enzyme has shown that the precursor tyrosine is bound to the Zn metal [Chen et al., 2000]. This

is the closest analogue to date of an intermediate in TPQ biogenesis. A mutation of one of the copper ligands, histidine 624 to a cysteine, is also thought to accumulate this Cu(II)-Tyr species. Upon addition of Cu(II) to apo-H624C-HPAO enzyme, an absorbance at 400 nm, most likely a Cys  $\rightarrow$  Cu(II) CT band from a type 2 Cu complex, appears and persists anaerobically [Dove et al., 2000]. An additional oxygen-dependent absorbance, which accumulates at 390 nm during H624C biogenesis, is thought to be a tyrosinate  $\rightarrow$  Cu(II) ligand-metal charge transfer band. Preliminary RR experiments were performed by this lab to obtain evidence for either Cu-Cys or Cu-Tyr ligation in H624C, but no definitive spectra were obtained. This experiment is made more difficult due to the fact that neither type 2 Cu-S nor Cu-tyrosinate are strong RR scatterers, and the sample was photolabile. It would be worthwhile to discover another mutant of a copper ligand that is less photosensitive than the H624C mutant.

Finally, it is imperative that the crystal structures for the HPAO mutants be solved. The crystal structures of active site base (position 383 in ECAO) mutants (D383A, D383N, and D383E) of *E. coli* amine oxidase have been solved [Murray et al., 1999]. The electron density of the TPQ ring for the D383A-ECAO mutant shows even greater disorder than for wild-type. The D383N-ECAO mutant exhibits similar disorder for the electron density associated with the TPQ ring as observed in the wild type. Thus, for the D383A-ECAO and D383N-ECAO mutants, the TPQ cofactor still retains great mobility. However, the D383E-ECAO mutant shows clear electron density for the TPQ ring resting in a productive conformation. This is in contrast to the TPQ orientation that was predicted for the D319E-HPAO mutant. However, it should be noted that the D383E and D383N mutants of ECAO behaved quite differently with respect to cofactor orientation. Furthermore, the crystal structure and RR data predict that the TPQ cofactors in the wild-type HPAO and ECAO enzymes behave quite differently. Therefore, it is not unreasonable to suspect that the active site base mutants of ECAO do not reflect the exact same properties as the active site base mutants of HPAO.

It would be of benefit to examine the rate of exchange for the active site base mutants of ECAO, as well as to examine the crystal structures for the HPAO mutants.



We predict that the D319E and D319N mutants of HPAO will display a flipped orientation for the TPQ cofactor. Additionally, we predict that the crystal structure for the N404A-HPAO mutant will display an ECAO-like cofactor, with the TPQ electron density being disordered. Finally, we predict a fast rate of C5=O exchange for the D383N-ECAO and D383E-ECAO mutants, a rapid rate of C3-H exchange for the D383N-ECAO mutant, and a slow C3-H exchange for the D383E-ECAO mutant.

## 5.5 Characterization of the Heme Cofactor in CBS

Human CBS is a unique heme protein that contains two essential cofactors: PLP and heme. The function of the PLP cofactor is to catalyze the  $\beta$ -replacement reaction in the condensation of homocysteine and serine to give cystathionine. However, the role of the heme cofactor is not obvious. The activity of CBS has been shown to be dependent on the oxidation [Taoka et al., 1998], ligation [Taoka et al., 1999b], and coordination state [Taoka and Banerjee, 2001] changes in the heme, suggesting a possible regulatory role for the heme cofactor. Recent EPR and X-ray absorption spectroscopic studies implicate histidine and cysteine as the heme axial ligands in both the ferrous and ferric states [Ojha et al., 2000].

In Chapter 4, we described the characterization of the heme cofactor in CBS by RR spectroscopy. We positively identified the axial heme ligands in the resting enzyme to be Cys and His, in agreement with the low-spin nature of the heme. Furthermore, we showed that homocysteine substrate does not bind to the heme cofactor by displacement of the cysteine axial ligand.

### 5.5.1 Determination of Heme Axial Ligands

Excitation of oxidized CBS within the Soret band at 428 nm produces a RR spectrum dominated by porphyrin modes (Fig. 4.2). Vibrational peaks in the high-frequency region (1200–1700  $\text{cm}^{-1}$ ) are sensitive indicators of the oxidation state ( $\nu_4$ ) and spin and coordination states ( $\nu_2$ ,  $\nu_3$ , and  $\nu_{10}$ ) of the heme iron [Spiro and Li, 1988]. For oxidized cystathionine  $\beta$ -synthase, the heme cofactor was six-coordinate low-spin. Through isotopic substitution, we have identified the peak at 312  $\text{cm}^{-1}$  as

the Fe-S(Cys) stretching frequency, which downshifts 3  $\text{cm}^{-1}$  with globally  $^{34}\text{S}$ -labeled enzyme. The observation of the Fe-S(Cys) stretch in CBS is unique in that it is the first detection of this vibration in a 6cLS heme species. Previously, the Fe-S(Cys) vibration had only been observed in 5cHS species where  $\nu(\text{Fe-S})$  occurs at  $\sim 350 \text{ cm}^{-1}$ . The decreased frequency could result from an inherently weaker Fe-S bond in the six-coordinate species.

Excitation at 442 nm within the Soret band of reduced CBS gives a RR spectrum characteristic of a 6cLS ferrous heme. The low-frequency RR spectrum shows marked changes, including loss of the Fe-S(Cys) vibrational peak at  $312 \text{ cm}^{-1}$ . It is expected that the Fe-S(Cys) vibration would be weaker in the ferrous heme, due to the lower positive charge on the iron atom, resulting in a lower observed frequency for the  $\nu[\text{Fe-S(Cys)}]$  than in the oxidized enzyme. However, we were unable to detect any isotope-sensitive peaks in the RR spectrum of the reduced enzyme, suggesting that the Fe-S(Cys) vibration has fallen out of resonance in the ferrous heme complex. The 450-nm Soret band and the high-frequency RR spectrum support the presence of a thiolate ligand to a 6cLS heme, indicating that Cys and His are still ligated to the ferrous heme.

Formation of a ferrous heme-CO complex results in a blue shift of the Soret peak from 450 to 422 nm. The vibrational modes of the CO complex were identified by  $^{12}\text{CO}/^{13}\text{CO}$  isotopic substitution. Appearance of  $\nu(\text{C=O})$  and  $\nu(\text{Fe-CO})$  at 1961 and  $497 \text{ cm}^{-1}$ , respectively, confirms that CO binds to the heme by displacement of one of the original axial ligands. Analysis of the observed  $\nu(\text{Fe-CO})$  and  $\nu(\text{C=O})$  frequencies by means of a back-bonding correlation diagram (Fig. 5.1) yields two pieces of information. First, it can be seen that the CBS data fall on the plot corresponding to CO adducts in which the sixth ligand is a neutral histidine. Second, the position of the CBS data along the correlation line is typical of a CO-ligand in a hydrophobic environment. Thus, we conclude that the cysteine ligand is displaced by CO. Finally, it is the displacement of the Cys ligand, upon binding CO, that inactivates the protein by altering the homocysteine-binding site.

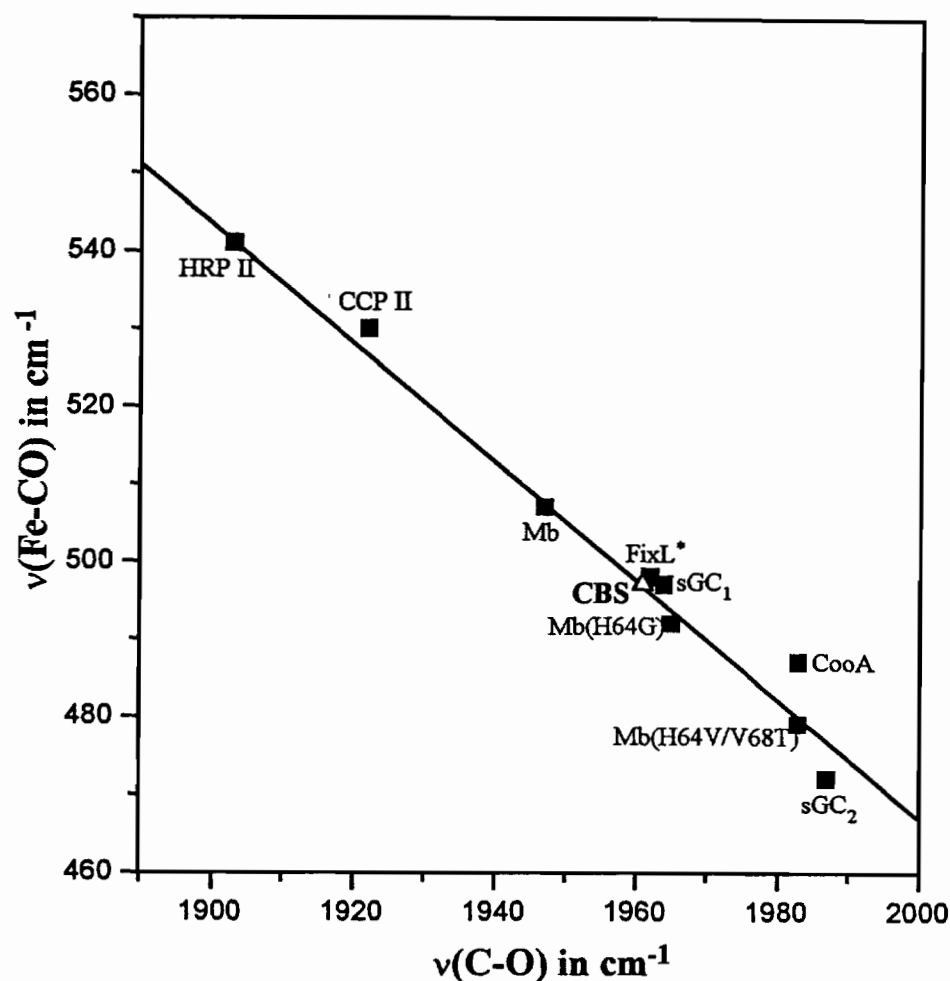


**Fig. 5.1** Plot of observed (Fe-CO) versus (C-O) frequencies for six-coordinate CO adducts of ferrous hemoproteins. The solid line indicates the back-bonding correlation for proximal neutral imidazole ligation. Data obtained in the present study for CBS is denoted by an open triangle. Solid squares represent data points for other CO adducts obtained from: HRP I, horseradish peroxidase [Evangelista-Kirkup et al., 1986]; CCP, cytochrome *c* peroxidase [Smulevich et al., 1986]; Mb, myoglobin [Tsubaki et al., 1982]; FixL\*, soluble truncated form of O<sub>2</sub>-sensing protein [Miyatake et al., 1999]; sGC<sub>1</sub>, soluble guanylate cyclase reconstituted with heme [Fan et al., 1998; Vogel et al., 1999b]; sGC<sub>2</sub>, soluble guanylate cyclase isolated with heme intact [Deinum et al., 1996; Kim et al., 1996; Tomita et al., 1997]; Mb(H64G) [Morikis et al., 1989]; Mb(H64V/V68T) [Biram et al., 1991]; CoxA, CO oxidation activator [Vogel et al., 1999a].

### 5.5.2 Ligation and Spin-State Changes with HgCl<sub>2</sub>

Treatment of oxidized CBS with the thiol chelator, HgCl<sub>2</sub>, results in a blue-shifting and broadening of the sharp Soret band at 428 nm to ~390 nm. The high-frequency RR spectrum is consistent with a 5cHS ferric heme. Marked changes are observed for the low-frequency RR spectrum of HgCl<sub>2</sub>-treated CBS. Disappearance of the Fe–S(Cys) vibration at 312 cm<sup>-1</sup> and lack of any observable frequency shifts upon global <sup>34</sup>S isotopic substitution supports the loss of the cysteine ligand and the formation of a five-coordinate heme species.

Reduction of oxidized CBS treated with HgCl<sub>2</sub> results in the broad Soret band shift from ~390 to ~422 nm. The high-frequency RR spectrum of HgCl<sub>2</sub>-treated ferrous CBS indicates conversion back to a 6cLS species. The optical absorption spectrum also supports a six-coordinate ferrous heme in which the Cys ligand has been replaced [Reynolds et al., 2000]. Global <sup>34</sup>S-isotope substitution resulted in no observable shifts in either the low- or the high-frequency regions. This is consistent with loss of the Cys ligand or could be attributed to the fact that the Fe–S(Cys) was not detected in the RR spectrum of reduced CBS and is not resonance enhanced.

### 5.5.3 Examination of Homocysteine Binding

Reaction of oxidized, <sup>34</sup>S globally labeled CBS with homocysteine resulted in no perturbation of the  $\nu(\text{Fe-S})$  at 309 cm<sup>-1</sup>. If homocysteine were to displace the coordinated cysteine residue, then the 309 cm<sup>-1</sup> peak of the <sup>34</sup>S-labeled enzyme would be expected to shift back to 312 cm<sup>-1</sup>, provided that the Fe–S(Cys) and Fe–S(homocysteine) bonds were of comparable strengths. Furthermore, no changes were detectable in any region of the RR spectrum in the presence of a large excess of homocysteine. Addition of a large excess of homocysteine to CBS treated with the thiol chelator, HgCl<sub>2</sub>, resulted in religation of the endogenous cysteine, indicated by the  $\nu(\text{Fe-S})$  located at 310 cm<sup>-1</sup>, consistent with the retention of the <sup>34</sup>S-labeled cysteine ligand [Taoka et al., 2001]. Thus, we have demonstrated that homocysteine is not activated by the heme cofactor through direct coordination to the heme.

## 5.6 Future Directions for Cystathionine $\beta$ -Synthase Research

Cystathionine  $\beta$ -synthase is a key enzyme involved in homocysteine metabolism in humans. The role of the recently discovered heme in this protein remains an important and open question. In yeast, it has been shown that the CBS enzyme does not contain the heme cofactor, arguing against an important catalytic role for the heme cofactor. It is plausible that the heme cofactor in CBS is a sensor for small molecules much in the same way as observed in guanylate cyclase, the transcriptional cofactor CooA, and implicated in cytochrome *c'* [Deinum et al., 1996; Tomita et al., 1997; Fan et al., 1998; Vogel et al., 1999a; Lawson et al., 2000; Reynolds et al., 2000; Andrew et al., 2001]. It has been shown that carbon monoxide binding inactivates CBS, and CO is a competitive inhibitor with respect to homocysteine binding [Taoka et al., 1999a]. However, we have shown that homocysteine does not covalently bind to the heme cofactor, so the displacement of the axial cysteine ligand by CO must be altering the homocysteine-binding site through the loss of the cysteine ligation.

Binding of nitric oxide to CBS results in displacement of the histidine ligand and the transient formation of a six-coordinate intermediate that converts to a five-coordinate ferrous nitrosyl species in which both endogenous ligands have been lost [Taoka and Banerjee, 2001]. As is the case with CO, binding of NO leads to complete loss of enzymatic activity. We have examined NO binding by RR spectroscopy but have been unable to identify either the Fe-NO or NO stretching modes. The NO complex shows rapid reversible photodissociation, even at low laser power and low temperatures. EPR studies of the ferrous-NO complex show a mixture of the five and six coordinate species, and suggest that for the six coordinate NO species it is the histidine ligand that is displaced by NO [Taoka and Banerjee, 2001]. In contrast, CO binding displaces the cysteine ligand [Green et al., 2001]. These results support CO and NO binding to opposite faces of the heme cofactor, a phenomenon observed in the crystal structure and RR studies of cytochrome *c'* [Lawson et al., 2000; Andrew et al., 2001]. Binding of CO, but not NO, activates CooA as a transcriptional regulator of the *coo* operon [Reynolds et al., 2000]. It is

possible that the differential effect of CO versus NO on CooA activation arises from the binding of these molecules to opposite sides of the heme. For hemes complexed with CO or NO, the frequency of the observed  $\nu(\text{Fe-CO})$  versus the  $\nu(\text{CO})$  or the  $\nu(\text{Fe-NO})$  versus the  $\nu(\text{NO})$  stretch can provide information on the extent of back-bonding, which in turn can be used to determine the electrostatic environment of the heme pocket. Thus, it would be beneficial to characterize the ferrous NO complex by RR spectroscopy and show retention of the thiolate ligand in the six-coordinate intermediate.

Another important experiment would be to obtain the crystal structure for CBS with homocysteine substrate bound. This could then answer the question as to how the homocysteine substrate interacts with the heme cofactor and which amino acid residue is acting as a catalytic base to activate homocysteine. Additionally, it would be beneficial to collect the crystal structure for both the CO and NO adducts of CBS to observe whether or not these small molecules bind to opposite sides of the heme as is predicted.

Finally, treatment of oxidized CBS with  $\text{HgCl}_2$  results in the loss of the cysteine ligand and formation of a 5cHS heme species. Reduction of this species results in the formation of a 6cLS species in which the endogenous cysteine ligand is not coordinated to the heme. Through mutagenesis studies and by growing the enzyme in different isotopically labeled amino acids, we could use RR spectroscopy to identify the sixth ligand in this species.

## LITERATURE CITED

- Andrew, C. R., Green, E. L., Lawson, D. M., and Eady, R. R. (2001) Resonance Raman studies of cytochrome *c'* support binding of NO and CO to opposite sides of the heme: implications for ligand discrimination in heme-based sensors. *Biochemistry* **40**, 4115–4122.
- Anthony, C. (1996) Quinoprotein-catalysed reactions. *Biochem. J.* **320**, 697–711.
- Aono, S., Ohkubo, K., Matsuo, T., and Nakajima, J. (1998) Redox-controlled ligand exchange of the heme in the CO-sensing transcriptional activator CooA. *J. Biol. Chem.* **273**, 25757–25764.
- Bangcharoenpaurpong, O., Champion, P. M., Hall, K. S., and Hager, L. P. (1986) Resonance Raman studies of isotopically labeled chloroperoxidase. *Biochemistry* **25**, 2374–2378.
- Biram, D., Garratt, C. J., and Hester, R. E. (1991) Resonance Raman investigations of carbon monoxide binding to mutant myoglobins. In *Spectroscopy of Biological Molecules* (Hester, R. E., and Girling, R. B., Eds.). Royal Society of Chemistry, Cambridge, pp. 433–434.
- Borcsok, E., and Abeles, R. H. (1982) Mechanism of activation of cystathionine synthase. *Arch. Biochem. Biophys.* **213**, 695–707.
- Cai, D., and Klinman, J. P. (1994a) Copper amine oxidase: heterologous expression, purification, and characterization of an active enzyme in *Saccharomyces cerevisiae*. *Biochemistry* **33**, 7647–7653.
- Cai, D., and Klinman, J. P. (1994b) Evidence for a self-catalytic mechanism of 2,4,5-trihydroxyphenylalanine quinone biogenesis in yeast copper amine oxidase. *J. Biol. Chem.* **269**, 32039–32042.
- Cai, D., Dove, J., Nakamura, N., Sanders-Loehr, J., and Klinman, J. P. (1997) Mechanism-based inactivation of a yeast methylamine oxidase mutant: implications for the functional role of the consensus sequences surrounding topaquinone. *Biochemistry* **36**, 11472–11478.

- Champion, P. M., Stallard, B. R., Wagner, G. C., and Gunsalus, I. C. (1982) Resonance Raman detection of an Fe-S Bond in cytochrome P450<sub>cam</sub>. *J. Am. Chem. Soc.* **104**, 5469–5472.
- Chen, Z., Schwartz, B., Williams, N. K., Li, R., Klinman, J. P., and Mathews, F. S. (2000) Crystal structure at 2.5 Å resolution of zinc-substituted copper amine oxidase of *Hansenula polymorpha* expressed in *Escherichia coli*. *Biochemistry* **39**, 9709–9717.
- Choi, Y. H., Matsuzaki, R., Fukui, T., Shimizu, E., Yorifuji, T., Sato, H., Ozaki, Y., and Tanizawa, K. (1995) Copper/topa quinone-containing histamine oxidase from *Arthrobacter globiformis*. Molecular cloning and sequencing, overproduction of precursor enzyme, and generation of topa quinone cofactor. *J. Biol. Chem.* **270**, 4712–4720.
- Clarke, R., Smith, A. D., Jobst, K. A., Refsum, H., Sutton, L., and Ueland, P. M. (1998) Folate, vitamin B 12, and serum total homocysteine levels in confirmed Alzheimer disease. *Arch. Neurol.* **55**, 1449–1455.
- Dawson, J. H., and Sono, M. (1987) Cytochrome P-450 and chloroperoxidase: thiolate-ligated heme enzymes. Spectroscopic determination of their active site structures and mechanistic implications of thiolate ligation. *Chem. Rev.* **87**, 1255–1276.
- Deinum, G., Stone, J. R., Babcock, G. T., and Marletta, M. A. (1996) Binding of nitric oxide and carbon monoxide to soluble guanylate cyclase as observed with resonance Raman spectroscopy. *Biochemistry* **35**, 1540–1547.
- Dove, J. E., Schwartz, B., Williams, N. K., and Klinman, J. P. (2000) Investigation of spectroscopic intermediates during copper-binding and TPQ formation in wild-type and active-site mutants of a copper-containing amine oxidase from yeast. *Biochemistry* **39**, 3690–3698.
- Drummond, J. T., Jarrett, J., Gonzalez, J. C., Huang, S., and Matthews, R. G. (1995) Characterization of nonradioactive assays for cobalamin-dependent and cobalamin-independent methionine synthase enzymes. *Anal. Biochem.* **228**, 323–329.
- Ekblom, J., Grönvall, J., Lennernäst, B., Nilsson, S., Garpenstrand, H., and Orelund, L. (1999) Elevated activity of semicarbazide-sensitive amine oxidase in blood from patients with skeletal metastases of prostate cancer. *Clin. Sci. (Lond.)* **97**, 111–115.
- Evangelista-Kirkup, R., Smulevich, G., and Spiro, T. G. (1986) Alternative carbon monoxide binding modes for horseradish peroxidase studied by resonance Raman spectroscopy. *Biochemistry* **25**, 4420–4425.



- Fan, B., Gupta, G., Danziger, R. S., Friedman, J. M., and Rousseau, D. L. (1998) Resonance Raman characterization of soluble guanylate cyclase expressed from baculovirus. *Biochemistry* **37**, 1178–1184.
- Ferraro, J. R., and Nakamoto, K. (1994) *Introductory Raman Spectroscopy*. Academic Press, Boston.
- Green, E. L., Taoka, S., Banerjee, R., and Loehr, T. M. (2001) Resonance Raman characterization of the heme cofactor in cystathionine  $\beta$ -synthase. Identification of the Fe–S(Cys) vibration in the six-coordinate low-spin heme. *Biochemistry* **40**, 459–463.
- Hartmann, C., Brzovic, P., and Klinman, J. P. (1993) Spectroscopic detection of chemical intermediates in the reaction of para-substituted benzylamines with bovine serum amine oxidase. *Biochemistry* **32**, 2234–2241.
- Holt, A., Alton, G., Scaman, C. H., Loppnow, G. R., Szpacenko, A., Svendsen, I., and Palcic, M. M. (1998) Identification of the quinone cofactor in mammalian semicarbazide-sensitive amine oxidase. *Biochemistry* **37**, 4946–4957.
- Janes, S. M. (1990) Mechanistic and structural characterization of bovine serum amine oxidase. Ph.D. Dissertation, University of California, Berkeley, CA.
- Janes, S. M., and Klinman, J. P. (1991) An investigation of bovine serum amine oxidase active site stoichiometry: evidence for an aminotransferase mechanism involving two carbonyl cofactors per enzyme dimer. *Biochemistry* **30**, 4599–4605.
- Janes, S. M., Mu, D., Wemmer, D., Smith, A. J., Kaur, S., Maltby, D., Burlingame, A. L., and Klinman, J. P. (1990) A new redox cofactor in eukaryotic enzymes: 6-hydroxydopa at the active site of bovine serum amine oxidase. *Science* **248**, 981–987.
- Janes, S. M., Palcic, M. M., Scaman, C. H., Smith, A. J., Brown, D. E., Dooley, D. M., Mure, M., and Klinman, J. P. (1992) Identification of topaquinone and its consensus sequence in copper amine oxidase. *Biochemistry* **31**, 12147–12154.
- Jeter, R. M., and Ingraham, J. L. (1984) Isolation and characterization of mutant *Pseudomonas aeruginosa* strains unable to assimilate nitrate. *Arch. Microbiol.* **138**, 124–130.
- Jhee, K. H., McPhie, P., and Miles, E. W. (2000) Yeast cystathionine  $\beta$ -synthase is a pyridoxal phosphate enzyme but, unlike the human enzyme, is not a heme protein. *J. Biol. Chem.* **275**, 11541–11544.
- Kim, I. C., and Deal, W. C., Jr. (1976) Isolation and properties of a new, soluble, hemoprotein (H-450) from pig liver. *Biochemistry* **15**, 4925–4930.

Kim, S., Deinum, G., Gardner, M. T., Marletta, M. A., and Babcock, G. T. (1996) Distal pocket polarity in the unusual ligand binding site of soluble guanylate cyclase: implications for the control of <sup>•</sup>NO binding. *J. Am. Chem. Soc.* **118**, 8769–8770.

Klinman, J. P., and Mu, D. (1994) Quinoenzymes in biology. *Annu. Rev. Biochem.* **63**, 299–344.

Knowles, P. F., and Dooley, D. M. (1994) Amine oxidases. In *Metal Ions in Biological Systems, Vol. 30: Metalloenzymes Involving Amino Acid-Residue and Related Radicals* (Sigel, H. and Sigel, A., Eds.). Marcel Dekker, New York, pp. 361–403.

Kraus, J. P., and Rosenberg, L. E. (1983) Cystathionine  $\beta$ -synthase from human liver: improved purification scheme and additional characterization of the enzyme in crude and pure form. *Arch. Biochem. Biophys.* **222**, 44–52.

Kraus, J., Packman, S., Fowler, B., and Rosenberg, L. E. (1978) Purification and properties of cystathionine  $\beta$ -synthase from human liver. Evidence for identical subunits. *J. Biol. Chem.* **253**, 6523–6528.

Kumar, V., Dooley, D. M., Freeman, H. C., Guss, J. M., Harvey, I., McGuirl, M. A., Wilce, M. C., and Zubak, V. M. (1996) Crystal structure of a eukaryotic (pea seedling) copper-containing amine oxidase at 2.2 Å resolution. *Structure* **4**, 943–955.

Lawson, D. M., Stevenson, C. E. M., Andrew, C. R., and Eady, R. R. (2000) Unprecedented proximal binding of nitric oxide to heme: implications for guanylate cyclase. *EMBO J.* **19**, 5661–5671.

Lee, Y., and Sayre, L. M. (1995a) Model reactions for the quinone-containing copper amine oxidases. Anaerobic reaction pathways and catalytic aerobic deamination of activated amines in buffered aqueous acetonitrile. *J. Am. Chem. Soc.* **117**, 3096–3105.

Lee, Y., and Sayre, L. M. (1995b) Model studies on the quinone-containing copper amine oxidases. Unambiguous demonstration of a transamination mechanism. *J. Am. Chem. Soc.* **117**, 11823–11828.

Lee, Y., Huang, H., and Sayre, L. M. (1996) Model studies support pyrrolylation of the topaquinone cofactor to explain inactivation of bovine plasma amine oxidase by 3-pyrrolines. Unusual processing of a secondary amine. *J. Am. Chem. Soc.* **118**, 7241–7242.

Li, R., Klinman, J. P., and Mathews, F. S. (1998) Copper amine oxidase from *Hansenula polymorpha*: the crystal structure determined at 2.4 Å resolution reveals the active conformation. *Structure* **6**, 293–307.

- Liu, Y., Moënné-Loccoz, P., Hildebrand, D. P., Wilks, A., Loehr, T. M., Mauk, A. G., and Ortiz de Montellano, P. R. (1999) Replacement of the proximal histidine iron ligand by a cysteine or tyrosine converts heme oxygenase to an oxidase. *Biochemistry* **38**, 3733–3743.
- Loehr, T. M., and Sanders-Loehr, J. (1993) Techniques for obtaining resonance Raman spectra of metalloproteins. *Methods Enzymol.* **226**, 431–470.
- Mandal, S., Lee, Y., Purdy, M. M., and Sayre, L. M. (2000) Chemical simulation of biogenesis of the 2,4,5-trihydroxyphenylalanine quinone cofactor of copper amine oxidases: mechanistic distinctions point toward a unique role of the active site in the *o*-quinone water addition step. *J. Am. Chem. Soc.* **122**, 3574–3584.
- Matsuzaki, R., Fukui, T., Sato, H., Ozaki, Y., and Tanizawa, K. (1994) Generation of the topa quinone cofactor in bacterial monoamine oxidase by cupric ion-dependent autooxidation of a specific tyrosine residue. *FEBS Lett.* **351**, 360–364.
- McGuirl, M. A., McCahon, C. D., McKeown, K. A., and Dooley, D. M. (1994) Purification and characterization of pea seedling amine oxidase for crystallization studies. *Plant Physiol.* **106**, 1205–1211.
- McIntire, W. S. (1994) Quinoproteins. *FASEB J.* **8**, 513–521.
- McIntire, W. S., and Hartmann, C. (1993) Copper-containing amine oxidases. In *Principles and Applications of Quinoproteins* (Davidson, V. L., Ed.). Marcel Dekker, New York, pp. 97–171.
- McIntire, W. S., Wemmer, D. E., Chistoserdov, A., and Lidstrom, M. E. (1991) A new cofactor in a prokaryotic enzyme: tryptophan tryptophylquinone as the redox prosthetic group in methylamine dehydrogenase. *Science* **252**, 817–824.
- Mills, J. L., McPartlin, J. M., Kirke, P. N., Lee, Y. J., Conley, M. R., Weir, D. G., and Scott, J. M. (1995) Homocysteine metabolism in pregnancies complicated by neural-tube defects. *Lancet* **345**, 149–151.
- Mitchell, J. B. O., Nandi, C. L., McDonald, I. K., Thorton, J. M., and Price, S. L. (1994) Amino/aromatic interactions in proteins: is the evidence stacked against hydrogen bonding? *J. Mol. Biol.* **239**, 315–331.
- Miyatake, H., Mukai, M., Adachi, S., Nakamura, H., Tamura, K., Iizuka, T., Shiro, Y., Strange, R. W., and Hasnain, S. S. (1999) Iron coordination structures of oxygen sensor FixL characterized by Fe K-edge extended X-ray absorption fine structure and resonance Raman spectroscopy. *J. Biol. Chem.* **274**, 23176–23184.

- Moënné-Loccoz, P., Nakamura, N., Steinebach, V., Duine, J. A., Mure, M., Klinman, J. P., and Sanders-Loehr, J. (1995) Characterization of the topa quinone cofactor in amine oxidase from *Escherichia coli* by resonance Raman spectroscopy. *Biochemistry* **34**, 7020–7026.
- Morikis, D., Champion P. M., Springer, B. A., and Sligar, S. G. (1989) Resonance Raman investigations of site-directed mutants of myoglobin: effects of distal histidine replacement. *Biochemistry* **28**, 4791–4800.
- Mudd, S. H., Levy, H. L., and Skovby, F. (1995) Disorders of transsulfuration. In *The Metabolic and Molecular Bases of Inherited Diseases* (Scriver, C. R., Beaudet, A. L., Sly, W. S., and Valle, D., Eds.). McGraw-Hill, New York, pp. 1279–1328.
- Mure, M., and Klinman, J. P. (1993) Synthesis and spectroscopic characterization of model compounds for the active site cofactor in copper amine oxidases. *J. Am. Chem. Soc.* **115**, 7117–7127.
- Mure, M., and Klinman, J. P. (1995a) Model studies of topaquinone-dependent amine oxidases. 1. Oxidation of benzylamine by topaquinone analogs. *J. Am. Chem. Soc.* **117**, 8698–8706.
- Mure, M., and Klinman, J. P. (1995b) Model studies of topaquinone-dependent amine oxidases. 2. Characterization of reaction intermediates and mechanism. *J. Am. Chem. Soc.* **117**, 8707–8718.
- Murray, J. M., Saysell, C. G., Wilmot, C. M., Tambyrajah, W. S., Jaeger, J., Knowles, P. F., Phillips, S. E. V., and McPherson, M. J. (1999) The active site base controls cofactor reactivity in *Escherichia coli* amine oxidase: X-ray crystallographic studies with mutational variants. *Biochemistry* **38**, 8217–8227.
- Nakamura, N., Matsuzaki, R., Choi, Y. H., Tanizawa, K., and Sanders-Loehr J. (1996) Biosynthesis of topa quinone cofactor in bacterial amine oxidases. Solvent origin of C-2 oxygen determined by Raman spectroscopy. *J. Biol. Chem.* **271**, 4718–4724.
- Nakamura, N., Moënné-Loccoz, P., Tanizawa, K., Mure, M., Suzuki, S., Klinman, J. P., and Sanders-Loehr, J. (1997) Topaquinone-dependent amine oxidase: identification of reaction intermediates by Raman spectroscopy. *Biochemistry* **36**, 11479–11486.
- Ojha, S., Hwang, J., Kabil, Ö., Penner-Hahn, J. E., and Banerjee, R. (2000) Characterization of the heme in human cystathionine  $\beta$ -synthase by X-ray absorption and electron paramagnetic resonance spectroscopies. *Biochemistry* **39**, 10542–10547.

- Omura, T., Sadano, H., Hasegawa, T., Yoshida, Y., and Kominami, S. (1984) Hemoprotein H-450 identified as a form of cytochrome P-450 having an endogenous ligand at the 6<sup>th</sup> coordination position of the heme. *J. Biochem. (Tokyo)* **96**, 1491–1500.
- Parsons, M. R., Convery, M. A., Wilmot, C. M., Yadav, K. D., Blakeley, V., Croner, A. S., Phillips, S. E., McPherson, M. J., and Knowles, P. F. (1995) Crystal structure of a quinoenzyme: copper amine oxidase of *Escherichia coli* at 2 Å resolution. *Structure* **3**, 1171–1184.
- Plastino, J., Green, E. L., Sanders-Loehr, J. and Klinman, J. P. (1999) An unexpected role for the active site base in cofactor orientation and flexibility in the copper amine oxidase from *Hansenula polymorpha*. *Biochemistry* **38**, 8204–8216.
- Ray, G. B., Li, X.-Y., Ibers, J. A., Sessler, J. L., and Spiro, T. G. (1994) How Far can proteins bend the FeCO unit? Distal polar and steric effects in heme proteins and models. *J. Am. Chem. Soc.* **116**, 162–176.
- Refsum, H., Ueland, P. M., Nygard, O., and Vollset, S. E. (1998) Homocysteine and cardiovascular disease. *Annu. Rev. Med.* **49**, 31–62.
- Reynolds, M. F., Parks, R. B., Burstyn, J. N., Shelper, D., Thorsteinsson, M. V., Kerby, R. L., Roberts, G. P., Vogel, K. M., and Spiro, T. G. (2000) Electronic absorption, EPR, and resonance Raman spectroscopy of CooA, a CO-sensing transcription activator from *R. rubrum*, reveals a five-coordinate NO-heme. *Biochemistry* **39**, 388–396.
- Ruggiero, C. E., Smith, J. A., Tanizawa, K., and Dooley, D. M. (1997) Mechanistic studies of topa quinone biogenesis in phenylethylamine oxidase. *Biochemistry* **36**, 1953–1959.
- Schwartz, B., Green, E. L., Sanders-Loehr, J., and Klinman, J. P. (1998) Relationship between conserved consensus site residues and the productive conformation for the TPQ cofactor in a copper-containing amine oxidase from yeast. *Biochemistry* **37**, 16591–16600.
- Schwartz, B., Dove, J. E., and Klinman, J. P. (2000) Kinetic analysis of oxygen utilization during cofactor biogenesis in a copper-containing amine oxidase from yeast. *Biochemistry* **39**, 3699–3707.
- Shan, X., and Kruger, W. D. (1998) Correction of disease-causing CBS mutations in yeast. *Nat. Genet.* **19**, 91–93.

- Shelver, D., Kerby, R. L., He, Y., and Roberts, G. P. (1997) CooA, a CO-sensing transcription factor from *Rhodospirillum rubrum*, is a CO-binding heme protein. *Proc. Natl. Acad. Sci. U.S.A.* **94**, 11216–11220.
- Shelver, D., Thorsteinsson, M. V., Kerby, R. L., Chung, S. Y., Roberts, G. P., Reynolds, M. F., Parks, R. B., and Burstyn, J. N. (1999) Identification of two important heme site residues (cysteine 75 and histidine 77) in CooA, the CO-sensing transcription factor of *Rhodospirillum rubrum*. *Biochemistry* **38**, 2669–2678.
- Skovby, F., Kraus, J. P., and Rosenberg, L. E. (1984) Biosynthesis and proteolytic activation of cystathionine  $\beta$ -synthase in rat liver. *J. Biol. Chem.* **259**, 588–593.
- Smulevich, G., Evangelista-Kirkup, R., English, A., and Spiro, T. G. (1986) Raman and infrared spectra of cytochrome *c* peroxidase–carbon monoxide adducts in alternative conformational states. *Biochemistry* **25**, 4426–4430.
- Spiro, T. G., and Li, X.-Y. (1988) Resonance Raman spectroscopy of metalloporphyrins. In *Biological Application of Raman Spectroscopy, Vol. 3: Resonance Raman Spectra of Hemes and Metalloproteins* (Spiro, T. G., Ed.). John Wiley and Sons, New York, pp. 1–37.
- Sun, J., Chang, C. K., and Loehr, T. M. (1997) Q-Band resonance Raman enhancement of Fe–CO vibrations in ferrous chlorin complexes: possible monitor of axial ligands in *d* cytochromes. *J. Phys. Chem. B* **101**, 1476–1483.
- Svastits, E. W., Alberta, J. A., Kim, I. C., and Dawson, J. H. (1989) Magnetic circular dichroism studies of the active site structure of hemoprotein H-450 comparison to cytochrome P-450 and sensitivity to pH effects. *Biochem. Biophys. Res. Commun.* **165**, 1170–1176.
- Taoka, S., and Banerjee, R. (2001) Activity of human cystathionine  $\beta$ -synthase is regulated by CO and NO: possible role for the heme protein in CO sensing. *J. Inorg. Biochem.*, in press.
- Taoka, S., Ojha, S., Shan, X., Kruger, W. D., and Banerjee, R. (1998) Evidence of heme-mediated redox regulation of human cystathionine  $\beta$ -synthase activity. *J. Biol. Chem.* **273**, 25179–25184.
- Taoka, S., West, M., and Banerjee, R. (1999a) Characterization of the heme and pyridoxal phosphate cofactors of human cystathionine  $\beta$ -synthase reveals nonequivalent active sites. *Biochemistry* **38**, 2738–2744.
- Taoka, S., Widjaja, L., and Banerjee, R. (1999b) Assignment of enzymatic functions to specific regions of the PLP-dependent heme protein cystathionine  $\beta$ -synthase. *Biochemistry* **38**, 13155–13161.

Taoka, S., Green, E. L., Loehr, T. M., and Banerjee, R. (2001) Mercuric chloride-induced spin or ligation state changes in ferric or ferrous human cystathionine  $\beta$ -synthase inhibit enzyme activity. *J. Inorg. Biochem.*, in press.

Tipping, A. J., and McPherson, M. J. (1995) Cloning and molecular analysis of the pea seedling copper amine oxidase. *J. Biol. Chem.* **270**, 16939–16946.

Tomita, T., Ogura, T., Tsuyama, S., Imai, Y., and Kitagawa, T. (1997) Effects of GTP on bound nitric oxide of soluble guanylate cyclase probed by resonance Raman spectroscopy. *Biochemistry* **36**, 10155–10160.

Tsubaki, M., Srivastava, R. B., and Yu, N. T. (1982) Resonance Raman investigation of carbon monoxide binding in (carbon monoxy)hemoglobin and -myoglobin: detection of Fe–CO stretching and Fe–C–O bending vibrations and influence of the quaternary structure change. *Biochemistry* **21**, 1132–1140.

Vogel, K. M., Spiro, T. G., Shelper, D., Thorsteinsson, M. V., and Roberts, G. P. (1999a) Resonance Raman evidence for a novel charge relay activation mechanism of the CO-dependent heme protein transcription factor CooA. *Biochemistry* **38**, 2679–2687.

Vogel, K. M., Hu, S., Spiro, T. G., Dierks, E. A., Yu, A. E., and Burstyn, J. N. (1999b) Variable forms of soluble guanylyl cyclase: protein–ligand interactions and the issue of activation by carbon monoxide. *J. Biol. Inorg. Chem.* **4**, 804–813.

Wagner, G., and Wüthrich, K. (1982) Amide proton exchange and surface conformation of the basic pancreatic trypsin inhibitor in solution. Studies with two-dimensional nuclear magnetic resonance. *J. Mol. Biol.* **160**, 343–361.

Wang, F., Bae, J.-Y., Jacobson, A. R., Lee, Y., and Sayre, L. M. (1994) Synthesis and characterization of models for the 2,4,5-trihydroxyphenylalanine (TOPA)-derived cofactor of mammalian copper amine oxidases, and initial amine reactivity studies. *J. Org. Chem.* **59**, 2409–2417.

Wang, S. X., Mure, M., Medzihradszky, K. F., Burlingame, A. L., Brown, D. E., Dooley, D. M., Smith, A. J., Kagan, H. M., and Klinman, J. P. (1996) A crosslinked cofactor in lysyl oxidase: redox function for amino acid side chains. *Science* **273**, 1078–1084.

Wang, S. X., Nakamura, N., Mure, M., Klinman, J. P., and Sanders-Loehr, J. (1997) Characterization of the native lysine tyrosylquinone cofactor in lysyl oxidase by Raman spectroscopy. *J. Biol. Chem.* **272**, 28841–28844.

Wilce, M. C., Dooley, D. M., Freeman, H. C., Guss, J. M., Matsunami, H., McIntire, W. S., Ruggiero, C. E., Tanizawa, K., and Yamaguchi, H. (1997) Crystal structures of the copper-containing amine oxidase from *Arthrobacter globiformis* in the holo and apo forms: implications for the biogenesis of the topaquinone. *Biochemistry* **36**, 16116–16133.

Wilmot, C. M., Murray, J. M., Alton, G., Parson, M. R., Convery, M. A., Blakeley, V., Corner, A. C., Palcic, M. M., Knowles, P. F., McPherson, M. J., and Phillips, S. E. V. (1997) Catalytic mechanism of the quinoenzyme amine oxidase from *Escherichia coli*: exploring the reductive half-reaction. *Biochemistry* **36**, 1608–1620.



## BIOGRAPHICAL SKETCH

Edward L. Green was born in Portland, Oregon on May 21, 1974. He developed a love for science at an early age at Buckman Elementary School. There he participated in the T.A.G. program and further explored the scientific field. Three years at Harriet Tubman Middle School provided much fun in all areas of study. He then attended Cleveland High School for four years where he enjoyed such activities as baseball, photography, and his first real experience with chemistry. Under the tutelage of Bernie Carlson he developed his skills as a chemist and was encouraged to further explore this area in college. He started his college education in the fall of 1992. He obtained his B.S. degree in Chemistry from Pacific University in 1996. He started his Ph.D. studies in the Department of Biochemistry and Molecular Biology at the Oregon Graduate Institute of Science and Technology in the summer of 1996. After graduation, Edward aspires for a career in the chemical industry.

### Publications:

Schwartz, B., Green, E. L., Sanders-Loehr, J., and Klinman, J. P. (1998) Relationship between conserved consensus site residues and the productive conformation for the TPQ cofactor in a copper-containing amine oxidase from yeast. *Biochemistry* **37**, 16591–16600.

Plastino, J., Green, E. L., Sanders-Loehr, J. and Klinman, J. P. (1999) An unexpected role for the active site base in cofactor orientation and flexibility in the copper amine oxidase from *Hansenula polymorpha*. *Biochemistry* **38**, 8204–8216.

Melville, C. R., Green, E. L., Sanders-Loehr, J., and Klinman, J. P. (2000) Reassessment of the active site quino-cofactor proposed to occur in the *Aspergillus niger* amine oxidase AO-I from the properties of model compounds. *Biochemistry* **39**, 7589–7594.

Green, E. L., Taoka, S., Banerjee, R., and Loehr, T. M. (2001) Resonance Raman characterization of the heme cofactor in cystathionine  $\beta$ -synthase. Identification of the Fe-S(Cys) vibration in the six-coordinate low-spin heme. *Biochemistry* **40**, 459–463.

Andrew, C. R., Green, E. L., Lawson, D. M., and Eady, R. R. (2001) Resonance Raman studies of cytochrome *c'* support binding of NO and CO to opposite sides of the heme: implications for ligand discrimination in heme-based sensors. *Biochemistry* **40**, 4115–4122.

Green, E. L., Nakamura, N., Dooley, D. M., Klinman, J. P., and Sanders-Loehr, J. (2001) Rates of oxygen and hydrogen exchange as indicators of TPQ cofactor orientation in amine oxidases. *Biochemistry*, in press.